12-2015

DEVELOPMENT OF A MINIATURIZED AMBIENT GLOW DISCHARGE IONIZATION SOURCE AND ITS APPLICATION IN ELEMENTAL AND MOLECULAR ANALYSIS

Xinyan Zhang
Clemson University, xinyanz@clemson.edu

DEVELOPMENT OF A MINIATURIZED AMBIENT GLOW DISCHARGE IONIZATION SOURCE AND ITS APPLICATION IN ELEMENTAL AND MOLECULAR ANALYSIS

A Dissertation

Presented to

the Graduate School of

Clemson University

In Partial Fulfillment

of the Requirements for the Degree

Doctor of Philosophy

Chemistry

---

by

Xinyan Zhang

December 2015

Accepted by:

R. Kenneth Marcus, Committee Chair

George Chumanov

Jeffrey N. Anker

Brian N. Dominy

ABSTRACT

Since the liquid sampling-atmospheric pressure glow discharge (LS-APGD) was first developed as an excitation source for atomic emission spectroscopy, it has been improved upon and demonstrated as an ionization source for elemental mass spectrometry, molecular mass spectrometry, and ambient desorption mass spectrometry. Multiple functions coming from one package allowed the LS-APGD to hold a unique position among all atmospheric pressure glow discharges. It also has the capabilities to work with different sample forms including liquids, bulk solids, and solution residues. The high salt/matrix tolerance reduces sample prep work and thus provides convenience for its potential use as a field-Based ionization source. These versatilities all come on a small platform.

It all started with Marcus and co-workers, who have developed a liquid sampling-atmospheric pressure glow discharge (LS-APGD) as a low power, small footprint, and cost efficient ionization source for mass spectrometry. The glow discharge is sustained between the surface of an electrolytic solution (5-50 μL min^{-1}), introduced through a 0.28 mm (i.d.) capillary housed inside a 1 mm (i.d.) metal capillary (with 0.1-1.0 L min^{-1} helium sheath gas flows between the two capillaries), and a solid stainless steel counter electrode mounted at a 90° angle with discharge currents of <60 mA, and d.c. powers of <50 W. Presented here, the design and fundamental operational aspects of the LS-APGD used as various spectroscopic sources will be demonstrated graphically. Sample analysis involving direct elemental analysis, organometallic speciation and organic compound in liquid solution, and direct surface analysis of solid sample and liquid residue will be

presented to further explain the ability of the LS-APGD. It is believed that the LS-APGD ionization source holds a unique position and has great potential to be utilized in many fields of chemical analysis.

DEDICATION

This dissertation is dedicated to everyone who believed in me. It is the love and support that each individual provided that assisted me in obtaining all of the goals set in my path.

To my love, Daniel, your companionship is the main reason that walked me through this journey, oh, and all of our lovely “arguments” throughout the years helped me so much about American logic and English Speaking. My cat, Bean, all those nights you sit by my feet while I am working on data processing, kept me company and warm.

To my close friends, Wang, Sting, Jerry and Fan, I am thankful to have you guys here in Clemson with me, we had so much fun together, for all the trips to Atlanta, GA, and to all those meals we ate together. Those memories will always be with me, and we sure are going to make more together.

To Ben, who have impacted my life tremendously through the years, a friend and colleague, provided both knowledge and support, thanks you.

I would like to thank my Clemson friends, and the whole Marcus group for all the help and support. I love you all!

Finally, to my parents and brother, thanks for believing in me, and support me through my whole life, financially and spiritually, I will not be here without you guys. 爸，妈，辛苦了！谢谢你们！

ACKNOWLEDGMENTS

First of all, I would like to thank my advisor, Dr. R. Kenneth Marcus for his support and guidance throughout my time at Clemson University and for teaching me how to be a scientist, and more importantly made me a better person! I really appreciate all the opportunities Dr. Marcus provided for me to expand my scientific background and build professional networking, such as attending conferences and collaborations. These experiences have made me learn, grow and mature, I am really thankful to have him as my advisor.

The whole Marcus group, I am really thankful to have you all, for all the help and support. Dr. Benjamin Manard, Dr. Derrick Quarles, Dr. Carolyn Burdette, Dr. Abby Schadock-Hewitt, Jerry Liu, Marissa Pierson, Paul Haupt-Renaud, Sarah Harris and Edward Hoegg for their support throughout my graduate degree. I would also like to acknowledge my graduate committee Jeffery Anker, George Chumanov and Brian Dominy.

TABLE OF CONTENTS

Page

Table of Contents (Continued) Page

Table of Contents (Continued) Page

LIST OF FIGURES

List of Figures (Continued)

Figure Page

List of Figures (Continued)

Figure Page

List of Figures (Continued)

Figure Page

List of Figures (Continued)

Figure Page

List of Figures (Continued)

Figure Page

LIST OF TABLES

CHAPTER ONE

INTRODUCTION

1.1 Introduction of Mass Spectrometry

Mass spectrometry is an analytical technique that measures the mass to charge ratio (m/z) of the analytes/fragments of analytes to provide useful information including elemental composition and some aspects of the molecular structure of an analyte. Mass spectrometry can also be used to selectively detect and determine the amount of a given analyte. These tasks are accomplished through the experimental measurements of the mass of gas-phase ions produced from molecules of an analyte under vacuum condition. As stated earlier, one unique features of mass spectrometry includes its capacity for direct determination of the nominal mass of an analyte, and to produce and detect fragments of the molecule that reveal structural features. Mass spectrometry has the capacity to generate more structural information through the mass spectrum generated from the analyte which is a plot of the ion signal intensity as a function of the mass-to-charge ratio.

In general, a mass spectrometry instrument consists of three components operating fully or partially under vacuum condition: an ion source, a mass analyzer, and a detector as presented in Figure 1.1. However, there are various types for each component that benefits different analytes as a result of their chemical and physical properties.

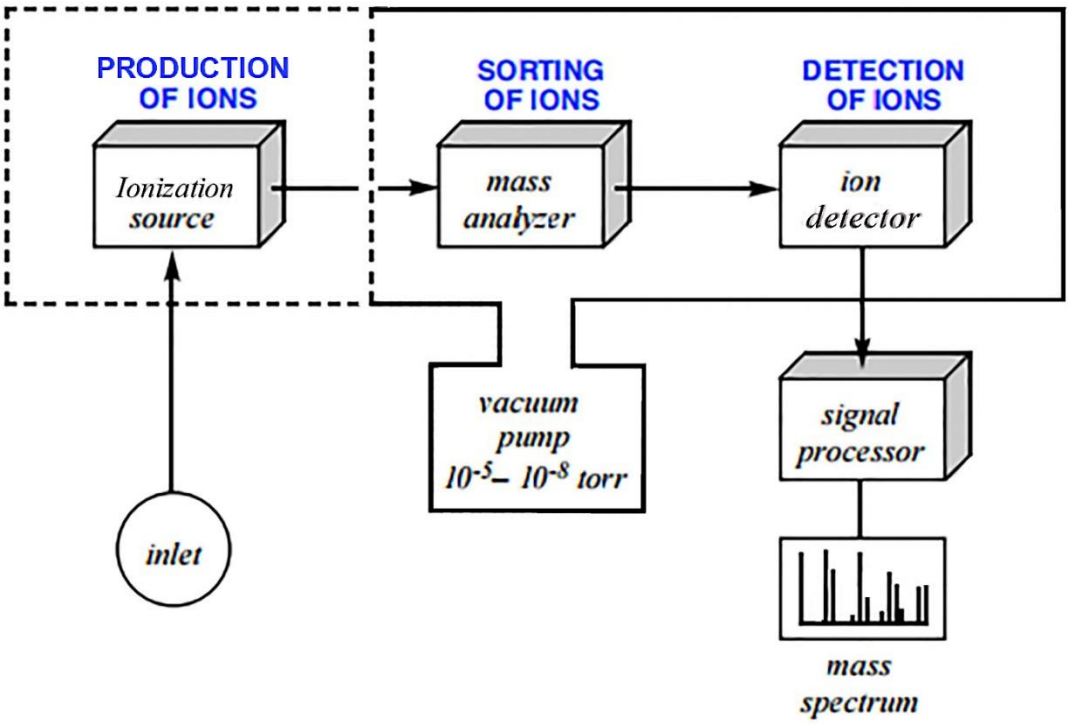

Figure 1.1 Basic diagram for a mass spectrometer.

This dissertation is focused on the development and characterization of an ionization source designed in this laboratory: the liquid sampling atmospheric pressure glow discharge coupled with a Thermal® LCQ Advantage ™ mass analyzing system. The development focuses on using this system towards applications such as gathering elemental and molecular information of target analytes, including atomic speciation, molecular structural information and metal-ligand speciation in aqueous solution.

There are many different types of ionization sources available that benefit different analytes. In general, most of the ionization sources can be divided into two categories, inorganic ionization sources that provide elemental information, and organic ionization sources that produces molecular ions.

1.1.1 Inorganic Ionization Sources

Thermal ionization[1], spark[2] and arc[3] ionization sources have been used for decades for elemental analysis of samples introduced in solid mode. However, inductively coupled plasma (ICP) is the most commonly used ionization source for atomic speciation including isotopic ratio in the sample.[4-7] ICP-MS was commercially introduced in 1983 and has gained general acceptance in many types of laboratories. Geochemical analysis labs were early adopters of ICP-MS technology because of its superior detection capabilities, particularly for the rare-earth elements. Under the typical operation of ICP-MS, a liquid sample is introduced (typically by a peristaltic pump at 1-2 mL min^{-1}) into an analytical nebulizer, which converts the liquid solution into an aerosol of droplets through a high flow-rate gas such as N_2. The droplets are then separated by a spray chamber in which the larger droplets are removed and the fine droplets become dry particles due to solvent evaporation. These dry particles can then be swept into the plasma torch for atomization and ionization to create ions. The plasma used in an ICP-MS typically is made by partially ionizing argon gas (up to 16 L min^{-1}) utilizing a coil that surround the argon gas and powered by a radio frequency power supply. After the dry particles is injected into the torch, the extremely high temperature of the plasma can cause the sample to dissociate into individual atoms, known as the atomization step. Following this is the ionization step in which the neutral atoms will be ionized through Penning ionization, charge transfer, direct electron impact, ect, so that they can be detected by the mass spectrometer.

ICP-MS has many benefits in comparison to other elemental techniques (such as atomic absorbance spectroscopy, glow discharge mass spectrometry and thermal ionization mass spectrometry), with better analytical figures of merit including limit of detection (LOD), sensitivity, and robustness.[8] However it has a high amount of interfering species produced by the argon from the plasma, component gasses of air that leak through the cone orifices, and contamination from glassware and the cones are some of the disadvantages of ICP along with the high operating cost.[9-13] This dissertation will discuss an approach with an atomic ionization source utilizing a miniaturized plasma with a small footprint and relatively low operating costs.

1.1.2 Organic Ionization Sources

The classic organic ionization sources include electron ionization (EI) and chemical ionization (CI). EI is also referred to as “electron impact” and is one of the oldest and also the most commonly used on commercial MS instruments.[14-16] A beam of electrons passes through a gas-phase sample, and one of the electrons that collides with a neutral analyte molecule (M) can knock off another electron or a part of the molecule, resulting in a positively charged molecular ion (M^+) or a fragment ion ($M-X^+$) through mechanisms in Figure 1.2. Generally electrons with energies of 70 eV are used and such energy produces very similar spectra for the same analytes even performed on different instruments, thus libraries exist for identifying unknown compounds through spectral “fingerprints”.[17] EI is also the best characterized among all ionization sources and therefore more commonly used when coupled with gas chromatography(GC).[17]

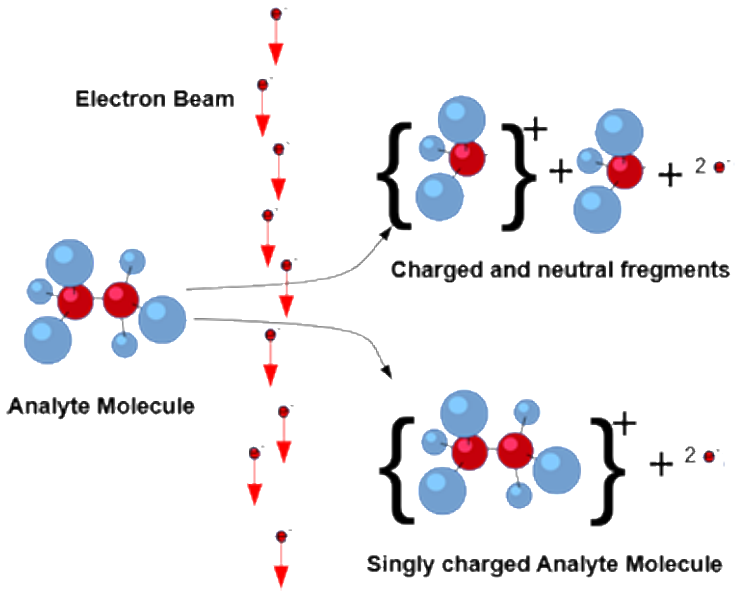

Figure 1.2 Electron Ionization mechanism.

Chemical ionization (CI) begins with a reagent gas (R) being ionized by electron impact, then subsequently reacts with analyte molecules to produce analyte ions.[14,18-20] This method provides more molecular weight information and reduced fragmentation in comparison to EI, in another word, CI is a softer ionization technique than EI. An example of ionization mechanism when using methane as reagent gas is showing below:

$$CH_4 + e^- \rightarrow CH_4^{+\bullet} + 2e^-$$
$$CH_4 + CH_4^{+\bullet} \rightarrow CH_5^+ + CH_3^\bullet$$
$$M + CH_5^+ \rightarrow CH_4 + [M+H]^+$$

However, other reactions can occur as well, such as the ion-molecule reactions between the reagent gas ions and reagent gas neutrals in situations under a high reagent gas pressure or long reaction time.[21] Some of the products of these ion-molecule reactions can react with the analyte molecules to produce analyte ions. The commonly used reagent gas types, their molecular ions

generated through electron impact and their reactive reagent ions formed are listed in Table 1.1.

Table 1-1 Reagent gas types and their reactive ions for chemical ionization.

reagent gas (R)	molecular ion	reactive reagent ion
H_2	$H_2^{+\bullet}$	H_3^+
C_4H_{10}	$C_4H_{10}^{+\bullet}$	$C_4H_{11}^+$
NH_3	$NH_3^{+\bullet}$	NH_4^+
CH_3OH	$CH_3OH^{+\bullet}$	$CH_3OH_2^+$
NO	$NO^{+\bullet}$	NO^+

The classic organic ionization techniques are require vacuum conditions to operate, however, there are ionization techniques developed for the operation at atmospheric pressure and are termed atmospheric pressure ionization (API) sources. Electrospray (ESI) and atmospheric pressure chemical ionization (APCI) are two typical representatives of this category. Both ESI and APCI are for direct liquid-phase sampling mode, therefore they are also the most commonly used ionization sources for the analysis of organic compounds while using liquid chromatography (LC)-MS coupling. ESI is generally accomplished by forcing an analyte solution with nebulizer gas through a small fused silica capillary, the fluid sprays into an electric field, thereby generating very fine droplets as illustrated conceptually in Figure 1.3.[22-26] The electric field is imposed between the tip of the spraying capillary and a counter electrode. It is very important to have this imposed field which keeps the droplets from freezing during the loss of solvent (endothermic evaporation process) by causing the charged droplets to endure collisions through

which some kinetic energy is converted to internal energy.[27] Such collisions also help the removal of solvent on the droplets to produce more gas phase analyte ions.

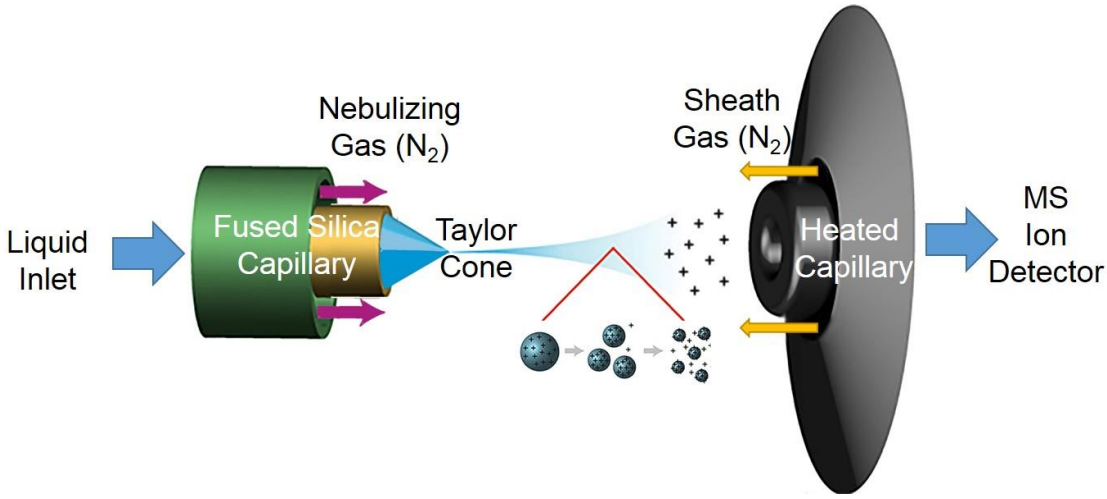

Figure 1.3 Ionization mechanism of electrospray.

ESI brings many new benefits/features into classic mass spectrometry, which has traditionally relied on gas-phase analytes introduction. Beyond the advantage of producing ions for nonvolatile, thermally labile compounds and the ability of direct analysis of inorganic cations and anions, ESI can also produce multiple charged ions, which permits the detection of high-mass compounds such as biological macromolecules The limitation is that multiple charged species require interpretation and mathematical transformation to calculate. Also, ESI is not quit useful when analytes are uncharged or are low-polarity compounds such as steroids. For inorganic speciation in aqueous solution, ESI is also not the ideal ionization source as the high voltage and the electrical field along with the nebulization process brings many variations into the speciation analysis in aqueous solution.[28-30] This dissertation will discuss an ionization source that is

more suitable for metal-ligand speciation in aqueous environment utilizing a miniaturized plasma that can directly perform liquid phase sampling.

APCI is complementary to ESI, it is particularly effective for less-polar compounds.[30,31] The ionization process is initiated by low-energy electrons generated by either a radioactive beta source or a corona discharge (more common for modern APCI source) under atmospheric region.[32,33] And because the ion source operates under atmospheric pressure, a heated filament cannot be used to produce electrons as the primary source of ionization. Same with CI source, a reagent gas is required (i.e., N_2, O_2, H_2O) for the ionization process which involving a complex series of ion/molecule reactions, efficiently produces positive and negative ions of the analyte. The basic processes of ionization by APCI have been reviewed, typically through several steps as in equations below, and a drawing of such process is presented in Figure 1.4.

$$S + e^- \rightarrow S^+ \cdot + 2e^-$$

$$S^+ \cdot + S \rightarrow [S + H]^+ + [S - H]$$

$$[S + H]^+ + M \rightarrow S + [M + H]^+ \; or \; S^+ \cdot + M \rightarrow M^+ \cdot + S$$

In which S is the solvent/reagent gas, usually as a complex mixture of H_2O, CH_3CN/CH_3OH and mobile phase modifiers. S abstracts a hydrogen atom from other solvent gas molecules then further ionizes analyte (M) by proton transfer/proton abstraction or charge transfer.[34]

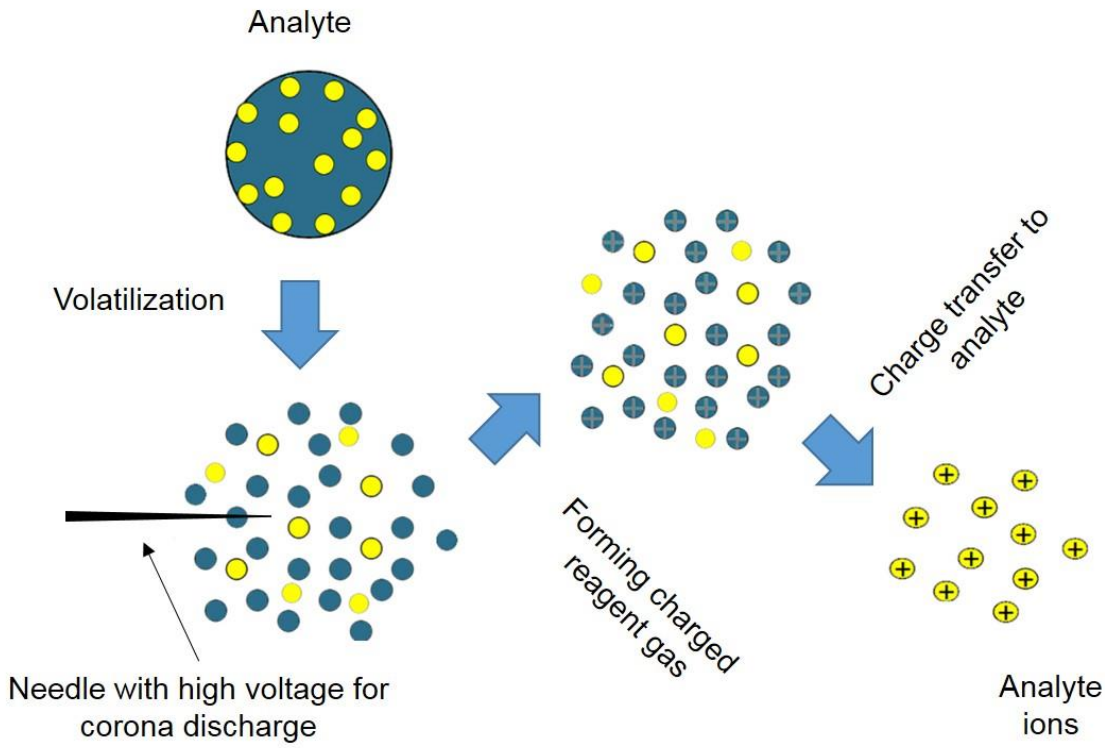

Figure 1.4 Ionization mechanism of atmospheric pressure chemical ionization.

Efficient ionization for less polar compounds is a major benefit for APCI. The fact that APCI does not require liquid phase sampling permits it the ability to couple with both LC and GC.[35-37] The limitation is analytes that are thermally labile or polar. Also high molecular weight compounds should be avoided due to the vaporization process since fragmentations beyond EI-like could occur.

1.1.3 Desorption Ionization Source

Desorption ionization sources all involve the unifying aspect of the rapid addition of energy onto a condensed-phase sample (solid sample or dried sample solution residue), with subsequent generation and release of ions into a mass analyzer. The energy used for the desorption of analyte sample can be in many different forms, including laser beam, plasma, and/or kinetic energy. Matrix

assistant laser desorption/ionization (MALDI) source is one unique desorption source, which operates under vacuum condition, with the assistance of an organic matrix compound which is pre-mixed with the analytes.[38]

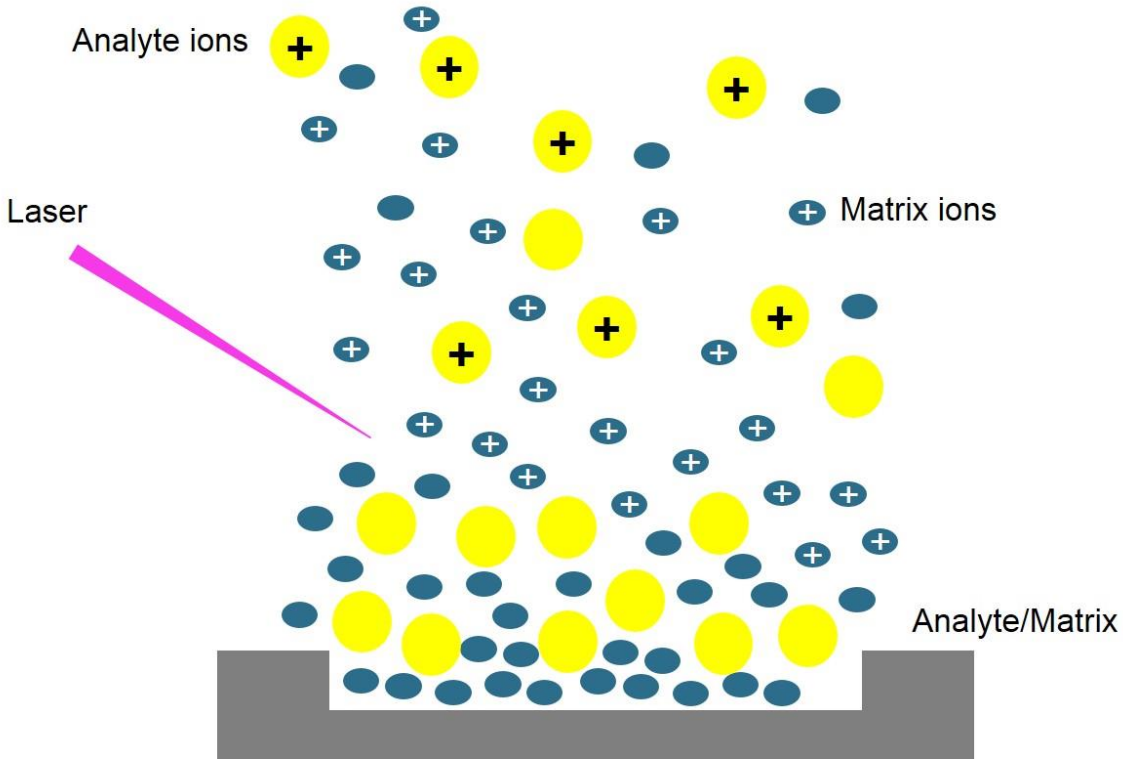

Figure 1.5 Ionization mechanism of matrix assist laser desorption/ionization source.

As seen in Figure.1.5, the high energy density at the spot illuminated by the laser causes the solid sample to evaporate into the gas phase, during which the localized segment of matrix and analyte expand and disperses into neutral molecules along with some ions. Through proton transfer, cation/anion transfer, or in some rare cases charge transfer between the matrix ions and analyte neutral molecules, analytes are being ionized.[39] The species have high kinetic energy (initial velocities of 400 to 800 m s^{-1}), however, very little increase in the internal

energy of the analyte occurs during the laser shot, which leads to very little or no fragmentation of the analyte and makes MALDI a soft ionization technique.

There are several adsorption ionization sources that operates under ambient conditions, they are categorized into ambient desorption ionization (ADI) sources. ADI-MS allows the direct analysis of ordinary objects in the open atmosphere of the laboratory or in some situations, in their natural environment, which typically require little or no sample preparation. These techniques can be related into the classic atmospheric ionization sources, ESI and APCI, based on the ionization mechanism. The development of ADI started with the introduction of desorption electrospray ionization (DESI)[40] and direct analysis in real time (DART)[41] into this field. For the first time you have an ionization technique that allows for the ionization of samples directly in their native condition under ambient condition, bypassing steps like the sample preparation and matrix matching. In the DESI process, solvent is forced through a capillary and nebulized while a high voltage is applied, the solvent solution forms into aqueous droplets (charged or neutral), with diameters less than 10 μm and velocities typically higher than 100 m/s, that impact on a sample surface, as as showing in Figure 1.6a.[42] The analyte ionization mechanism is believed to be initiated as the surface is pre-wetted by initial solvent droplets to form localized analyte-solvent layer. When later arriving solvent droplets impact this analyte-solvent-layer and break it up they create numerous off-spring droplets including the dissolved analytes. During this collision, charge transfer and/or proton transfer occurs as well. Thus, for DESI, the analyte

desorption occurs by momentum transfer, and analyte ionization occurs by the charge transfer initiated by the charged droplets through the ESI mechanisms.

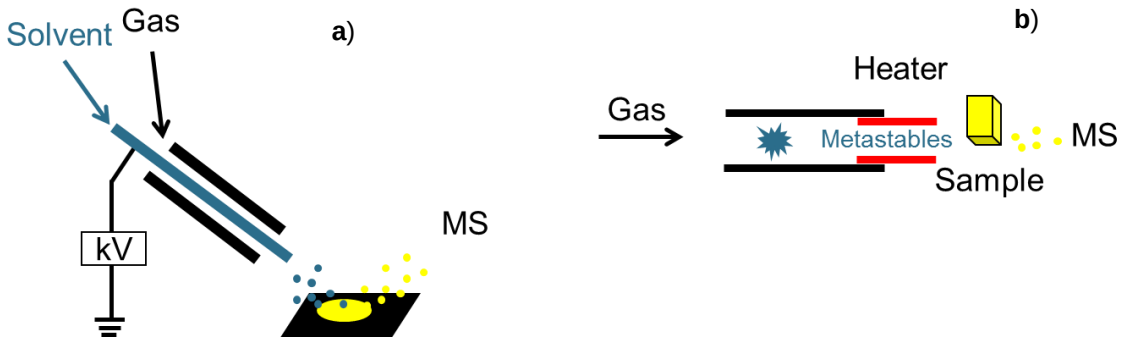

Figure 1.6 Basic drawing of desorption electrospray ionization (a) and direct analysis in real time (b).

In DART, the discharge occurs further away from the sample surface, and a stream of heated gas is used to carry the metastables towards the sample as showing in Figure 1.6b. The thermal energy combined with the kinetic energy desorb the analyte from the localized solid form into single molecular analyte. The ionization mechanism in DART is APCI-like, initiated with metastable helium atoms originating in the plasma which react with ambient water, oxygen, or other atmospheric components during transit to produce the reactive ionized species. The analyte ionization mechanism is different for positive and negative ions. The positive-ion detection mode where analytes with high proton affinity are ionized by proton-transfer and non-polar analyte are in general ionized through Penning ionization, which is through the electron removal from the analyte molecule during the collision with excited states of He or N_2 to form analyte radical cations. However, for the negative-ion mode, the dominant reactions are deprotonation or combination with various anions in analyte sample, including chloride, acetate, and

nitrate anions to form negatively charged analyte ions. There are more than 50 different ADI sources in the literature, they are all either DESI-like or DART-like, but with different geometry and/or operating conditions that lead to different benefits when analyzing particular analyte samples. Presenting in this dissertation, is an ADI source that combines the ionization mechanism and benefits of both DESI and DART, which uses solvent droplet, thermal energy and kinetic energy to desorb solid analyte, and ionize analyte through proton transfer, Penning ionization and ion adduction.

1.1.4 Liquid-Sampling Atmospheric Glow Discharge

Miniaturization of instrumentation recently is of interest to increase access to sophisticated methodologies in addition to reducing operating costs, reducing the sample size and the amount of waste generated, and minimizing footprint with a given instrument for the potential of field deployment. Advances regarding miniaturization have been seen in many areas except atomic spectroscopy. The atomic ionization sources including inductively coupled plasma (ICP) and thermal ionization (TI) sources have not changed significantly in their commercial implementations over the past three decades. However, the efforts to develop glow discharge mass spectrometry (GDMS) sources started in the 1980s.[43,44] In terms of elemental analysis using spectroscopy methods, ion sputtering of the cathode surface is a versatile means of introducing sample material into the low temperature plasma, wherein atoms are excited and ionized by collisions with electrons and metastable discharge gas atoms (e.g. Penning ionization), providing for bulk and depth-resolved analysis of metals and electronic materials.[45] Among

all designs, APGD is the most desired and suitable technique due to the lack of vacuum. There have been two basic designs described for the generation of low power, continuous plasmas using direct liquid sampling and having the ability of performing elemental analysis using optical emission spectroscopy (OES). The electrolyte cathode discharge (ELCAD) was designed by Cserfalvi and co-workers,[46] and then further characterized and improved by Hieftje and co-workers under the name of solution cathode discharge (SCD).[47,48] The device utilizes a d.c. glow discharge formed between the grounded tungsten or titanium anode and the surface of the electrolyte solution that flows out from a u-shaped glass pipette placed <1 cm above the waste reservoir. The electrolyte solution acts as the cathode electrode in this case. Marcus and Davis developed the liquid sampling-atmospheric pressure glow discharge (LS-APGD) as a low power (<50 W), reduced cost, and small sample flow rate (<100 µL min^{-1}) excitation source.[49] In the LS-APGD, the microplasma is sustained between the surface of the electrolyte solution and a metallic counter electrode mounted at a 90° angle and parallel to the lab bench, with a spacing of only 1-2 mm as seen in Figure 1.7. A primary difference with the ELCAD-based designs is the fact that a very high power density is realized in the microplasma (>10 W mm^{-3}) providing sufficient energy for operation in a total-consumption (i.e., no liquid waste) mode.[50] The combination of high power density and the ever-presence of the electrolyte solution yields a high tolerance for matrix effects from salt-heavy samples.

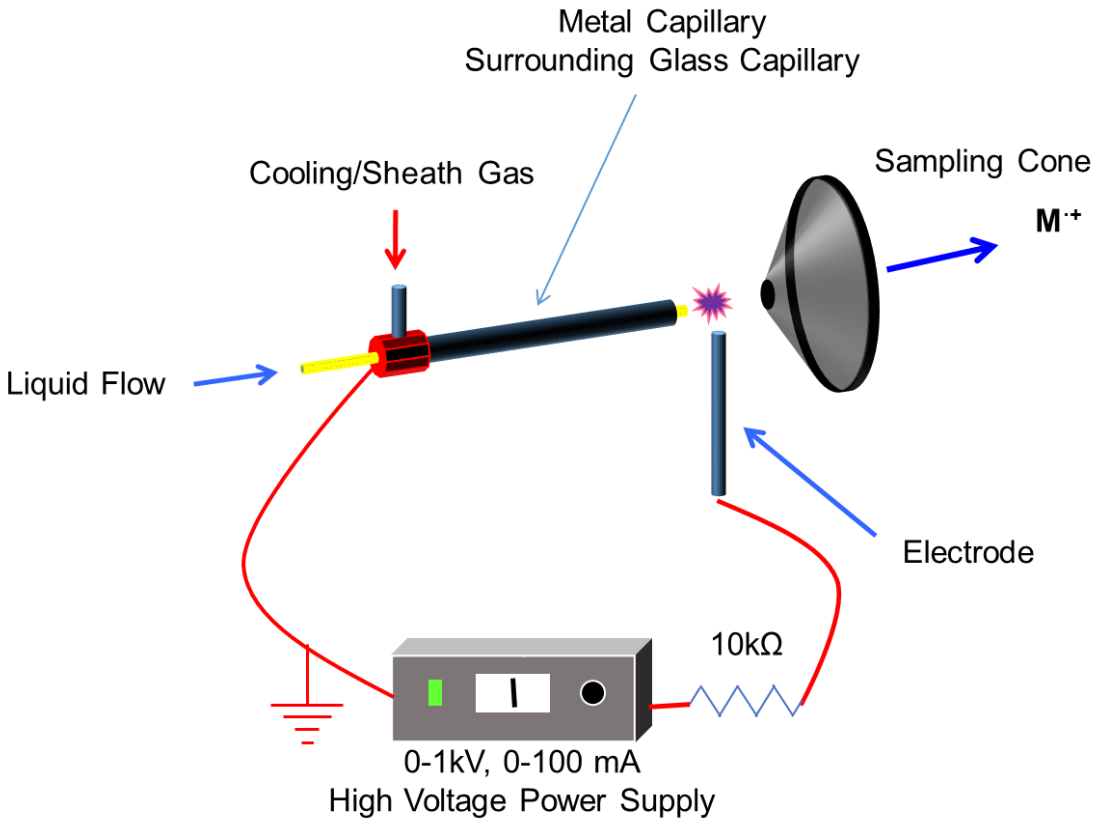

Figure 1.7 Liquid Sampling-Atmospheric Pressure Glow Discharge Ion Source.

The LS-APGD has recently been utilized as an ionization source for elemental mass spectrometry presenting.[51,52] The device can be easily integrated onto the atmospheric ionization source interface common to organic/biological ambient mass spectrometers as a source for direct liquid sample analyzing ion source or an ADI source. The proposed research involves attaching the LS-APGD ionization source to a Thermo Finnigan LCQ Advantage quadrupole ion trap mass analyzer to fully characterize and evaluate all parameters to provide better performance for the potential applications of the source, including the uranyl speciation in aqueous solution or detection of a variety of drugs of abuse in buffers and simulated biofluids. This work is both significant and innovative because the

development and characterization of LS-APGD microplasma will further improve this ionization source which is highly effective with low cost, small sample size requirement, compact footprint and has easy integration into most of the commercially available mass spectrometers.

As a new ionization source, a full understanding of the operating parameters and how they contribute to the ionization step and how to optimize the operating conditions are very important. Thus, a parametric evaluation of the operating parameters (i.e., solution flow rate, He sheath/cooling gas flow rate, discharge current, and ion sampling distance), when LS-APGD is used as atomic emission ionization source, is presented in Chapter 2. Then a different geometry of the set-up allowing for the analyses of solid samples directly as an ADI source is presented in Chapter 3. Presented in Chapter 4 involves the direct liquid phase sampling of uranyl-acetate system, the LS-APGD ionization source was slightly modified and was employed for the determination of metal-ligand speciation in aqueous solution. The same system presented in Chapter 4 is determined to be a much softer ionization source in comparison to the initial LS-APGD design, this system was tested for the ionization of organic compounds, and the results are presented in Chapter 5.

1.2 References

1. Todd, P. J.; McKown, H. S.; Smith, D. H. *International Journal of Mass Spectrometry and Ion Processes* **1982**, *42*, 183-190.

2. Shiloh, J.; Chupp, W.; Faltens, A.; Keefe, D.; Kim, C.; Rosenblum, S. S.; Tiefenback, M. *Bulletin of the American Physical Society* **1979**, *24*, 999-999.

3. Venkatasubramanian, V. S.; Swaminathan, S.; Rajagopalan, P. T. *International Journal of Mass Spectrometry and Ion Processes* **1977**, *24*, 207-217.

4. Gunther, D.; Hattendorf, B. *Trac-Trends in Analytical Chemistry* **2005**, *24*, 255-265.

5. Ammann, A. A. *Journal of Mass Spectrometry* **2007**, *42*, 419-427.

6. Beauchemin, D. *Analytical Chemistry* **2010**, *82*, 4786-4810.

7. Giner Martinez-Sierra, J.; Galilea San Bias, O.; Marchante Gayon, J. M.; Garcia Alonso, J. I. *Spectrochimica Acta Part B-Atomic Spectroscopy* **2015**, *108*, 35-52.

8. Cottingham, K. *Analytical Chemistry* **2004**, *76*, 35A-38A.

9. Ramsey, M. H.; Thompson, M. *J. Anal. At. Spectrom.* **1986**, *1*, 185-193.

10. Olesik, J. W.; Williamsen, E. J. *Applied Spectroscopy* **1989**, *43*, 1223-1232.

11. Tripkovic, M. R.; Holclajtnerantunovic, I. D. *J. Anal. At. Spectrom.* **1993**, *8*, 349-365.

12. Agatemor, C.; Beauchemin, D. *Analytica Chimica Acta* **2011**, *706*, 66-83.

13. Pak, Y.-N. *Bulletin of the Korean Chemical Society* **2014**, *35*, 3482-3488.

14. Dorman, F. H. *J. Chem. Phys.* **1965**, *43*, 3507-&.

15. Bely, O.; Vanregem.H. *Annual Review of Astronomy and Astrophysics* **1970**, *8*, 329-&.

16. Bell, K. L.; Gilbody, H. B.; Hughes, J. G.; Kingston, A. E.; Smith, F. J. *Journal of Physical and Chemical Reference Data* **1983**, *12*, 891-916.

17. Sanchez-Guijo, A.; Hartmann, M. F.; Wudy, S. A. In *Hormone Assays in Biological Fluids, 2nd Edition*, Wheeler, M. J., Ed., 2013, pp 27-44.

18. Volkov, N. F.; Karachev.Gv; Marutkin, A. Z.; Kholodov, A. I. *Pribory I Tekhnika Eksperimenta* **1974**, 7-12.

19. Munson, B. *Analytical Chemistry* **1977**, *49*, A772-&.

20. Richter, W. J.; Schwarz, H. *Angewandte Chemie-International Edition in English* **1978**, *17*, 424-439.

21. Hunter, R. L.; McIver, R. T. *Analytical Chemistry* **1979**, *51*, 699-704.

22. Dole, M.; Cox, H. L.; Gieniec, J. *Abstracts of Papers of the American Chemical Society* **1971**, 44-&.

23. Dole, M.; Cox, H. L.; Gieniec, J. *Advances in Chemistry Series* **1973**, 73-84.

24. Yamashita, M.; Fenn, J. B. *Journal of Physical Chemistry* **1984**, *88*, 4451-4459.

25. Geisow, M. *Trends in Biotechnology* **1990**, *8*, 301-303.

26. Shumate, C. B.; Hill, H. H. *Acs Symposium Series* **1992**, *508*, 192-205.

27. Kebarle, P. *Journal of Mass Spectrometry* **2000**, *35*, 804-817.

28. Dion, H. M.; Ackerman, L. K.; Hill, H. H. *Talanta* **2002**, *57*, 1161-1171.

29. Cole, R. B. *Electrospray and MALDI Mass Spectrometry: Fundamentals, Instrumentation, Practicalities, and Biological Applications*, 2nd ed.; John Wiley & Sons: Hoboken, 2010.

30. Awad, H.; Khamis, M. M.; El-Aneed, A. *Applied Spectroscopy Reviews* **2015**, *50*, 158-175.

31. Van Breeman, R. B.; Huang, C.-R.; Tan, Y.; Schilling, A. B. *Abstracts of Papers American Chemical Society* **1995**, *210*, 51-ANYL 51.

32. Byrdwell, W. C. *Lipids* **2001**, *36*, 327-346.

33. Klee, S.; Derpmann, V.; Wissdorf, W.; Klopotowski, S.; Kersten, H.; Brockmann, K. J.; Benter, T.; Albrecht, S.; Bruins, A. P.; Dousty, F.; Kauppila, T. J.; Kostiainen, R.; O'Brien, R.; Robb, D. B.; Syage, J. A. *Journal of the American Society for Mass Spectrometry* **2014**, *25*, 1310-1321.

34. Kolakowski, B. M.; Grossert, J. S.; Ramaley, L. *Journal of the American Society for Mass Spectrometry* **2004**, *15*, 301-310.

35. Mitchum, R. K.; Korfmacher, W. A.; Moler, G. F.; Stalling, D. L. *Analytical Chemistry* **1982**, *54*, 719-722.

36. Kolakowski, B. A.; Grossert, J. S.; Ramaley, L. *Journal of the American Society for Mass Spectrometry* **2004**, *15*, 311-324.

37. Andrade, F. J.; Shelley, J. T.; Wetzel, W. C.; Webb, M. R.; Gamez, G.; Ray, S. J.; Hieftje, G. M. *Analytical Chemistry* **2008**, *80*, 2646-2653.

38. Boyd, R. K. *Biological Mass Spectrometry* **1994**, *23*, 806-806.

39. Kruger, R.; Karas, M. *Journal of the American Society for Mass Spectrometry* **2002**, *13*, 1218-1226.

40. Calbiani, F.; Careri, M.; Elviri, L.; Mangia, A.; Pistarà, L.; Zagnoni, I. *Journal of Chromatography A* **2004**, *1042*, 123-130.

41. Cody, R. B.; Laramee, J. A.; Durst, H. D. *Anal. Chem.* **2005**, *77*, 2297-2302.

42. Takats, Z.; Wiseman, J. M.; Cooks, R. G. *Journal of Mass Spectrometry* **2005**, *40*, 1261-1275.

43. Harrison, W. W.; Hess, K. R.; Marcus, R. K.; King, F. L. *Analytical Chemistry* **1986**, *58*, 341A-356A.

44. Duckworth, D. C.; Marcus, R. K. *Analytical Chemistry* **1989**, *61*, 1879-1886.

45. Marcus, R. K. *Glow Discharge Spectroscopies*; Plenum Press: New York, 1993.

46. Cserfalvi, T.; Mezei, P. *J. Anal. At. Spectrom.* **1994**, *9*, 345-349.

47. Webb, M. R.; Andrade, F. J.; Gamez, G.; McCrindle, R.; Hieftje, G. M. *J. Anal. At. Spectrom.* **2005**, *20*, 1218-1225.

48. Webb, M. R.; Chan, G. C. Y.; Andrade, F. J.; Gamez, G.; Hieftje, G. M. *J. Anal. At. Spectrom.* **2006**, *21*, 525-530.

49. Davis, W. C.; Marcus, R. K. *J. Anal. At. Spectrom.* **2001**, *16*, 931-937.

50. Manard, B. T.; Gonzalez, J. J.; Sarkar, A.; Dong, M. R.; Chirinos, J.; Mao, X. L.; Russo, R. E.; Marcus, R. K. *Spectrochim. Acta B* **2014**, *94-95*, 39-47.

51. Marcus, R. K.; Quarles, C. D.; Barinaga, C. J.; Carado, A. J.; Koppenaal, D. W. *Anal Chem* **2011**, *83*, 2425-2429.

52. Quarles, C. D., Jr.; Carado, A. J.; Barinaga, C. J.; Koppenaal, D. W.; Marcus, R. K. *Anal Bioanal Chem* **2012**, *402*, 261-268.

CHAPTER TWO

EVALUATION OF THE OPERATING PARAMETERS OF THE LIQUID SAMPLING-ATMOSPHERIC PRESSURE GLOW DISCHARGE (LS-APGD) IONIZATION SOURCE FOR ELEMENTAL MASS SPECTROMETRY

2.1 Introduction

A worthy direction of mass spectrometry (MS) instrumentation development over the past two decades has been focused on various aspects of miniaturization [1-3]. Improvements are driven towards lower operating costs, implementation of versatile atmospheric pressure ionization (API) sources, ease of interfacing with diverse mass analyzers, and overall system portability. These advances have almost exclusively been in the realm of "organic" MS as little work has focused on analyzer or ion source miniaturization in regards to elemental MS. Historically, the inductively coupled plasma (ICP) and thermal ionization (TI) sources have not changed significantly in their commercial implementations over the past three decades [4-7]. Perhaps the greatest evolutionary efforts in atomic mass spectrometry systems have involved the introduction of dissociation/reaction cell technologies as applied to ICP-MS [8,9].

While not of the commercial scale of ICP-MS and TIMS, the developments in glow discharge mass spectrometry (GDMS) sources have seen increased activity since the 1980s. In the simplest terms, a GD plasma is formed by the passage of electric current (d.c.) between two electrodes (anode and cathode) in

a low pressure (1-10 Torr) inert gas environment [10,11]. In terms of elemental analysis, ion sputtering of the cathode surface is a versatile means of introducing sample material into the low temperature plasma, wherein atoms are excited and ionized by collisions with electrons and metastable discharge gas atoms (e.g. Penning ionization), providing for bulk and depth-resolved analysis of metals and electronic materials [12]. The scope of applicability was greatly expanded with the advent of radio frequency (rf) powering schemes, permitting direct analysis of non-conductive materials (i.e. glass, ceramic, and polymeric materials) [13,14]. At present, the majority of the activity in "solids" GD-MS is devoted to the combination of rf powering and time-of-flight (ToF) mass analyzers, providing a powerful combination for diverse materials analysis [15,16].

A more recent development in the use of GD devices in mass spectrometry has been their implementation as ambient desorption/ionization (ADI) sources for the direct analysis of solid samples. To be clear, in this application, the primary analytical classes are small organic molecules adsorbed to surfaces, existent in solution residues, or introduced as gases [17,18]. ADI-MS has a number of practical advantages including zero sample preparation/pretreatment, rapid analysis time, and 2-D imaging of sample surfaces. Direct analysis in real time (DART) is the most common GD-based ADI-MS technique and can be utilized for a variety of applications including explosives and chemical warfare agents [18]. Indeed, there are a plethora of ADI designs which employ GD sources of various geometries and powering modes (d.c., rf, capacitive coupling) [19-21]. The primary attribute being exploited in these efforts are low capital costs, low operational overhead in terms

of consumables, small footprint, and ease of implementation on diverse mass analyzer systems. In practice, any MS system designed for the sampling of atmospheric pressure ionization (API) sources used in organic analysis (e.g., electrospray) are all suitable.

Perhaps the most active area of GD source development has been sources designed for the direct sampling of flowing solutions at atmospheric pressure [22-24]. There have been two basic designs described for the generation of low power, continuous plasmas using direct liquid sampling and having the ability of performing elemental analysis using optical emission spectroscopy (OES) [22]. The electrolyte cathode discharge (ELCAD) was designed by Cserfalvi and co-workers [25,26], and then further characterized and improved by Hieftje and co-workers under the name of solution cathode discharge (SCD) [27-29]. The device utilizes a d.c. glow discharge formed between the grounded tungsten or titanium anode and the surface of the electrolyte solution that flows out from a u-shaped glass pipette placed <1 cm above the waste reservoir. The electrolyte solution acts as the cathode electrode in this case. Reported LODs for this OES device range from 0.06 ng mL^{-1} to 270 ng mL^{-1} for 25 µL injections [29]. Marcus and Davis [30-32] developed the liquid sampling-atmospheric pressure glow discharge (LS-APGD) as a low power (<50 W), low cost, and low sample flow rate (<100 µL min^{-1}) excitation source. In the LS-APGD, the microplasma is sustained between the surface of the electrolyte solution and a metallic counter electrode mounted collinearly and parallel with the lab bench, with a spacing of only 1-2 mm. A primary difference with the ELCAD-based designs is the fact that a very high power

density is realized in the LS-APGD microplasma (>10 W mm^{-3}) providing sufficient energy for operation in a total-consumption (i.e., no liquid waste) mode. The combination of high power density and the ever-presence of the electrolyte solution yields a high tolerance for matrix effects for salt-heavy samples [33].

Recently, the LS-APGD has been utilized as an ionization source for elemental mass spectrometry [34,35]. The device can be easily integrated onto the electrospray ionization (ESI)/atmospheric-pressure chemical ionization (APCI) interfaces common to organic/biological ambient mass spectrometers. The device was originally reported by Marcus and co-workers as an ionization source coupled with a high resolution Thermo Scientific LTQ Orbitrap mass spectrometer [34], in which the basic design aspects and spectral characteristics observed when sampling the LS-APGD were presented. A cursory parametric evaluation [35] revealed that the individual parameters effect the intensity, the level and distributions of spectral background, signal-to-background ratio (S/B), and the limits of detection (LODs) for target analytes. However, the initial parametric evaluation was performed where individual parameters were tested independent of each other, holding the other parameters constant at their assumed “best condition”. As such, there was not enough information to thoroughly determine an optimized set of operating conditions, especially including the inter-parameter effects. More recently, the use of the LS-APGD as a source for ADI-MS has been described [36].

Table 2-1 Operating parameters evaluated for LS-APGD-MS source.

Parameter	Test Range
Current	5-50 mA
Sample flow rate	5-40 μL min^{-1}
Gas Flow rate	0.1-0.9 L min^{-1}
Distance between the sampling cone and center of plasma	0.25-1.0 cm

Presented here is a more thorough parametric evaluation of the LS-APGD interfaced with a Thermo Scientific LCQ ion trap mass spectrometer. Parameters investigated for optimization include the discharge current, liquid (sample) flow rate, sheath/cooling gas flow rate, and the distance between the plasma and the sampling cone as seen in Table 1. Evaluation studies were initially conducted using 10^{-4} mol L^{-1} $CsNO_3$ in 1 mol L^{-1} HNO_3 as the test solution to map out the general parameter space. After the general behavior of the parameters was determined, a mixture of $AgNO_3$, $Pb(NO_3)_2$, $Ni(NO_3)_2$, and $La(NO_3)_3$ (10^{-4} mol L^{-1} in 1 mol L^{-1} HNO_3) was employed to determine whether the optimized operating conditions were analyte-specific. These elements were selected due to their range of first and second ionization potentials, propensity to form oxide ions, and their mass distribution as listed in Table 2. Lastly, consideration for element selection was focused on areas of current research emphasis in atomic MS [37-39]. The nitrate salts were used to alleviate potential differences that might be attributed to anion identity (the focus of future work). Parametric evaluation was performed by

observing the resulting ion intensities and signal-to-background (S/B) characteristics at each elements' major isotopic masses. Since the LS-APGD source also produces oxides, hydroxides or water clusters depending on the chemical properties of the elements, an intensity ratio of the atomic peak to the most intense cluster (oxides in most of cases) was also employed for the investigation. The results demonstrate that there are a series of interrelated plasma operation and ion sampling parameters that affect the intensity, S/B ratio, and the composition of the mass spectrum derived for the LS-APGD ion source. LODs were also established at the best operating conditions for the corresponding elements using the signal-to-background ratio/relative standard deviation of the background (SBR-RSDB) approach [40-42]. It is believed that the detailed parametric evaluation presented here provides better understanding of the operating principles of the LS-APGD source and points to future directions in its developments and more applications as a miniaturized, low cost alternative ionization source for elemental isotopic MS.

Table 2-2 Elements used for parametric studies and their properties: ionization potentials, major isotopes and their abundance

Element	**1st ionization potential (eV)**	**2nd ionization potential (eV)**	**Major isotopes and abundance**	**Metal oxide ion strength (kJ mol^{-1})** *
Nickel	7.64	18.17	^{58}Ni 68.1 %; ^{60}Ni 26.2 %	392
Silver	7.58	21.49	^{107}Ag 51.8 %; ^{109}Ag 48.2 %	213
Cesium	3.89	23.16	^{133}Cs 100 %	297
Lanthanum	5.58	11.08	^{139}La 99.9 %	799
Lead	7.42	15.03	^{206}Pb 24.1 %; ^{207}Pb 22.1 %; ^{208}Pb 52.4 %	378

* Dean JA (1999) Lange's Handbook of Chemistry, 15th Ed. McGRAW-HILL, INC., New York.

2.2 Materials and Methods

2.2.1 Sample preparation

Stock solutions (Cs, Ag, La, Ni, Pb) were prepared as $1x10^{-2}$ M in de-ionized H_2O from their nitrate salts; ($La(NO_3)_3$ (GFS Chemicals, Inc., Powell, OH, USA), and $AgNO_3$, $CsNO_3$, $Ni(NO_3)_2$, and $Pb(NO_3)_2$ (Sigma-Aldrich Co. LLC, St. Louis, MO, USA). These stock solutions were diluted to $1x10^{-4}$ M in deionized H_2O as the tuning solutions for the ion trap analyzer. To make the test solutions for the inter-parametric evaluation, the stock solutions ($1x10^{-2}$ M) were diluted using 1 M HNO_3 to their final concentrations as $1x10^{-4}$ M in 1 M HNO_3. The stock solutions were diluted to $1x10^{-5}$ M in 1 M HNO_3 as the test solution for the LODs determinations.

2.2.2 LS-APGD ionization source

As described in previous work [34,35], for safety considerations the glass capillary through which the electrolytic (sample) solution flows serves as the ground electrode. Power was provided to the counter electrode by a direct current (d.c.) Bertan Model 915 series power supply (Hickville, NY, USA); 0-100 mA, 0-1 kV (positive polarity), through a 10 kΩ, 225 W ballast resistor. Helium (99.99% purity) was introduced in between the surrounding stainless steel capillary and the glass capillary as sheath/cooling gas (0.1-1.2 L min^{-1}), while the electrolyte flow (5-50 µL min^{-1}) was pumped through the glass capillary using a syringe pump (NE-1000, New Era Pump Systems, Farmingdale NY, USA). As depicted in Fig. 2.1, the stainless steel counter electrode was placed perpendicular to the tip of the

capillary (~2 mm separation distance), with the discharge that is formed in between the electrodes being in-line with the MS sampling cone (0.1-1.0 cm in distance). The range of operation parameters studied is presented in Table 1. The testing order of each set of parameters was randomly generated, by sorting the number assigned by the formula =RAND() which generates a random number between 0 and 1 in Microsoft® Excel software. Sample and gas flow were continuously delivered into the plasma, and integrated signals from a 1 min data acquisition period were obtained. Such acquisitions were run in triplicate, with the reported values being the average of the three. The repeatability of such measurements generally displayed precision of better than 10 %RSD. After completion of a given parametric evaluation, the initial set of parameters was re-set and that acquisition repeated to ensure reproducibility.

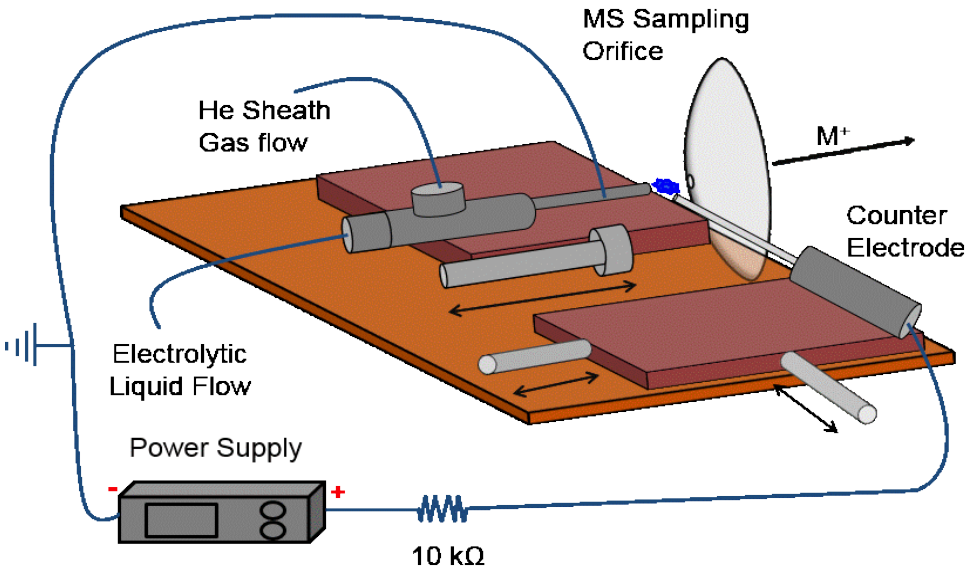

Figure 2.1 Diagrammatic representation of the components of the LS-APGD device as an ionization source for mass spectrometry

2.2.3 Mass analyzer system

A Thermo Scientific (Waltham, MA, USA) LCQ Advantage Max^{TM} ion trap mass analyzer (operating in the positive ion mode) and the accompanying Xcalibur^{TM} data acquisition software were used as the MS system. This system contains five major components: atmospheric pressure ionization (API) source housing, ion sampling interface and optics, ion trap, continuous dynode detector, and electronics for system control and data collection. The system was originally outfit with an ESI and an APCI source. Other than the API housing which is mounted on the main frame, the rest of the system is held under a vacuum of ~10^{-5} Torr. Ions are sampled through an ion transfer tube having an inner diameter of 0.45 mm, generating a suctional force to deliver the ions into the ion transfer tube of the mass analyzer. The mass analyzer system includes two octapoles, which are connected by an interoctapole lens, with the second octapole fitting in to the end cap of the ion trap. The mass range of the collected ions can be set through the system, as can the ion accumulation time, mass range, and scan-out rate. Mass spectra are acquired using mass-selective instability, where ions are sequentially ejected and detected. It is important to note that the lower mass limit for the octapole system is factory-set at 50 Da, and so the information space is limited in the lower mass region. Ultimately, lack of access to low masses and poor sensitivity below ~100 Da are analytical limitations of this system. On the other hand, while not exercised here, the octapoles could be employed in the same manner as the collision/reaction cells utilized in the first stage of modern ICP-quadrupole-MS systems [8,9]. This operational space will be investigated in detail in

future works. It is important to note that collision induced dissociation (CID) was not employed here as in the case of the previous Orbitrap work [35], and so the oxide levels are far higher in this study. The applied voltages on the ion optics, octapoles, ion trap, and the detection system have minor effects on the signal of selected ions, i.e. there is some bias. Therefore, the ion optics parameters need to be tuned based on the specific analyte. The system *auto-tune* function was employed based on the major atomic ion for each element as the parametric dependences for that element were being evaluated.

2.2.4 Assessment of Limits of Detection

The determination of LODs using ion trap mass spectrometers is complicated by the limited storage capacity of the devices. Thus, calibration functions covering dynamic ranges typical of atomic MS are not a viable approach, as the possibility of overloading the trap causes uncertainty in the response linearity [43]. Therefore, determinations of LODs were made based on the signal transients of 10 µL discrete sample injections introduced into the 1 mol L^{-1} HNO_3 electrolyte flow at a rate of 10 µL min^{-1}. LODs were generated using the relative standard deviation of the background (RSBD) method of calculation proposed by Boumans and Vrakking [40-42]; the so called "SBR-RSDB" approach. This approach is useful for assessing a single-point detection limit for a given element in a particular matrix; perhaps more correctly setting the *limit of detectability*. The SBR-RSDB approach allows the detection limit to be calculated from relative quantities that can be easily and accurately quantified without making comprehensive calibration functions. The LODs based on the SBR-RSDB approach is given by

$$LOD = \frac{(0.01)\ k\ (RSDB)m}{(S/B)} \quad (2.1)$$

Where RSDB is the relative standard deviation for the background (no sample introduction), m is the concentration of the test element in the specimen, S/B is the signal-to-background ratio, and the k is a statistical factor equal to 2, 3, $2\sqrt{2}$, or $3\sqrt{2}$, depending on the measuring procedure and the convention used. In this case, the multiplier is 3, which gives a 99% confidence interval.

2.3 Results and Discussion

2.3.1 General Parametric Evaluation

Previous studies involving the use of the LS-APGD reflect a series of physical processes that are much like those of combustion flames and ICP sources as depicted below (Eq. 2.2). Different from what has been proposed for ELCAD [44] and SCD devices [22,45], in the LS-APGD the passage of electric current (either ions or electrons) across the gas/liquid interphase provides thermal energy to convert the bulk liquid flow into an aerosol of analyte-containing droplets. It remains to be determined whether or not the coaxial He sheath/cooling gas provides a pneumatic nebulization component. Droplets are subjected to the modest gas temperature environment (~1000 K) [46], such that they are desolvated and the latent analyte salts are dissociated to produce free atoms. The rate and extent of decomposition to free atoms is a function of the chemical properties of the particular analyte, the plasma kinetic environment, and the residence time. These atoms are subjected to collisions with energetic species (i.e. electrons and perhaps He metastable

atoms) and can therefore be excited/ionized. Likewise, molecular species (e.g., oxides) could be ionized as well (Eq. 2.3), though perhaps to subsequently

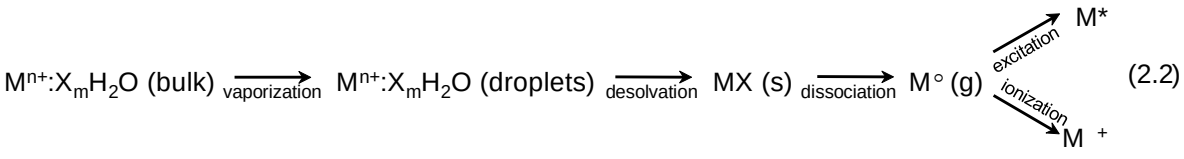

(2.2)

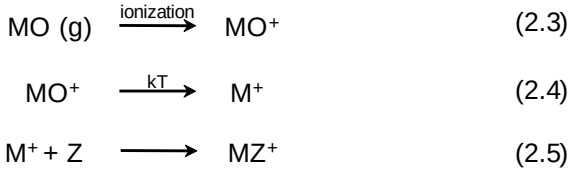

dissociate to the desired free metal ions when subjected to collisions in the plasma (Eq. 2.4). While the production of atomic ions is the primary goal in elemental MS, these ions may suffer the fate of collisions with ambient species (e.g., atmospheric gases and water (designated as Z) that will form molecular ions before reaching the MS entrance aperture (Eq. 2.5) and thus be a net loss from the desired atomic ion products. Thus, as with the case in combustion atomizers, and ICP-OES/MS sources, there can be expected to be different atom/ion populations as a function of microplasma operating conditions and sampling position.

Previous LS-APGD-MS studies demonstrated that changes in the individual parameters directly affect the observed metal ion intensities and signal-to-background (S/B) ratios [35]. The present, more comprehensive, parametric study shows that the parameters interact with each other to affect the intensity of atomic ions and the resultant S/B ratios. As an example, Fig. 2.2 illustrates the effect of changing both the liquid flow rate and cooling/sheath gas flow on the intensity of $^{133}Cs^+$ as a function of discharge current at two plasma sampling distances. Cesium was chosen in this demonstration due to its monoisotopic nature and

spectral simplicity (i.e., low abundance of doubly-charged ions, oxide, and hydroxide species). Figures 2.2 a-c represents the relative $^{133}Cs^{+}$ intensities at a 1.0 cm distance from the sampling cone for the discharge currents of 10 mA, 20 mA, and 30 mA, respectively. (As listed in Table 2.1, currents of 5 – 50 mA were investigated, but the currents presented were by far more analytically useful.) In increasing the current, the optimal liquid flow rate (~15 μL min^{-1}) does not change; however, the gas flow rate follows a slight negative correlation, as increasing the applied current, lower gas flow rates are preferred in order to obtain greater $^{133}Cs^{+}$ response. Higher current leads to faster vaporization of the liquid flow into gas phase (increasing the solvent loading [35]), and also an increase of the power density [46]. With regards to the differences in optimum gas flow rates, two processes are likely relevant. First, there may be some aspect (which will be the subject of future studies) of pneumatic nebulization, which would assist low-current conditions. Likewise, high gas flow rates would be expected to help confine and direct the plasma species toward the ion sampling orifice. At the higher currents, both of these aspects seem to be lost. Ultimately, and perhaps counter intuitively, the low current situation, with high gas flow rates, yields substantially higher $^{133}Cs^{+}$ signal response.

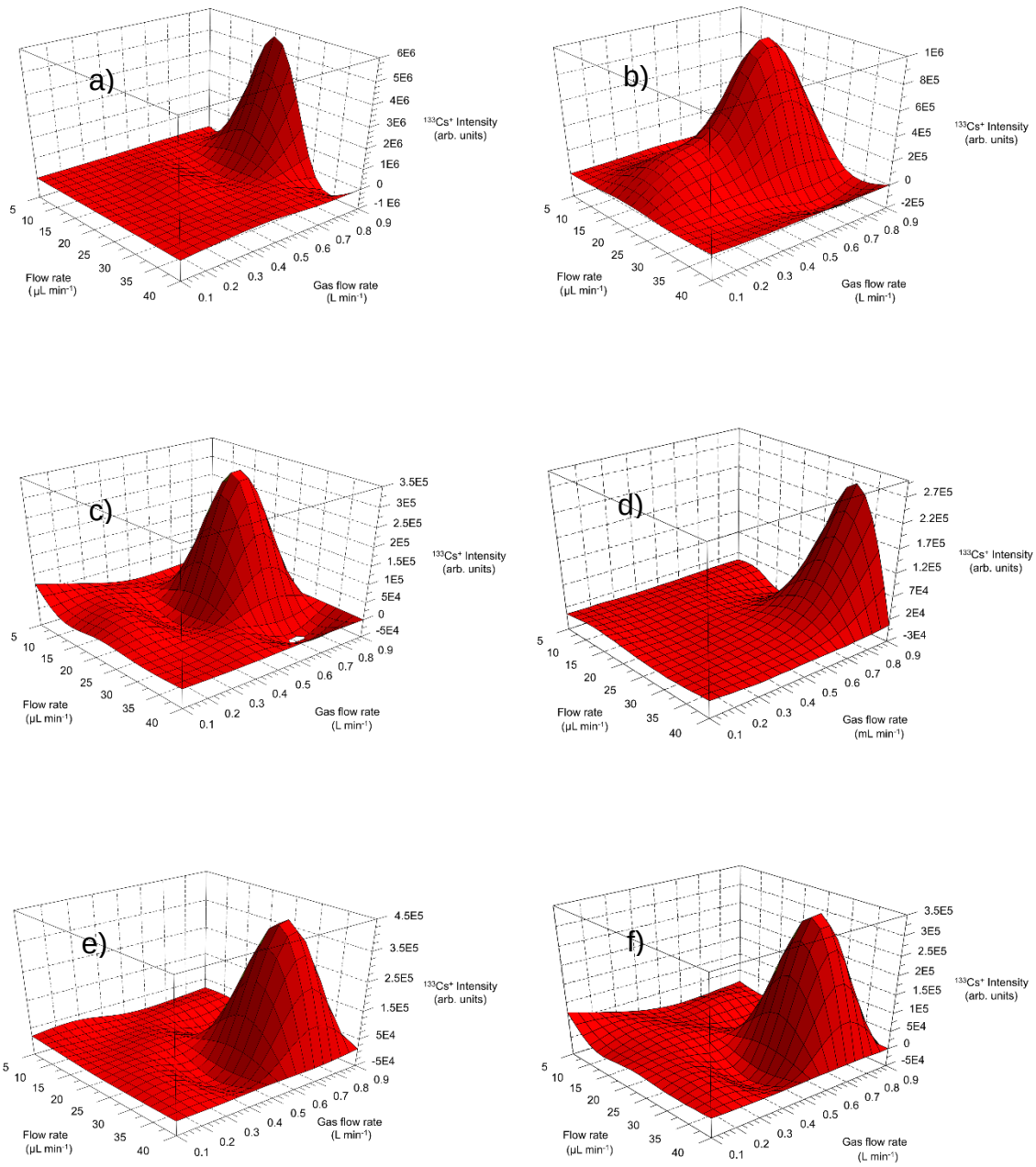

Figure 2.2 Inter-parametric evaluation of $^{133}Cs^+$ responses ([Cs] = 10^{-4} M in 1M HNO_3) as a function of liquid flow rate and sheath gas flow rate at a sampling distance of 1.0 cm from MS sampling cone at currents of a) 10 mA, b) 20 mA and c) 30 mA, and at a sampling distance of 0.75 cm from MS sampling cone at currents of e) 10 mA, e) 20 mA and f) 30 mA.

Figures 2.2 d-f depict the same parameters (changes in liquid and sheath gas flow rates) with the plasma is located closer to the sampling cone, at 0.75 cm. Similar to the first three plots (Figs. 2.2 a-c), the gas flow rate is negatively correlated to the applied current, with the optimum liquid flow rate unaffected to the change in current. The one difference between the two distances is that when the plasma is sustained closer to the sampling cone, a higher liquid flow rate is preferred, 27 μL min^{-1}, in comparison to 15 μL min^{-1}, respectively. Here, it appears that the kinetics of the processes that must take place (Eq. 2.2) require greater solution/analyte feed rates to see a maximum atomic ion responses. From a different point of view, the plasma placed further away will allow for longer residence times for the particles to stay in the plasma which then leads to a higher probability of forming M^+, with lower solvent loading being a result. Indeed, it is important to note that the maximum $^{133}Cs^+$ signal for the 1.0 cm sampling distance, occurs at a much lower liquid flow rate of ~15 μL min^{-1}, and the lowest discharge current, yet is a factor of 10 greater than any of the discharge currents at the shorter sampling distance. Thus, optimum metal ion signals are seen at conditions where there is overall low analyte feed rates, and thus lower solvent loading. As seen in the previous studies, conditions of high current and high liquid flow rates indeed generate spectra that become increasingly dominated by water-related clusters in lieu of atomic analyte ions [34].

As the lower solution delivery rates yielded the highest analytical responses in general, an evaluation of the role of the gas flow rates at that single current, while varying the liquid flow and ion sampling distance parameters is reasonable.

Figures 2.3 a-d illustrate the relationship between liquid flow rate and distance from sampling cone at an applied current of 10 mA and different gas flow rates (0.3, 0.5, 0.7, and 0.9 L min^{-1}), respectively, based on the intensity of $^{133}Cs^{+}$. In general, higher gas flow rates tend to favor greater ion sampling distances to yield the best atomic ion responses. This more clearly defines what was projected from the responses in Fig. 2.2. Here now, a residence time argument is reasonable. Specifically, at low gas flow rates, there is sufficient exposure to the plasma to affect the vaporization/dissociation/ionization processes at the shorter distances. As the gas flow rate increases, greater distance is required to spend the same period of time within the plasma environment to affect the same amount of "work". To be clear, a separation distance of 1 cm means that the sampling cone is more than 7 mm from the actual tip of the plasma, and so one must think that only thermal process are occurring over this space; i.e., loss of neutral species from analyte-containing molecular ions. Furthermore, one might expect an added contribution of a sheathing effect at the higher flow rates, which may tend to exclude ambient species and their reaction with the desired metal ions prior to entry in the MS interface. These results point clearly to an interplay amount the processes depicted in Eqs. 3 - 5 to affect the greatest metal ion response.

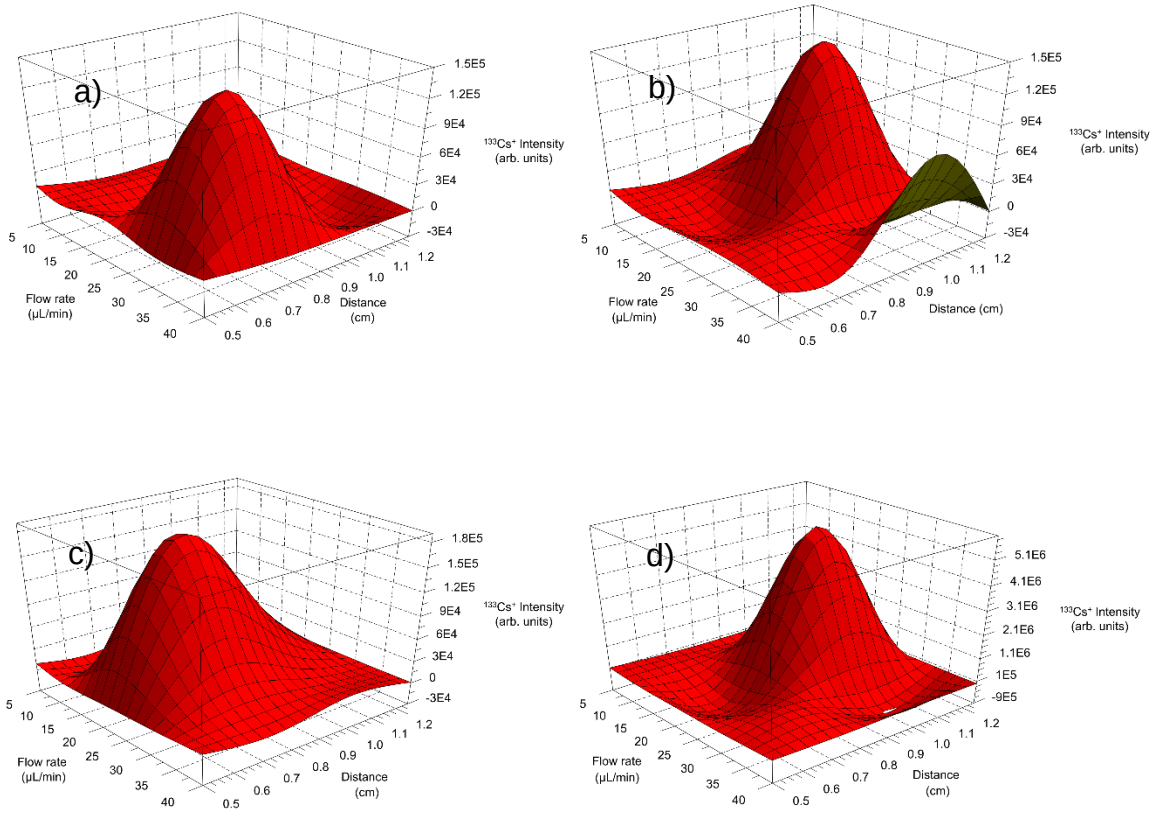

Figure 2.3 Inter-parametric evaluation of $^{133}Cs^{+}$ responses ([Cs] = 10^{-4} M in 1M HNO_3) as a function of liquid flow rate and ion sampling distance at a constant discharge current of 10 mA at sheath gas flow rates of a) 0.3 L min^{-1}, b) 0.5 L min^{-1}, c) 0.7 L min^{-1}, and d) 0.9 L min^{-1}.

As the present studies do not employ any sort of reaction/dissociation strategies to alleviate background molecular species, it is informative to understand the response of spectral background as a function of the discharge parameter as a means of discerning the origins of the spectral background. In the case of the LS-APGD, wherein the bulk of the plasma is composed of water vapor, there is any number of potential water-related cationic species that can be produced (anionic species exist as well, but are of no relevance here). Add to this, the fact that the electrolyte nitric acid will decompose to yield a range of

radicals/ions. The creation of background ions will likely be the result of diverse sequences of reactions that are initiated by plasma electrons or Penning-type collisions, with a multitude of subsequent chemical ionization events taking place. For example, these primary collisions will generate free protons, which in turn react with molecular water (which is in great excess) to form hydronium ions (H_3O^+), which are very strong BrØnsted acids. As with other ambient (atmospheric pressure) ionization sources, background species will emanate not only from the basic sample components (including solvent) but also atmospheric gases such as N_2, O_2, etc. which interact with the electrons, metastables, and reactive species emanating from the plasma. The various reviews of ambient ionization sources present the reactions that are likely producing background ions prominent in the LS-APGD [17,47,48]. The plasma operation conditions and ion sampling position will dictate the identity and magnitude of background species.

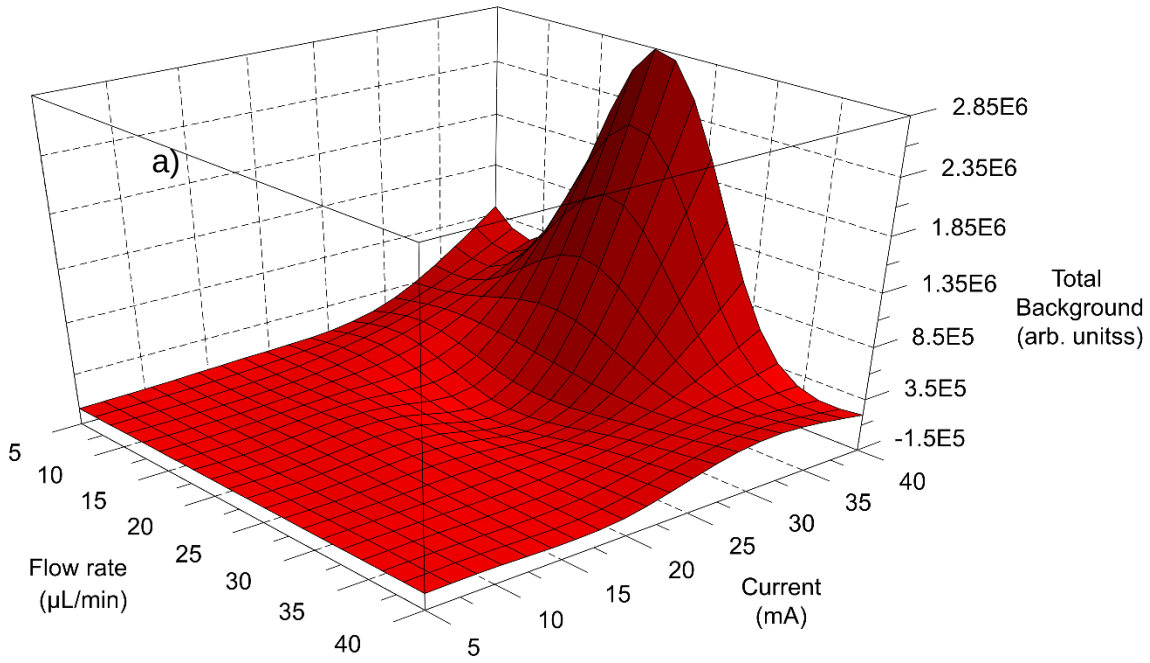

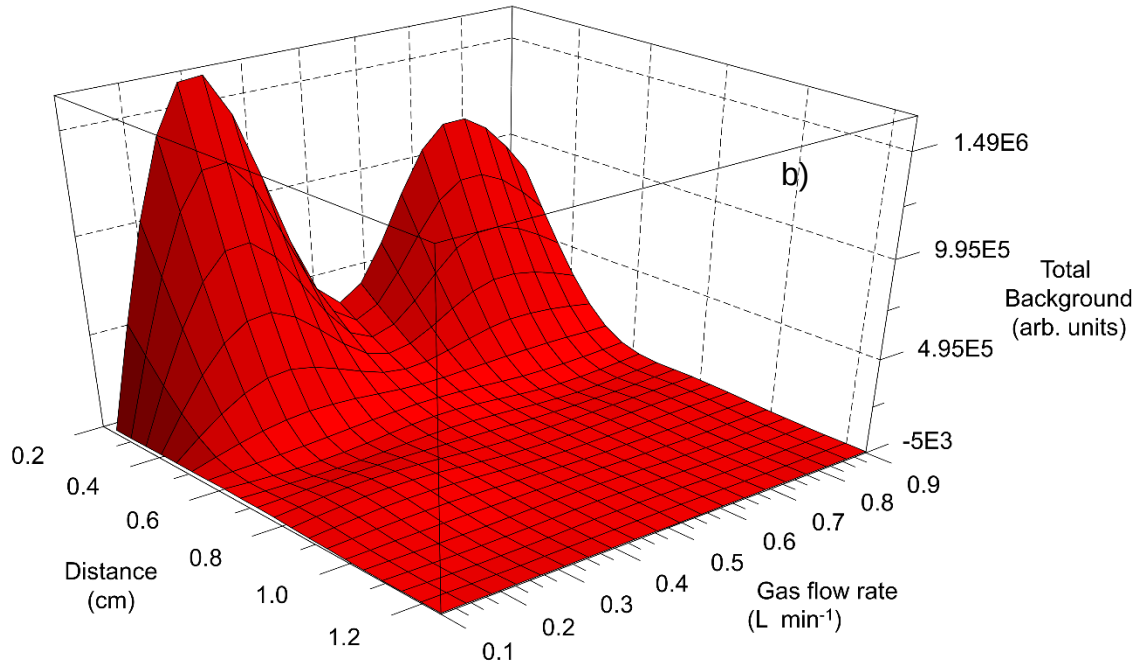

Figure 2.4 Inter-parametric evaluation of the total spectral background responses over m/z = 50 – 500 Da with the introduction of 1 M HNO_3 as the electrolytic solution. a) Roles of liquid delivery rate and discharge current (sampling distance = 1 cm, sheath gas flow = 0.9 L min^{-1}), and b) roles of sampling distance and sheath gas flow rate (discharge current = 10 mA, liquid flow rate = 10 µL min^{-1}).

As presented in the original manuscript describing the LS-APGD microplasma ion source [34], increases in discharge current have the unique effect in not increasing the intensities of representative background ions as much as creating new species, wherein the total background signal across all species increases. For example, at 5 mA the most prominent background ion is $(H_2O)_9H^+$, while at 50 mA the $(H_2O)_{12}H^+$ species is the spectral base peak. A more detailed parametric evaluation of the contributions of these species (in general) allows for a deeper level of understanding about how these ions are formed/decomposed in a way that reflects the processes depicted in Eqs. 2.2 - 2.4. Figures 2.4a and b present the total (integrated) ion signals derived for the mass range of 50 – 500

Da, using the basic electrolyte (1 M HNO_3) as the test solution, across the microplasma operational space. As might be expected, Fig. 2.4a (sampling distance = 1 cm, sheath gas flow rate = 0.9 L min^{-1}) reflects the case where increasing current is met with an increase in the total background signals for each of the solution flow rates. The most pronounced effect is the role of the solution flow rate. Here, increases in liquid flow have no real effect at the lower currents, but at the higher currents, there is a large increase in the background. At the higher currents (>25 mA), increases in flow rate yield pronounced increases in background. The maxima in the responses in terms of liquid flow and current reflect the situations where increases in liquid flow at each current provide more liquid than can be effectively turned into ions. The solvent vaporization is still complete, but there is not sufficient energy in the plasma to affect greater ionization. The roles of sampling distance and sheath gas flow rate (solution flow = 10 µL min^{-1} and discharge current = 10 mA) paint a fairly straightforward set of relationships. Clearly, longer sampling distances greatly suppress background ion contributions. The effects of increasing gas flow rate show two pronounced maxima at the shorter sampling distances. Close inspection of the mass spectral features shows that low flow rates (longer residence times) yield higher populations of lower-mass ions, while the higher flow rates yield higher-mass clusters. Thus, the overall picture for the production of background ions (in general) is that high currents, high solution flow rates, short residence times lead to increased background. As a final point, the quantitative aspects between Figs. 2.2, 2.3, and 2.4 can be compared, such that under the worst conditions, the total (integrated) signals for the background

species are approximately of the same order of magnitude as the 10^{-5} M $^{133}Cs^{+}$ signals.

In the present studies, which are more about fundamental characterization than ultimate analytical performance, dissociation/reaction processes are not employed. As described above, discharge conditions affect not only the intensities of background ions, but more clearly the spectral composition. In the case of the targeted ^{133}Cs species, there is in fact a background contribution that can be attributed to a water-related cluster, possibly of the form $(H_2O)_5CNOH^{+}$. Unfortunately, MS/MS of this species was unsuccessful as the products were of m/z < 50 Da. The signal-to-background ratio for 10 µL injection of 10^{-4} M CsNO3 were determined using the average background intensity (1 M HNO_3 mobile phase) over a 1 minute period before and after the injections and the average intensity during the injection transient, both at a mass of 133 Da. The relationship of ^{133}Cs S/B ratios were evaluated across the same set of parameters as described in the previous paragraphs and depicted in Fig. 2.2. As presented above, discharge currents above 30 mA produce an overwhelming amount of water clusters that could overwhelm the analyte species. The lowest current tested, 5 mA, provided large S/B ratios, but the $^{133}Cs^{+}$ intensity is significantly lower than is analytically practical.

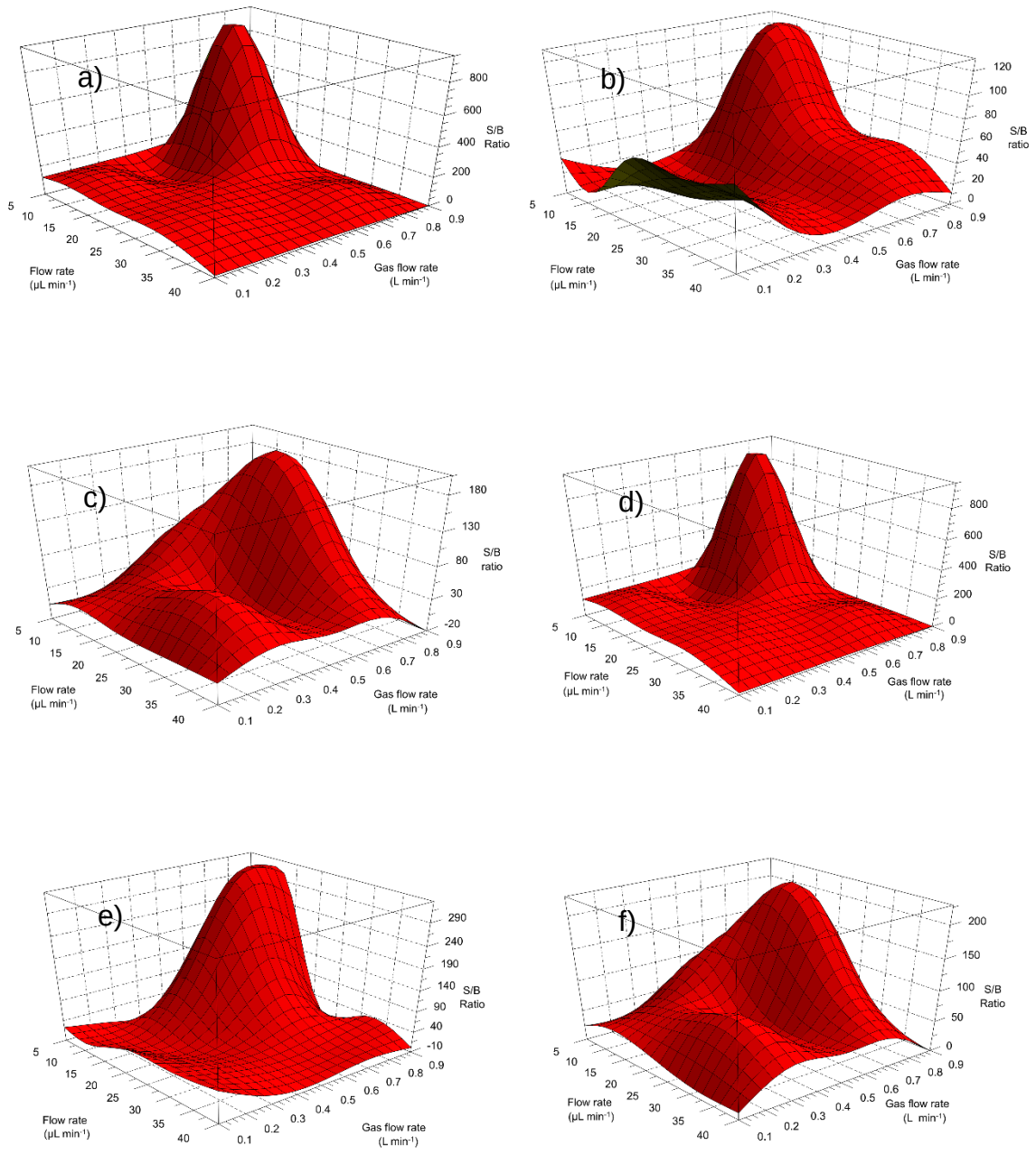

Figure 2.5 Inter-parametric evaluation of $^{133}Cs^{+}$ signal-to background ratio responses ([Cs] = 10^{-4} M in 1M HNO_3) as a function of liquid flow rate and sheath gas flow rate at a sampling distance of 1.0 cm from MS sampling cone at currents of a) 10 mA, b) 20 mA and c) 30 mA, and at a sampling distance of 0.75 cm from MS sampling cone at currents of e) 10 mA, e) 20 mA and f) 30 mA.

Figures 2.5a - c and Figs. 2.5d - f represent the relationship of ^{133}Cs S/B ratios with different liquid and gas flow rates at distances of 1.0 cm and 0.75 cm (respectively) from the sampling cone and currents ranging from 10-30 mA. (As would be expected based on the responses plotted in Fig. 2.4b, shorter sampling distances resulted in much-degraded S/B values.) In all cases the greatest S/B values were derived at a liquid flow rate of 15 µL min^{-1}. As with the atomic and background signal responses of Figs. 2.2 and 2.4, optimum responses were found at slightly higher gas flow rates for the longer sampling distance (1 cm) and at the lowest discharge current, 10 mA. Thus, the S/B characteristics consistently reflect conditions wherein low solvent loading and low levels of background species ionization are realized; low discharge current, low solution feed and high gas flow rates, and longer sampling distances.

2.3.2 Multi-element Parametric Dependencies

In the ideal case, the amount of energy provided by the plasma and the ionization potential of the analyte should be the only factors affecting the generation of singly charged atomic ions. As depicted in Eqs. 2.2 – 2.5, though, there is a large number of potential differences in analyte chemistry that will affect the ultimate observation of the desired atomic ions in the recorded mass spectra. The most relevant of these thermodynamic characteristics are presented in Table 2.2. In the context of the LS-APGD-MS sampling, the relationship between an element's 1^{st} and 2^{nd} ionization potential would represent the ease of making the primary ion, and then the potential "loss" of that species in lieu of forming the di-cation. Beyond this, the respective metal-oxide bond strengths will play a role in

two ways. In the first case, metal-oxides existing early in path through the plasma would need to be dissociated to yield free atomic ion. In the second case, it is ultimately true that metal ions present in ambient atmosphere will be oxidized if given the opportunity. Thus, the desired metal ions are lost if not sampled into the MS prior to such reactions. Therefore it would not be unexpected that there may be differences in the parametric responses for the sampling of free atomic ions between elements; though certainly such differences introduce the potential for operation under compromise analysis conditions, which might be problematic.

Inter-parametric relationships were determined for the remainder of the suite of test elements (Ni, Ag, La, and Pb) across the parameter space depicted for Cs in Figs. 2.2 and 2.3. Consistently, the highest atomic ion signals *for all elements studied* were observed at sampling distances of 0.75 - 1 cm and sheath gas flow rates of 0.7-1.0 L min^{-1}, but changes in current and sample flow rate resulted in significant differences among the elements. Not surprisingly, these are the two parameters that affect the solvent loading on the plasma and the subsequent reactions that might occur. The most straightforward example of interelement differences is Ag, which is relatively unreactive as reflected in its low metal-oxide bond energy. The maximum Ag^+ responses (both isotopes responding the same way) were obtained at a relatively high liquid delivery rate and discharge current; 25 µL min^{-1} and 30 mA, respectively. Both Ni and Pb produced their highest atomic ion signals at a relatively low current (~20 mA), dropping rapidly with increasing currents. However, the difference between these two elements are the liquid flow rate as Ni benefits from a lower solution flow rate

(17 µL min^{-1}), while Pb prefers a higher flow rate (30 µL min^{-1}). Finally, La provided the best atomic ion signals under two different sets of conditions: liquid flow rate of 10 µL min^{-1} and current of 10 mA; liquid flow rate of 50 µL min^{-1} and current of 40 mA. These are the two extreme sets of conditions, lowest flow rate coupled to the lowest current possible, highest flow rate works best with highest current employed in this study. As will be seen in subsequent discussions, La has a very high propensity to yield metal-oxide ions in the mass spectrum, and so these two conditions seem to reflect the conditions where LaO^+ is formed the least efficiently and when it is dissociated most efficiently in the plasma, respectively.

The individual atomic ion responses tend to reflect conditions that would be unfavorable for metal oxide/hydroxide/etc. formation through gas phase collisions with solvent vapors or ambient atmospheric gases. By the same token, for those elements that form molecular ions through the initial ionization events, gas phase collisions could also serve as a means of dissociating the primary ions down to the desired free metal ions. In essence, we are concerned with the following dynamic equilibrium situation, which would be a function of the plasma residence time (a function of sheath gas flow rate and ion sampling distance), the gas phase composition, and the thermal conditions. Equation 2.6 basically represents a composite of Eqs. 3 – 5, using the metal oxide as just one example.

$$MO^+ \rightleftharpoons M^+ + O \qquad (2.6)$$

As is common with other atomic spectrometry sources, dynamics such as depicted in Eq. 2.6 are readily revealed in spatial profiles of the various reactant/product species [49-53]. The atomic-to-oxide ratios (M^+/MO^+) for Ni, Cs, La,

and Pb, and the atomic to hydroxide (M^+/MOH^+) ratios for Ag, were determined as a function of ion sampling distances (from 0.25 cm to 1.25 cm), at a fixed discharge current of 10 mA, a liquid flow rate of 10 µL min^{-1}, and a sheath gas flow rate of 0.9 L min^{-1}, conditions that generally yield mass spectra more favorable to observe metal ions. Figure 2.6 illustrates the relationship of each element's metal ion-to-metal oxide/hydroxide ratio to the ion sampling distance for analyte concentrations of 10^{-5} M in 1 M HNO_3. Both the trends and the magnitudes point to differences in chemistry that are readily explained in light of expected plasma and sampling processes. First, and most distinct, is the very low M^+/MO^+ ratios seen for La, which is practically invariant with the sampling position, but having a slight upward trend. This behavior reflects clearly the very strong metal-oxide bond strength for LaO, which is a factor of two greater than any of the other metals, and suggests that the oxide is the primary ion formed in the plasma. Nickel shows a nearly exponential decrease from the shortest sampling distance, which suggests that NiO^+ is formed as the free metal ion traverses greater distances to the sampling cone. The last three metals, Ag, Pb, and Cs effectively show spatial profiles that suggest that the primary species formed are molecular in nature, which dissociate as more time is spent in the microplasma environment, with the free metal ions associating with background species at extended sampling distances. Notably, these three metals have the lowest M-O bond energies. That said, there are also kinetic aspects to the association/dissociation reactions occurring in the plasma, which contribute to the observed levels of oxides/hydroxides.

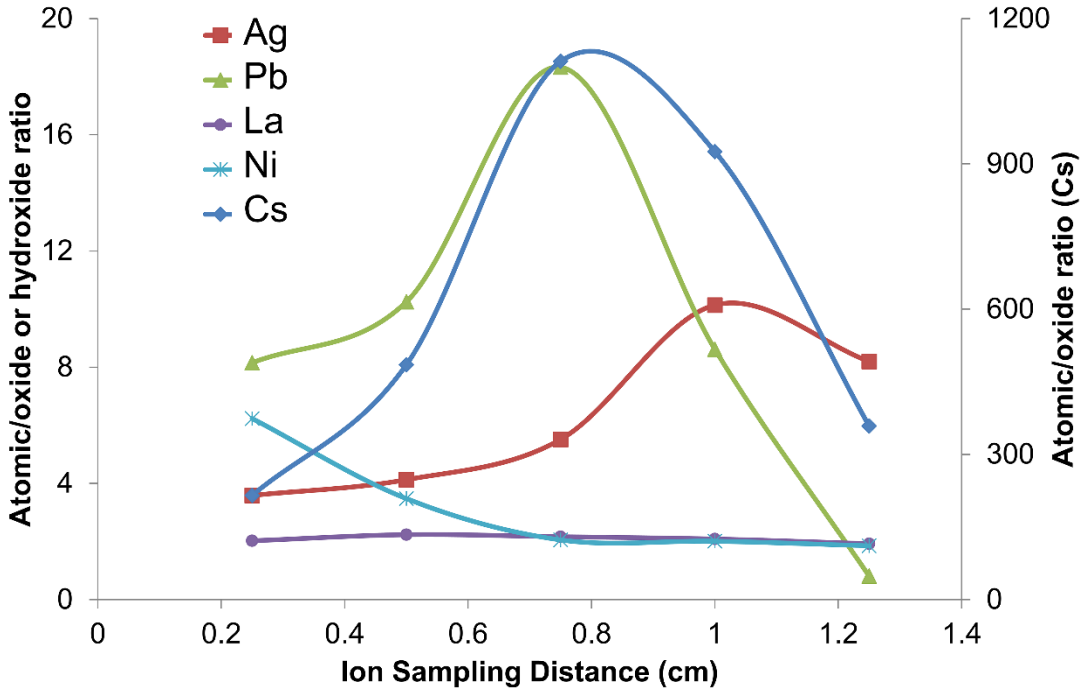

Figure 2.6 Atomic to oxide/hydroxide ratios (M^+/MO^+ and M^+/MOH^+) as a function of ion sampling distance for Ni, Ag, Cs, La, and Pb, at liquid flow rate of 10 µL min^{-1}, discharge current of 10 mA, and sheath gas flow rate of 0.9 L min^{-1}.

Ultimately, it must be recognized that element-specific plasma operation and ion sampling parameters are not a viable approach towards comprehensive, multielement analysis. Based on the parametric aspects that generally provide high analyte ion responses, low spectral backgrounds, and lower amounts of metal-oxide/hydroxide levels, a compromise set of conditions of a discharge current of 10 mA, a solution feed rate of 10 µL min^{-1}, a sheath gas flow rate of 1.0 L min^{-1}, and a 1.0 cm sampling position has been chosen. Figure 2.7 displays a typical mass spectrum obtained for a mixture containing 10^{-4} M of Ag, Cs, La, Ni, and Pb in 1 M HNO_3 under the compromise conditions. It is clear that the spectral composition is cluttered by the presence of oxide species far above what is likely tolerable for many applications. Indeed, comparison of this spectrum to that of the

initial LS-APGD-MS report [34] shows far worse performance in this case. In that work, in-source collision induced dissociation (CID = 63 eV) and/or high-energy collisional dissociation in the integrated HCD dissociation cell/trap (HCD voltage = 77 eV) were employed exactly as in the use of that instrument in ESI-MS. Cesium (10 µg mL^{-1}) and Pb (100 µg mL^{-1}) analytes in that work both showed oxide levels of <0.1 % of those metals. Thus, while the intent of the present work was a detailed study of the cumulative plasma processes, implementation of common collision/reaction strategies as applied in both organic and elemental (ICP) MS yield mass spectra that are indeed of high quality.

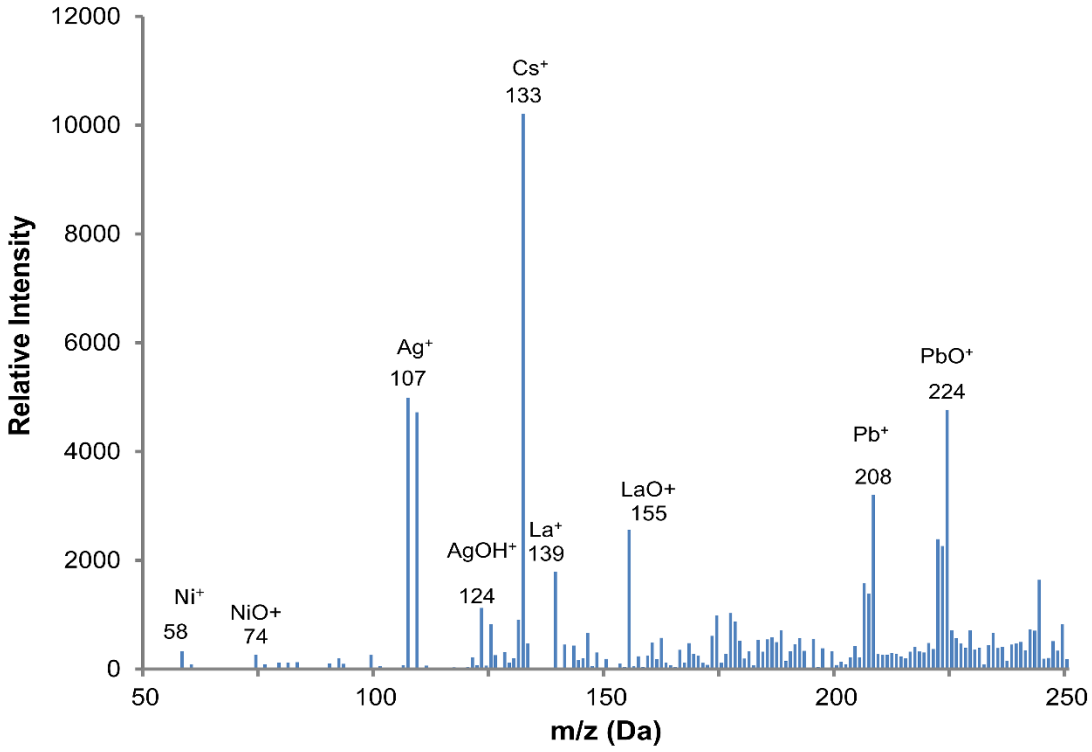

Figure 2.7 LS-APGD mass spectrum for a 10 µL injection of 10^{-4} M $CsNO_3$, $Pb(NO_3)_2$, $La(NO_3)_3$, $Ni(NO_3)_2$, and $AgNO_3$ in 1M HNO_3. Discharge current = 10mA, liquid flow rate = 10 µL min^{-1}, sheath gas flow = 1.0 L min^{-1}, and sampling distance = 1.0 cm

2.4 Limits of Detection

While the "raw" spectra extracted from the LS-APGD microplasma source are complicated by broadly dispersed background spectral contributions and target ion loss in the form of molecular ions, it is instructive to evaluate the sensitivity of the device without the use of collision/reaction strategies. To test the concentration-based LODs, 10 µL of 10^{-5} M in 1 M HNO_3 of $AgNO_3$, $CsNO_3$, $La(NO_3)_3$, $Ni(NO_3)_2$, and $Pb(NO_3)_2$ were injected into the LS-APGD source separately under their individual optimized operating conditions. The LODs were calculated using the SBR-RSDB approach, based on five repeating injections. As in the case of the S/B determinations, average background intensities and their standard deviations were assessed prior to the appearance of the injection transients, from which the average intensity of the plateau was used as the analytical signal. The calculated LODs for the test elements are presented in Table 3. The LODs range from 15-to-450 ng mL^{-1} for 10 µL injections, values which are on par with those obtained on the Exactive orbitrap where collisional dissociation was employed and lower electronic noise would be expected [35]. While not a practical goal in developing the LS-APGD, it is noteworthy that these values are quite competitive with first-generation ICP-MS devices [54]. The relative differences observed in the elemental LODs here are explained by the relative extents of metal oxides for La and Pb, and the poor MS performance for Ni at the very low end of the mass range. As one of the anticipated advantages of using a microplasma device is utilization of volume-limited samples, the mass-based LODs, ranging from ~0.2 – 4 ng in the 10 µL injection loops is indeed encouraging at this stage.

As a final note, based on ion physics, the absolute sensitivity of the octapole-ion trap analyzer system is not expected to be as good as quadrupole systems typical of ICP-MS. Therefore, the LS-APGD shows promising results for its applicability as elemental ionization source in converting an instrument designed for organic mass spectrometry to one employed for elemental analysis.

Element	LOD ($ng\ mL^{-1}$)	Absolute Mass (ng)
Nickel	310 ± 64	3.1 ± 0.64
Silver	27 ± 6	0.27 ± 0.06
Cesium	16 ± 2	0.16 ± 0.02
Lanthanum	56 ± 11	0.56 ± 0.11
Lead	415 ± 20	4.2 ± 0.2

Table 2-3 Determined limits of detection LODs of Ni, Ag, Cs, Pb and La via SBR-RSDB approach. 10 µL sample injections; average of 5 replicates

2.5 Conclusions

An inter-parametric evaluation of the operating space (i.e., solution flow rate, sheath/cooling gas flow rate, discharge current, and ion sampling distance) of the LS-APGD ionization source has been performed. Basic metrics of metal ion signal intensity, spectral background, S/B ratios, and metal-to-oxide/hydroxide ratios were evaluated using a suite of test elements including Ni, Ag, Cs, La, and Pb. As expected, there are interrelated effects among the parameters, with differences in optimum operation parameters based primarily on the occurrence of spectral background at the target masses and the propensity for metal-oxide/hydroxide formation. As a general rule, conditions that lead to lower amounts of solvent

loading (i.e., low discharge currents and solution flow rates) provide higher S/B ratios. In addition, trade-offs are seen with regards to the transit time between primary ion formation and the sampling orifice in terms of the formation/dissociation of oxide/hydroxide species.

In this study, collision/reaction protocols common to organic and ICP MS were not employed as it was desired to get a global picture of the plasma processes, as such the “raw” spectra show much higher levels of spectral background and analyte-containing molecular ions. The analytical utility is also limited in this system because of the low-mass cut-off at 50 Da, and overall low sensitivity below 100 Da. Even with these limitations, LODs on the levels of 20 – 400 ng mL^{-1} (0.2 – 4 ng absolute mass) were obtained; levels equivalent to previous works on higher performance analyzer systems. The lack of sacrifice in detectability is attributed in part to higher levels of ion source robustness and reproducibility as the ion source platform has evolved.

Future work will concentrate on the more practical aspects of developing the LS-APGD microplasma as a low cost, low power source for elemental/isotopic MS, and having a small footprint. The devices should be particularly attractive to laboratories already equipped with ambient sampling mass spectrometers (such as ESI or APCI) as the LS-APGD source can be easily mounted to those interfaces; converting an organic MS to an elemental MS system. Other efforts will continue the development in the analysis of aerosols generated by LA sampling and the development of field deployable OES and MS systems. Finally, the performance of the device will be assessed towards its ultimate analytical utility on highly-

evolved ICP-MS platforms. As stated previously, it is not envisioned that the microplasma would compete with the ICP, but may present a viable alternative in terms of cost and complexity for certain applications.

2.6 Acknowledgements

This work was supported in part by the Defense Threat Reduction Agency, Basic Research Award # HDTRA1-14-1-0010, to Clemson University.

2.7 References

1. LeGac, S.; VandenBerg, A. *Miniaturization and Mass Spectrometry*; Royal Society of Chemistry, 2008, p 1-315.

2. Xu, W.; Manicke, N. E.; Cooks, G. R.; Ouyang, Z. *J. Lab Autom.* **2010**, *15*, 433-439.

3. Wood, T. D.; Moy, M. A.; Dolan, A. R.; Bigwarfe, P. M.; White, T. P.; Smith, D. R.; Higbee, D. J. *Applied Spectroscopy Reviews* **2003**, *38*, 187-244.

4. Bacon, J. R.; Linge, K. L.; Parrish, R. R.; Van Vaeck, L. *J Anal Atom Spectrom* **2008**, *23*, 1130-1162.

5. Clough, R.; Harrington, C. F.; Hill, S. J.; Madrid, Y.; Tyson, J. F. *J Anal Atom Spectrom* **2013**, *28*, 1153-1195.

6. Evans, E. H.; Horstwood, M.; Pisonero, J.; Smith, C. M. M. *J Anal Atom Spectrom* **2013**, *28*, 779-800.

7. Ganeev, A. A.; Gubal, A. R.; Uskov, K. N.; Potapov, S. V. *Russ Chem Bull* **2012**, *61*, 752-767.

8. Koppenaal, D. W.; Eiden, G. C.; Barinaga, C. J. *J. Anal. At. Spectrom.* **2004**, *19*, 561-570.

9. Olesik, J. W.; Jones, D. R. *J. Anal. At. Spectrom.* **2006**, *21*, 141-159.

10. Marcus, R. K. *Glow Discharge Spectroscopies*; Plenum Press: New York, 1993.

11. Marcus, R. K.; Broekaert, J. A. C. *Glow Discharge Plasmas in Analytical Spectroscopy*; John Wiley & Sons: Chichester, 2003.

12. Harrison, W. W.; Hess, K. R.; Marcus, R. K.; King, F. L. *Anal Chem* **1986**, *58*, A341-&.

13. Duckworth, D. C.; Marcus, R. K. *Analytical Chemistry* **1989**, *61*, 1879-1886.

14. Marcus, R. K. *J Anal Atom Spectrom* **1996**, *11*, 821-828.

15. Reinsberg, K. G.; Schumacher, C.; Tempez, A.; Nielsch, K.; Broekaert, J. A. C. *Spectrochim Acta B* **2012**, *76*, 175-180.

16. Pisonero, J.; Bordel, N.; Gonzalez de Vega, C.; Fernandez, B.; Pereiro, R.; Sanz-Medel, A. *Analytical and bioanalytical chemistry* **2013**, *405*, 5655-5662.

17. Alberici, R. M.; Simas, R. C.; Sanvido, G. B.; Romao, W.; Lalli, P. M.; Benassi, M.; Cunha, I. B. S.; Eberlin, M. N. *Anal. Bioanal. Chem.* **2010**, *398*, 265-294.

18. Harris, G. A.; Galhena, A. S.; Fernandez, F. M. *Anal Chem* **2011**, *83*, 4508-4538.

19. Harper, J. D.; Charipar, N. A.; Mulligan, C. C.; Zhang, X.; Cooks, R. G.; Ouyang, Z. *Anal Chem* **2008**, *80*, 9097-9104.

20. Kratzer, J.; Mester, Z.; Sturgeon, R. E. *Spectrochim Acta B* **2011**, *66*, 594-603.

21. Shelley, J. T.; Wiley, J. S.; Hieftje, G. M. *Anal Chem* **2011**, *83*, 5741-5748.

22. Webb, M. R.; Hieftje, G. M. *Anal Chem* **2009**, *81*, 862-867.

23. Jamroz, P.; Greda, K.; Pohl, P. *Trac-Trend Anal Chem* **2012**, *41*, 105-121.

24. He, Q.; Zhu, Z.; Hu, S. *Appl. Spectrosc. Rev.* **2014**, *49*, 249-269.

25. Cserfalvi, T.; Mezei, P. *Journal of Analytical Atomic Spectrometry* **1994**, *9*, 345-349.

26. Mezei, P.; Cserfalvi, T.; Janossy, M. *J Phys D Appl Phys* **1998**, *31*, L41-L42.

27. Webb, M. R.; Chan, G. C. Y.; Andrade, F. J.; Gamez, G.; Hieftje, G. M. *J Anal Atom Spectrom* **2006**, *21*, 525-530.

28. Webb, M. R.; Andrade, F. J.; Hieftje, G. M. *J Anal Atom Spectrom* **2007**, *22*, 775-782.

29. Webb, M. R.; Andrade, F. J.; Hieftje, G. M. *Anal Chem* **2007**, *79*, 7899-7905.

30. Davis, W. C.; Marcus, R. K. *J Anal Atom Spectrom* **2001**, *16*, 931-937.

31. Davis, W. C.; Marcus, R. K. *Spectrochim Acta B* **2002**, *57*, 1473-1486.

32. Marcus, R. K.; Davis, W. C. *Anal Chem* **2001**, *73*, 2903-2910.

33. Venzie, J. L.; Marcus, R. K. *Spectrochim Acta B* **2006**, *61*, 715-721.

34. Marcus, R. K.; Quarles, C. D., Jr.; Barinaga, C. J.; Carado, A. J.; Koppenaal, D. W. *Anal Chem* **2011**, *83*, 2425-2429.

35. Quarles, C. D., Jr.; Carado, A. J.; Barinaga, C. J.; Koppenaal, D. W.; Marcus, R. K. *Anal Bioanal Chem* **2012**, *402*, 261-268.

36. Marcus, R. K.; Burdette, C. Q.; Manard, B. T.; Zhang, L. X. *Anal Bioanal Chem* **2013**, *405*, 8171-8184.

37. Liu, C.; Zhang, X.; Xiao, S.; Jia, B.; Cui, S.; Shi, J.; Xu, N.; Xie, X.; Gu, H.; Chen, H. *Talanta* **2012**, *98*, 79-85.

38. Montoro Bustos, A. R.; Ruiz Encinar, J.; Sanz-Medel, A. *Analytical and bioanalytical chemistry* **2013**, *405*, 5637-5643.

39. Lagad, R. A.; Alamelu, D.; Chaudhary, A. K.; Aggarwal, S. K. *Atomic Spectroscopy* **2012**, *33*, 109-116.

40. Boumans, P. W. J. M.; Vrakking, J. J. A. M. *Spectrochim Acta B* **1987**, *42*, 819-840.

41. Boumans, P. W. J. M. *Spectrochim Acta B* **1991**, *46*, 431-445.

42. Boumans, P. W. J. M. *Spectrochim Acta B* **1991**, *46*, 917-939.

43. *Practical Aspects of Ion Trap Mass Spectrometry*; CRC Press, Inc., 1995; Vol. II.

44. Cserfalvi, T.; Mezei, P. *Fresenius J. Anal. Chem.* **1996**, *355*, 813-819.

45. Schwartz, A. J.; Ray, S. J.; Elish, E.; Storey, A. P.; Rubinstein, A. A.; CHan, G. C. Y.; Pfeuffer, K. P.; Hieftje, G. M. *Talanta* **2012**, *102*, 26-33.

46. Manard, B. T., Gonzalez J. J., Sarker A., Dong M., Chirinos J. R., Chirions J. R., Xianglei M., Russo R. E., Marcus R. K. . *Spectrochim. Acta Part B*, *in press*.

47. Harris, G. A.; Galhena, A. S.; Fernandez, F. M. *Analytical Chemistry* **2011**, *83*, 4508-4538.

48. Venter, A. R.; Douglass, K. A.; Shelley, J. T.; Hasma, G., Jr.; Nonarvar, E. *Anal. Chem.* **2014**, *86*, 233-246.

49. Alkemade, C. T. J.; Hollander, T.; Snelleman, W.; Zeegers, P. J. T. *Metal Vapours in Flames*; Pergamon Press: Oxford, 1982.

50. Mavrodineanu, R.; Boiteux, H. *Flame Spectroscopy*; John Wiley and Sons: New York, 1965.

51. Blades, M. W.; Horlick, G. *Spectrochim. Acta, Part B* **1981**, *36*, 881-900.

52. Vickers, G. H.; Wilson, D. A.; Hieftje, G. M. *Spectrochim. Acta Part B* **1990**, *45*, 499-509.

53. Holliday, A. E.; Beauchemin, D. *Spectrochim. Acta, Part B* **2004**, *59*, 291-311.

54. Houk, R. S.; Fassel, V. A.; Flesch, G. D.; Svec, H. J.; Gray, A. L.; Taylor, C. E. *Analytical Chemistry* **1980**, *52*, 2283-2289.

CHAPTER THREE

PRELIMINARY ASSESSMENT OF POTENTIAL FOR METAL-LIGAND SPECIATION IN AQUEOUS SOLUTION VIA THE LIQUID SAMPLING-ATMOSPHERIC PRESSURE GLOW DISCHARGE (LS-APGD) IONIZATION SOURCE: URANYL ACETATE

3.1 Introduction

The general field of elemental speciation has been perhaps the area of greatest evolution in atomic spectroscopy over the last 30 years. The speciation of a metal such as oxidation state and ligand identity is important toward a number of aspects including the biochemical efficacy, chemical reactivity, and environmental transport of the metal. To this end, there is an entire field of biochemical science called *metallomics*[1,2]. The typical speciation determination involves chromatographic/electrophoretic separation of sample components that reflects the chemistry of the metal/ligand, followed by element-specific detection that allows identification and quantification of the metal composing the chromatographic fraction[3]. As the identity of the molecular entity can only be inferred by the chromatographic retention times, the development of "atomic" sources that provide "molecularly relevant" information is a goal of many research laboratories.

The behavior of uranium in the environment is profoundly influenced by the oxidation state and chemical species present. Generally aqueous concentrations of tetravalent uranium are low owing to the strong hydrolysis and eventual precipitation of U(IV) to form uraninite, UO_2(s) [4-6]. Hexavalent uranium is significantly more soluble as the uranyl dioxycation. Thus, active remediation at sites with subsurface uranium contamination from mining operations or legacy nuclear weapons production generally rely on reduction of soluble U(VI) to insoluble U(IV). However complexation of U(VI) can drastically alter uranium mobility in the subsurface and also facilitate reoxidation of U(IV). Wan et al. [7] examined biologically mediated reduction of U(VI) to U(IV) in soils amended with acetate to stimulate microbial activity. Though U(VI) was initially reduced to U(IV) and reducing conditions persisted throughout the experiment, reoxidation to U(VI) was facilitated through the formation of ternary alkali earth-uranyl-carbonate species [8,9]. Furthermore, the presence of small organic acids and natural organic matter has been shown to significantly influence uranium sorption to pure mineral surfaces.

A variety of spectroscopic techniques have been utilized to examine uranium and its speciation. X-ray absorption spectroscopy (XAS)[10-12], infrared absorption spectroscopy (IR)[13-15], Raman spectroscopy[16,17] and mass spectrometry (MS)[18-22] of various ionization modes are the commonly used for uranium speciation. Inductively coupled plasma–optical emission and mass spectrometries (ICP-OES/MS) are the benchmark elemental methods to detect

elemental uranium and determine isotopic ratios [21,23,24]. Methods reported using ICP-MS for metal-ligand speciation require sample pre-treatment steps including solvent extraction, ion exchange, or coprecipitation[25-27]. These procedures compromise overall sample throughput, analytical sensitivity, and may alter the oxidation state of the uranium, with the detection step providing no direct species information. On the other hand, electrospray ionization (ESI) - MS can be used for the determination of metal-ligand speciation[3,28,29]. ESI-MS was investigated at an alternative to ICP-MS for metals analysis (including the uranyl ion) in the 1990s by Horlick and co-workers[30-32]. On a first-principles basis, ESI-MS should be highly effective to address the challenges in metal speciation. Unfortunately, ESI spectra are difficult to interpret as they are influenced by a highly complex set of electrochemical, redox, solvent, and pH-dependent reactions. Clark and co-workers[33] recently illustrated the complexities of using ESI-MS in assessing the speciation of lanthanide-carboxylate complexes, using neodymium-acetate as the test system. Deviations between the observed spectral components and what would be expected based on thermodynamic calculations pointed to many experimental artifacts and deviations. Even so, ESI-MS has been used in the study of aqueous chemistry of the uranyl dication, UO_2^{2+} and its interaction with ligands in the aqueous solution[18,19,34-36], including different modalities, positive and negative ion monitoring, and a range of mass spectrometer platforms. As would be expected, given the complexities of metal-ligand electrospray processes[33], the overall results are as diverse as the number of reports.

In an effort to introduce microplasma technology to the field of metal speciation, Marcus et al. developed the liquid sampling-atmospheric pressure glow discharge (LS-APGD) as a low power (<50 W), low cost, and low sample flow rate (<100 μL min^{-1}) excitation source[37]. This device is related in concept to the electrolyte cathode discharge (ELCAD) by Cserfalvi and co-workers[38], further employed by Hieftje and co-workers as the solution cathode discharge (SCD)[39]. A primary difference between the ELCAD-based designs and the LS-APGD is the high power density of the LS-APGD microplasma (>10 W mm^{-3}) providing sufficient energy for operation in a total-consumption mode. The combination of high power density and the presence of the electrolyte solution yields a high tolerance for matrix effects of the high ion strength and/or extreme-pH samples[40,41].

The LS-APGD has also been utilized as an ionization source for elemental mass spectrometry, designed to easily integrate onto the ESI/atmospheric-pressure chemical ionization (APCI) interfaces common to organic/biological mass spectrometers. The device was originally described as an ionization source coupled with a high resolution Thermo Scientific Exactive Orbitrap mass spectrometer[42]. Detailed parametric evaluations were undertaken to understand factors affecting overall spectral composition, target analyte (metals) signal intensities and signal-to-background ratios (S/B), and the limits of detection (LODs)[43,44]. More recently, the use of the LS-APGD as a source for ambient desorption/ionization (ADI)-MS for small organic molecule detection has been described[45].

Presented here is the initial evaluation of the use of the LS-APGD microplasma ionization source for the monitoring of metal-ligand speciation in aqueous media. In spite of the difficulties realized in previous ESI-MS works, uranyl-acetate speciation in acidic aqueous solutions was chosen as the test case. This specific system was the topic of a recent Round Robin Test in Actinide Spectroscopy (RRT) wherein a variety of spectroscopic and computational methods were employed to evaluate the uranyl/acetate system as a function of pH (in acetic acid media). The materials used in this RRT (and the studies presented here) were prepared by the Helmholtz Zentrum Dresden Rossendorf (HZDR), who administered the broad-based study. Many types of optical, mass, NMR, x-ray absorption, and computation methods had shown large disparities in the ability to measure/predict the UO_2^{2+}:acetate stoichiometry. Thus this chemical system provides a formidable test of the abilities of the LS-APGD-MS source to yield spectra reflecting the solution chemistry. While much more detailed fundamental work remains, the ability to operate the LS-APGD-MS source in a mode that provides direct metal speciation information is promising, and is totally unique among other “atomic” ionization sources.

3.2 Experimental Section

3.2.1 Sample Preparation

A 0.025 M uranyl acetate in 0.95 M acetate solution (pH=2.5) solution was prepared and used for the optimization of the operating conditions. Uranyl acetate

($UO_2Ac_2 \cdot 2H_2O$) was purchased from International Bio-Analytical Industries, Inc. (Boca Raton, Florida), acetic acid (HPLC grade) was purchase from Thermo Fisher Scientific Inc. (Waltham, MA), DI water (18.2 MΩ cm^{-1}) was collected from a NANOpure Diamond Barnstead/Thermolyne Water System, (Dubuque, IA). All reagents were used without additional purification. The testing sample was provided to co-author BAP through the HZDR RRT program. Four samples were received from HZDR with 0.025 M uranyl, 0.95 M acetate, and 1 M ionic strength. The samples were adjusted to pH 1, 2, 2.5, and 3.5 to capture a range of uranyl:acetate complexes.

3.2.2 LS-APGD Mass Spectrometer

The interfacing of the LS-APGD ionization source to a ThermoScientific LCQ mass spectrometer system has been described previously in detail (presented diagrammatically in Fig. 2.1) [44]. As described, the glass capillary through which the sample solution flows serves as the ground electrode, which is mounted in-line with the MS ion-sampling capillary. The 1 mm diameter stainless steel counter electrode is mounted perpendicular to the capillary. The LS-APGD is housed within a plexiglass “safety box” to avoid contacting the high voltage electrodes when it is in use. Power (constant current mode) was provided to the counter electrode by a direct current Bertan 915-Series power supply (Hickville, NY, USA; 0-100 mA, 0-1 kV positive polarity), through a 10 kΩ, 225 W ballast resistor, with the reported operating current read from the supply panel. Helium (99.99% purity) was introduced through the stainless steel capillary surrounding

the glass capillary as sheath/cooling gas (0.1-1.2 L min^{-1}), while the electrolyte flow was pumped through the glass capillary using a syringe pump (NE-1000, New Era Pump Systems, Farmingdale NY, USA). The electrodes of the LS-APGD ionization source are mounted on an aluminum optical breadboard, which is coupled to the Thermo Scientific (Waltham, MA, USA) LCQ Advantage Max™ ion trap mass analyzer using the standard API source mounts. All MS experiments performed here were in the positive ion sampling mode, operating under the control of the accompanying Xcalibur™ data acquisition software. No form of in-source activation was performed to assist in de-clustering solvent molecules from the base ions. During the microplasma parametric evaluation, each set of operating conditions was tested 3 times, and the testing order of each set of parameters randomly determined by sorting (ascending) based on the random numbers (between 0 and 1) generated using formula = RAND() in Microsoft® Excel Software.

3.3 Results and Discussion

The essence of metal speciation experiment is the determination of the chemical form of a given system in a particular chemical environment. This would preferably be obtained by direct spectroscopic evidence that is not biased by the act of making the measurement. Thus, the four samples from the RRT vary in pH to capture the expected $UO_2(Ac)_x^{2-x}$ species, with x ranging from 0 to 3. The expected aqueous species in these samples versus pH were calculated using the

stability constants reported by Rao and co-workers[11] (Fig. 3.1). The general trends reflect sequentially greater prominence of the ligated uranyl ion at increasing pH, with the solution composition dominated by the cationic species UO_2^{2+} and UO_2Ac^+ at pH 1 and 2, respectively, and the anionic $UO_2(Ac)_3^-$ species above pH 3. The neutrally charged $UO_2(Ac)_2^0$ species is present from pH 1.5 to 3.5 but is not the dominant species at any pH. Thus any means of speciation should be able to generate spectral data that reflects this distribution of species; if not directly, by rational implication.

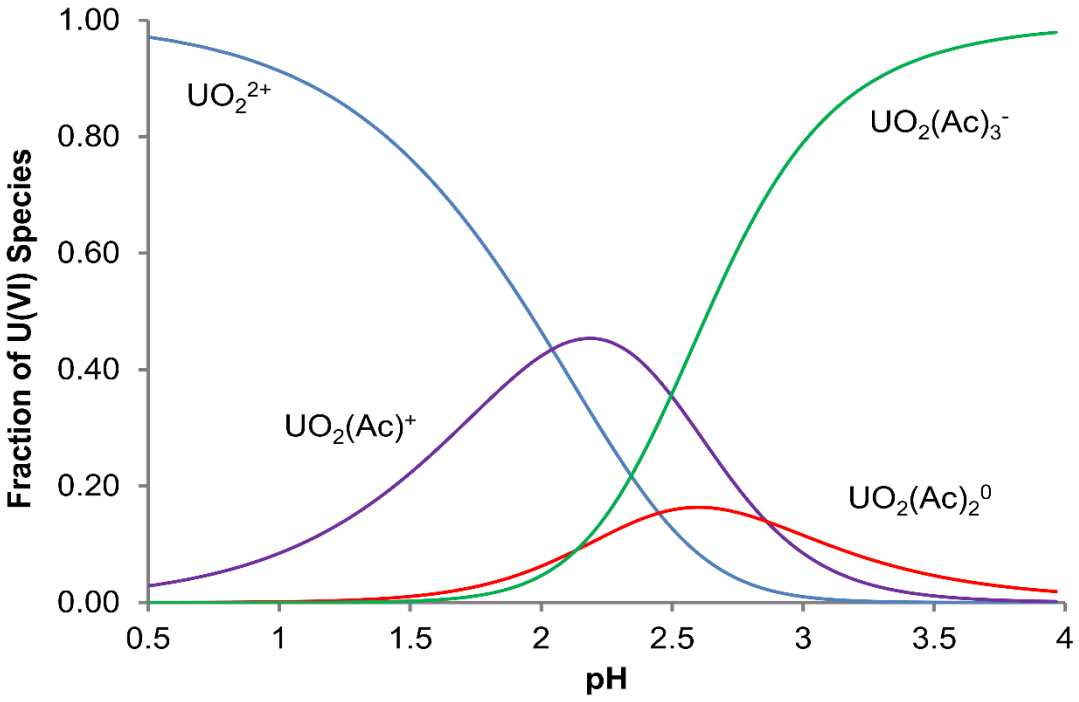

Figure 3.1 Predicted solution-phase speciation of the uranyl acetate system as a function of pH.

3.3.1 Evaluation of microplasma operating parameters

Previous reports from this laboratory have described the roles of the LS-APGD microplasma operating parameters in its performance as an ion source for elemental/isotopic analysis[43,44] as well as in an ADI-MS mode[45]. It is not unreasonable to expect that conditions which effectively convert metal ions in aqueous solution to free, atomic ions would not be the same as those which would affect the desired "molecular" mass spectra. The primary concern is delivery in a solvent for which the molecule is soluble and provides the ionization agents appropriate to affect soft ionization. Additionally, there is a need to operate at conditions of sufficiently low kinetic temperatures that would limit metal-ligand bond dissociation. Finally, one must be cognizant that the ion sampling distance would affect the length of time that the ions are subjected to the dissociating plasma environment. Thus, the key parameters that must be evaluated include the electrolyte solution composition, and the inter-related discharge current, electrolyte flow rate, sheath gas flow rate, and ion sampling distance. Perhaps more importantly (relative to what is seen in ESI-MS), would be a minimization of the roles of source operation parameters that might bias the spectral composition.

3.3.1.1 Role of Mobile Phase Composition

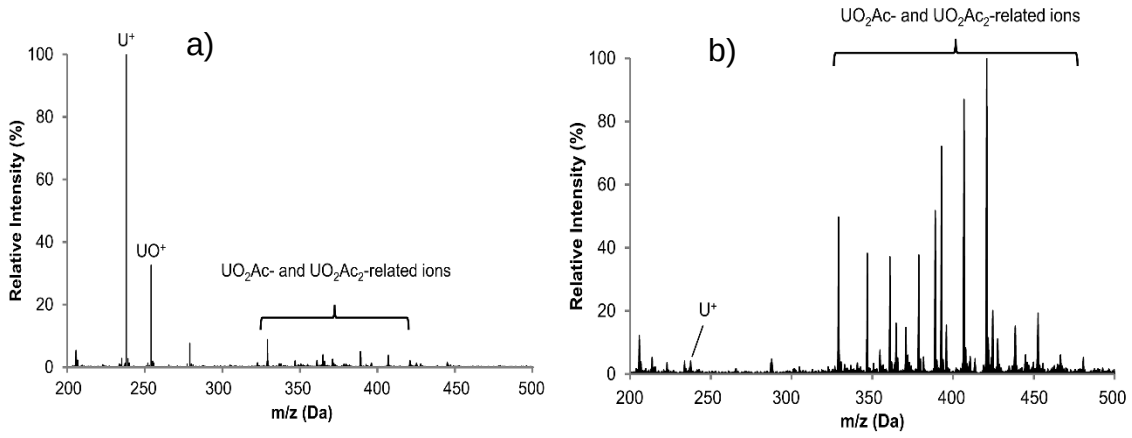

Figure 3.2 LS-APGD mass spectrum of 0.025 M UO_2Ac_2 in 0.95 M acetic acid solution (pH=2.5) introduced in a) 1 M HNO_3 and b) 70:30 MeOH:H_2O electrolyte solution flows.

Use of an electrically conductive feed solution is required for LS-APGD microplasma operation. In the case of elemental analysis, a 1 M aqueous HNO_3 solution is typically used[43,46], though operation of the device with alkali salt solutions is valid. In the case of the ADI-MS implementation, molecular mass spectra could be preferentially observed upon addition of an organic modifier (methanol). It is felt that methanol (CH_3OH), rather than nitric acid, yielded a lower temperature (less kinetically-energetic) plasma, while also providing an effective gas-phase proton donor, ($CH_3OH_2^+$). To better characterize the role of mobile phase composition, solutions ranging from 10:90 MeOH:H_2O (v:v) to 90:10 MeOH:H_2O (v:v) were tested. Solutions having lower amounts of MeOH tended to yield lower fractions of the desired molecular ions in lieu of greater amounts of U^+ and UO_2^+ species. This response is demonstrated in the mass spectra presented in Fig. 3.2 of uranyl acetate prepared in a pH = 2.5 acetate solution, where the

spectrum derived from the a) 1 M HNO_3 electrolyte yields almost exclusively "inorganic" species, while the b) 70:30 MeOH:H_2O, yields appreciable amounts of uranyl acetate (molecular) species. The differences in the mass spectra clearly reflect a situation where more extensive dissociation of the primary uranyl-acetate occurs in the plasma for the HNO_3 supporting electrolyte. Though it cannot be ruled-out that there are different ionization mechanisms that may be predominant under the two sets of solvent conditions. It is interesting to note that the raw intensities related to the base peaks in each spectrum (238 Da and 425 Da, respectively), are 98 k vs. 45 k, and so the most prominent peaks in each spectrum yield similar responses.

Table 3-1 Typical ionic species observed in LS-APGD mass spectra of UO_2Ac_2.

Ions	n=0	n=1	n=2	n=3	n=4
Inorganic uranyl					
U^+	238				
$U(OH)_n^+$		255	272	289	306
$UO_2(OH)_n^+$		287	304	321	338
$UO_2(H_2O)_n^+$		288	306	324	342
$UO_2(H_2O)_n(MeOH)_m^{2+}$					
m=0	135	144	153	162	171
m=1	151	160	169	178	187
m=2	167	176	185	194	203
m=3	183	192	201	210	219
m=4	199	208	217	226	235
$UO_2Ac(H_2O)_n(MeOH)_m^+$					
m=0	329	347	365	383	401
m=1	361	379	397	415	433
m=2	393	411	429	447	465
m=3	425	443	461	479	497
m=4	457	475	493	511	529
$UO_2Ac_2(H_2O)_n(MeOH)_m H^+$					
m=0	389	407	425	443	461
m=1	421	439	457	475	493
m=2	453	471	489	507	525
m=3	485	503	521	539	557
m=4	517	535	553	571	589

The composition of the uranyl-acetate mass spectrum taken with the 70:30 MeOH:H_2O solvent (Fig. 3.2b) consists of several major peaks corresponding to the uranyl ion with different degrees of acetate ligation (0, 1, or 2) and a range of associated solvent molecules, which can be categorized into three general groups as inorganic uranyl (i.e., no acetate ligands), $UO_2Ac(H_2O)_n(MeOH)_m^+$, and $UO_2Ac_2(H_2O)_n(MeOH)_mH^+$. In the first case, the ions appear as doubly- and singly-charged uranium and uranium oxides, with differing numbers of solvent molecules. To be sure, UO_2^+ does not exist in solution, and is likely the result of gas phase

reduction of UO_2^{2+} in the electron-rich gas phase[47]. That said, charge reduction of uranyl species has also been attributed to redox chemistry is ESI sources and through various CID studies or uranyl complexes[20,48]. The second group reflects the mono-acetate uranyl species, which are solvated to various extents and maintain a net +1 charge (as they are in solution). Finally, the di-acetate uranyl species contain some level of solvation, but in this case, the net charge is the result of the addition of one proton. This would tend to suggest that the principle ionization mechanism for these species in the LS-APGD microplasma is more akin to APCI than to ESI, as the neutral molecule would not be protonated in solution. The identities and masses of the various species observed throughout this study of U(VI):acetate complexation are summarized in Table 1. Each of the observed species is logical based on the starting material and the solvent system. For example, based on the variety of likely species, the base peak in the spectrum presented in Fig. 3.1b (m/z = 425 Da) could be either an ion of the formula $UO_2Ac(MeOH)_3H^+$or $UO_2Ac_2(H_2O)_2H^+$. Isolation of that ion in the ion trap, followed by collisional dissociation, yields the product ion (MS^2) spectrum shown in, Fig. 3.3. The major product peak at m/z = 407 reflects the loss of an 18 Da neutral (H_2O) and the loss of the second H_2O can be seen in the peak at 389 Da. The remainder of the fragment ions in the mass spectrum reflect the loss of expected functional groups/molecules from the $UO_2Ac_2(H_2O)_2H^+$ parent.

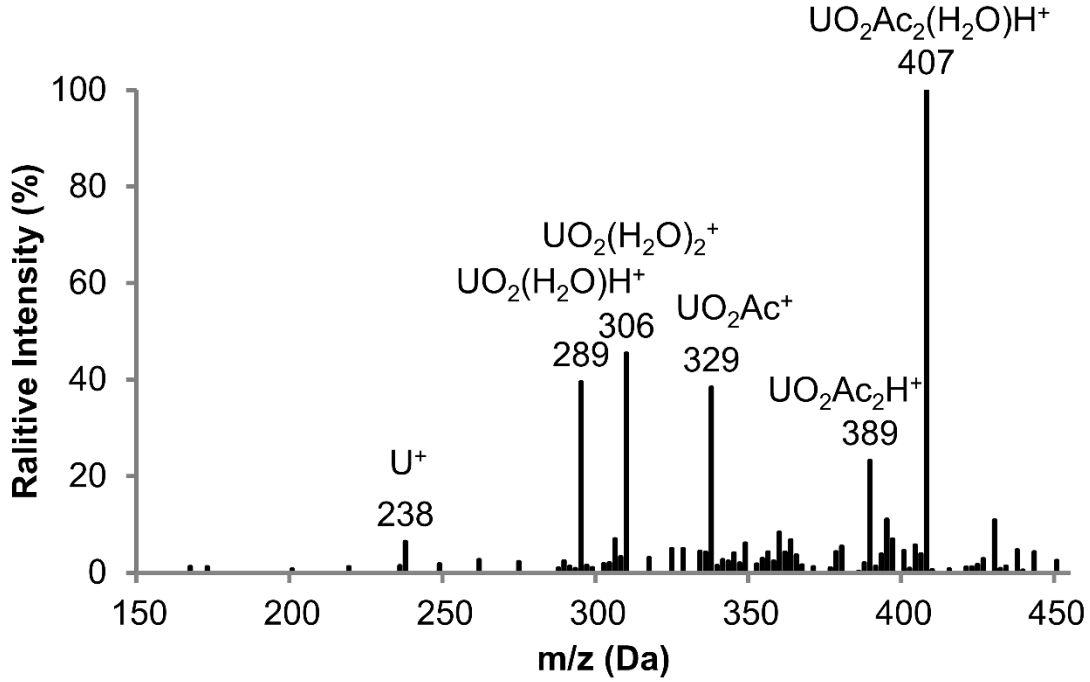

Figure 3.3 MS^2 spectrum of ions at m/z = 425 Da (in Fig. 3.1b) using 0.025 M UO_2Ac_2 in 0.95 M acetic acid solution (pH=2.5). Discharge current = 20 mA, solution flow rate = 10 µL min^{-1}, sheath gas flow rate = 0.9 L min^{-1}, and ion sampling distance = 0.75 cm.

In addition to the differences in the mass spectral features, operation of the microplasma across the range of MeOH:H_2O causes other changes in the plasma operation. Low MeOH compositions show greater instability, while solutions of greater than 70% MeOH yielded more of a combustion flame in appearance and operation than an electrical discharge. A direct comparison of the current-voltage (*i*-V) characteristics of the LS-APGD when employing 1 M HNO_3 (atomic mode) and 70:30 MeOH:H_2O (v:v) mobile phases (Fig. 3.4) indicates that both solvents operate in the abnormal glow discharge regime, as anticipated. Lower potentials for the HNO_3 solution reflect greater ease in affecting the plasma-sustaining

ionization. A greater departure from purely linear dependence for the case of the MeOH;H_2O solution, suggesting two potential operating modes. At low currents, solvent would likely evaporate at the liquid/gas interface at the base of the plasma, but as the current increases there may volatilization occurring from within the glass capillary. The results indicate that 70:30 MeOH:H_2O (v:v) is a suitable mobile phase, based on the mass spectral character and the plasma operation stability.

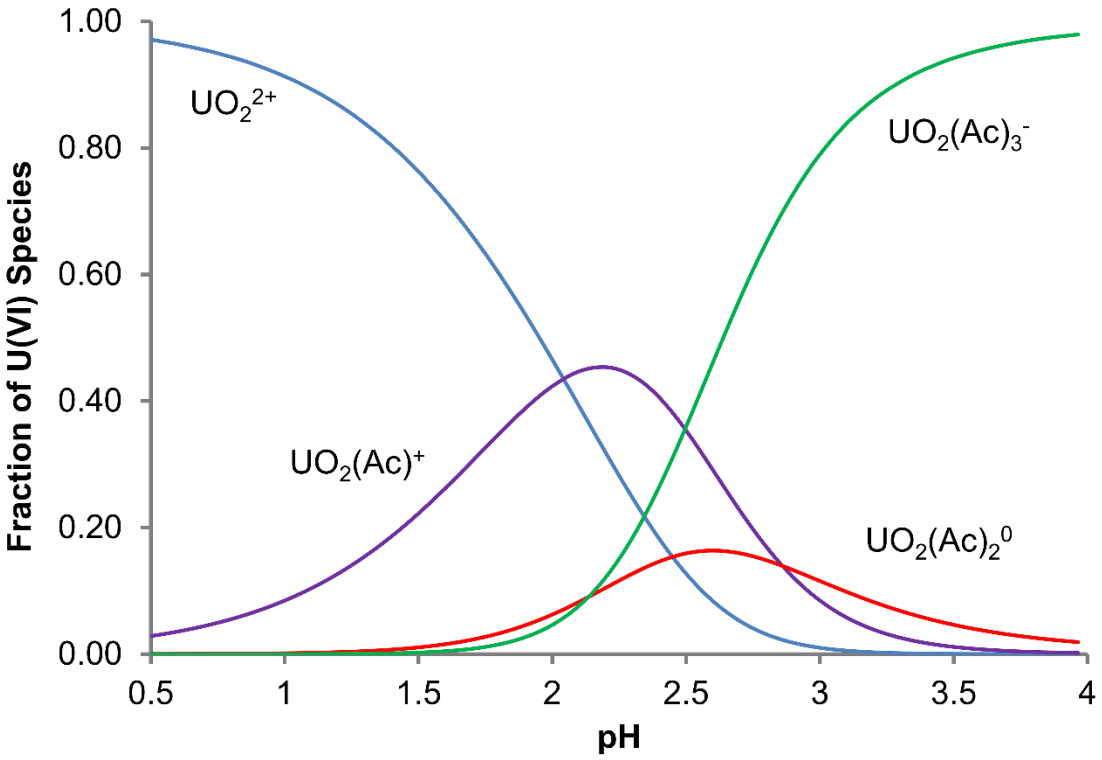

Figure 3.4 Current-voltage (*i*-V) characteristics of the LS-APGD ionization source with using 1 M HNO_3 and 70:30 MeOH:H_2O (v:v) electrolyte solutions

3.3.1.2 Roles of Plasma Operation Parameters

Different from the case of the "atomic"-MS implementation of the LS-APGD ionization source, where quantification is the primary goal, applications in metal

speciation must be concerned with qualitative spectral content. While the spectral content may not be an *exact* reflection of the solution chemistry, it should be a rational, predictable, and controllable situation. As described previously, ESI-MS studies of uranyl ion systems yield spectra whose compositions vary across the entirety of the operation space[11,33,35,36]. Thus an evaluation and optimization of all operating parameters/discharge conditions is necessary to understand whether or not this method of ionization biases the spectral character and thus the *apparent* solution chemistry.

In the case of the LS-APGD microplasma, the discharge current, liquid sampling flow rate, sheath/cooling gas flow rate and ion sampling distance likely have effects on the qualitative and quantitative nature of the resultant spectra. These parameters were varied using a single-composition uranyl acetate solution, assessing the raw signal intensities, the overall spectral composition, and the plasma stability across triplicate injections. Specifically, a 0.025M UO_2Ac_2 solution was prepared in acetate solution of pH = 2.5 due to the solution-phase abundance of the three uranyl species (UO_2^{2+}:UO_2Ac^+:UO_2Ac_2) of ~1:2:1, each of which should have distinct spectra signatures as described above. For each set of experimental parameters, the population for the respective solution species was characterized by the sum of the signals of the species listed in Table 1, along with the combined (total) uranyl-related signals as a measure of the overall solute ion yield. Presented in Fig. 3.5 are the parametric trends (relative to the maximum of the total-species' response) for triplicate, 20 µL injections at each condition, with

the error bars representing the range of the species' responses. It is noteworthy that under no set of microplasma conditions did the responses among injections vary by more than 10% relative standard deviation (RSD).

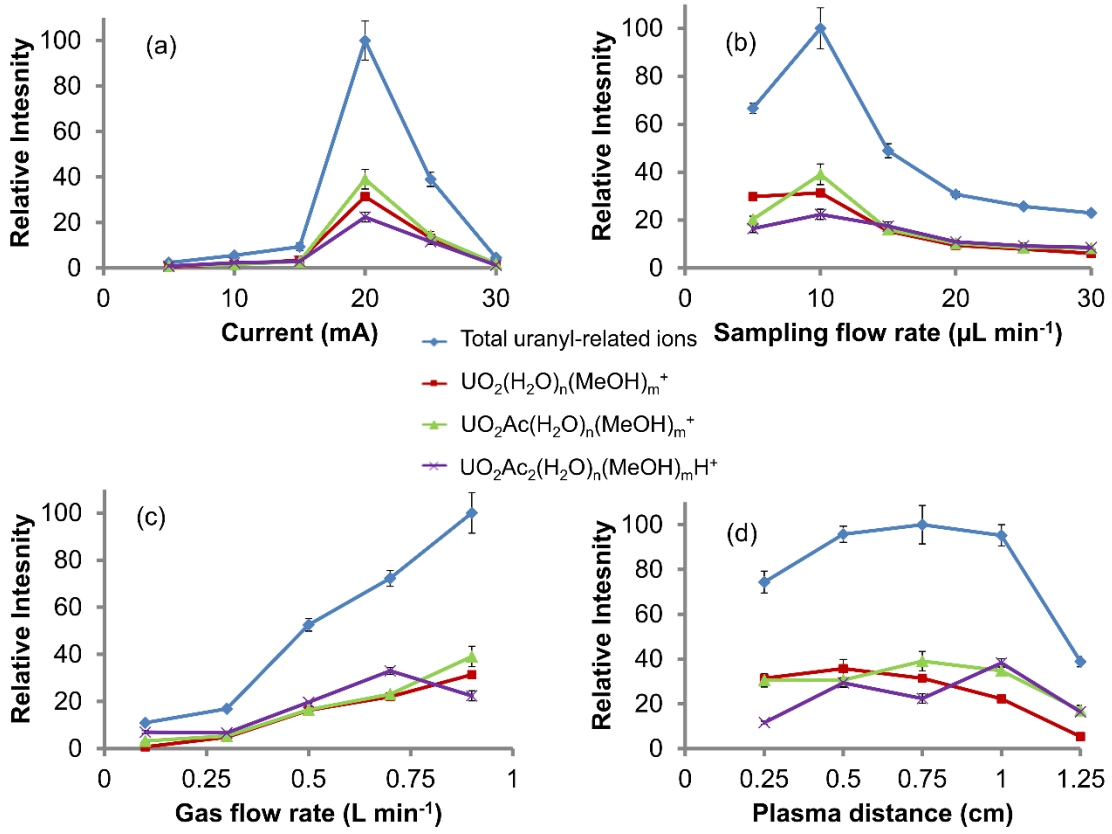

Figure 3.5 Parametric evaluation of total ion and UO_2Ac_2 species' responses using 0.025 M uranyl acetate in 0.95M acetic acid solution as a) function of discharge current (solution flow rate = 10 µL min^{-1}, gas flow rate = 0.9 L min^{-1}, sampling distance = 0.75 cm); b) function of electrolyte solution flow rate (current = 20 mA, gas flow rate = 0.9 L min^{-1}, sampling distance = 0.75 cm); c) function of sheath gas flow rate (current = 20 mA, solution flow rate = 10 µL min^{-1}, sampling distance = 0.75 cm); d) function of plasma sampling distances (current = 20 mA, gas flow rate = 0.9 L min^{-1}, solution flow rate = 10 µL min^{-1}). Signal intensities were normalized based on the highest intensity.

The discharge current in the LS-APGD controls a number of processes occurring in the microplasma. First, it controls the amount and efficiency of

converting the bulk solution flow into a vapor consisting of analyte and solvent species. The current, while a measure of the net charged particle flow between the electrodes, might also affect the electron number density. Finally, it could affect the thermal properties of the plasma. LS-APGD-OES studies of the normal, aqueous acid-based microplasma reflect a minimal change in electron number density, but increases in kinetic temperature with increasing current[40]. As depicted in Fig. 3.5a, there is a pronounced maximum in the solute ion responses at an operation current of 20 mA. Parametric studies of the LS-APGD operating as an "atomic" ionization source reflected a case where analyte ionization gives way to greater levels of solvent ionization with increases in discharge current[43,44]. Of greater relevance here, the signals attributable to the different solution species parallel each other, as well as the total ion response. Thus, discharge current does not affect the apparent species' distributions, only the absolute ion intensities.

The feed rate of the electrolyte increases the amount of analyte presented to the plasma per unit time, and also increases the overall solvent loading. As seen in Fig. 3.5b, there is a slight increase in the response of the signature ion populations as the flow is increased from 5 to 10 µL min^{-1}, representing a mass increase per unit time, followed by a steady decrease at higher feed rates. As would be hoped, the ion species show very similar response to the change in solution flow rate. The assumption is that high solution flow rates place a greater burden on the plasma energetics to affect vaporization of the solvent, leading to either lesser solute ionization efficiency or the preferential ionization of solvent.

Unfortunately, the 50 Da low-mass cut-off for this spectrometer system precludes the verification of this latter hypothesis.

Early LS-APGD-OES studies revealed the utility of a sheath gas around the liquid capillary to provide greater plasma stability and reducing the egress of atmospheric gases (e.g., N_2) into the plasma [49]. In MS sampling, the sheath gas will also effect the residence time of solutes in the plasma and act as a carrier toward the ion sampling orifice. These two aspects were found to counter-balance in the case of atomic ion analysis[44], as high flow rates at a fixed distance lead to greater amounts of metal oxide/hydroxide ions due to short residence times, but allowed for greater response at larger sampling distances (longer plasma exposure times). In the case of the uranyl-acetate solutes, one might imagine that differences in residence times would affect different degrees of solvent molecule retention. While this effect is seen for the various species monitored here, changes in the sheath gas flow rates serve to principally provide enhanced ion transport to the ion sampling orifice, as seen in Fig. 3.5c. There is some reduced response for the $UO_2Ac_2(H_2O)_n(MeOH)_mH^+$-related population at the highest gas flow rate. Closer inspection of the full mass spectra did not yield an obvious reason for the difference.

As suggested in the previous paragraph, there is a complementary set of relationships between the residence times and collection efficiencies of ions as a function of the ion sampling distance. More so than molecular ions, atomic ions would be expected to be more reactive with background (ambient) gases. In the

case of the uranyl-acetate species seen in Fig. 3.5d, each of the respective ion populations shows a broad, fairly-uniform distribution. By contrast, the signal for Cs^+ from the same source varies by orders of magnitude across a maximum between 0.8 and 1.1 cm sampling distance[44]. While the intent here is not an exhaustive assessment of the ionization mechanisms of the LS-APGD operating in a "molecular" mode, the basic response seen here suggests very different processes.

As an overall observation, the various ions reflective of the inorganic uranyl, $UO_2Ac(H_2O)_n(MeOH)_m^+$, and $UO_2Ac_2(H_2O)_n(MeOH)_mH^+$ species behave similarly to changes in the key LS-APGD operating conditions, indicating that the ions are formed through ionization mechanisms with having similar requirements of the plasma energetics and reactive species. Certainly, the dependences seen relative to changes in operating conditions suggest a lessened need for strict control in comparison to ESI-MS sources. By the same token, this would suggest that differences in spectral composition among different test solutions would be more likely to be representative of the chemical system, rather than how the microplasma was being operated.

3.3.2 Effect of Solution pH on LS-APGD-MS Spectra of Uranyl Acetate

The uranyl acetate system displays a well-defined equilibrium chemistry as a function of solution pH. The four samples analyzed contain 0.025 M UO_2^{2+} and 0.95 M acetic acid at pH values of 1.0, 2.0, 2.5, and 3.5. Note the high ionic strength and acetate concentration are necessary to capture all four U(VI):acetate

species within this pH range. Replicate mass spectra were taken for each of the test samples, using 70:30 MeOH:H_2O as the electrolyte solution. As demonstrated in Figs. 3.6a and b, the mass spectra obtained from the pH = 2.5 and and pH = 1.0 solutions, respectively, are appreciably different. (Unfortunately, the equivalent ESI-MS spectra that were anticipated to be part of the HZDR RRT were not published at the time of this writing.) Identified in each spectrum are the prominent species that can be assigned to the respective ion-type families summarized in Table 1: inorganic uranyl, $UO_2Ac(H_2O)_n(MeOH)_m^+$, and $UO_2Ac_2(H_2O)_n(MeOH)_mH^+$.

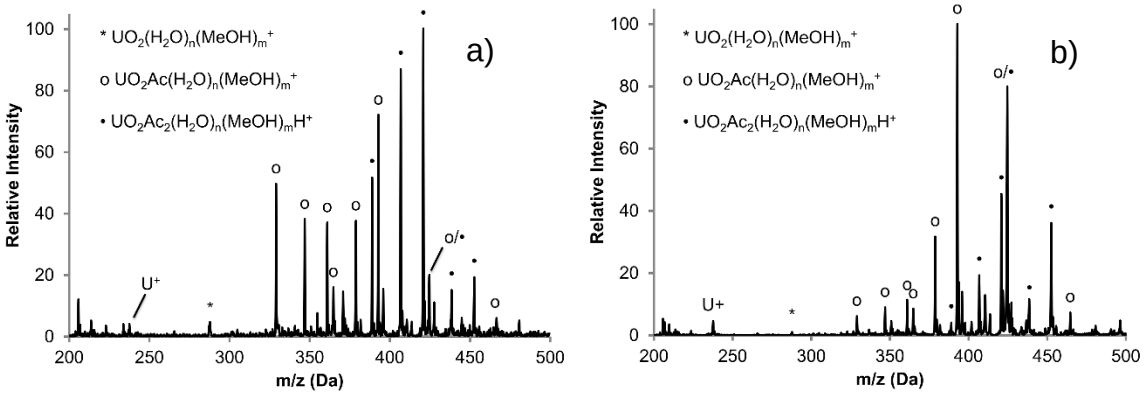

Figure 3.6 LS-APGD mass spectra obtained from source using 0.025 M UO_2Ac_2 in 0.95M acetic acid solutions at different pH values: a) pH=2.5 and b) pH=1. Discharge current = 20 mA, solution flow rate = 10 µL min^{-1}, sheath gas flow rate = 0.9 L min^{-1}, and ion sampling distance = 0.75 cm.

The quantitative differences between the spectra obtained across the range of sample pH values are presented in Fig. 3.7. Acknowledging that the key information desired in the uranyl:acetate speciation experiment are the relative populations of the UO_2^{2+}, UO_2Ac^+, and UO_2Ac_2 forms of the complex (Fig. 3.1), the total number of ions representing those solution-phase entities must be compared. Figure 3.5a presents the intensities of the summed responses for the different

molecular forms of the complex at the four pH values utilizing LS-APGD ionization source ($UO_2(H_2O)_n^+$ for inorganic uranyl, $UO_2Ac(H_2O)_n(MeOH)_m^+$ for UO_2Ac^+, and $UO_2Ac_2(H_2O)_n(MeOH)_mH^+$ for UO_2Ac_2), plotted as a fraction of each of the species' maximum response across the pH range. This is an admitted oversimplification, but it represents the best possible scenario as the sum of ions in the various populations would literally reflect the solution species distribution. Simply, the three ion families have different behavior in relation to the pH values. On a species-specific basis, it is seen that the inorganic uranyl-related ion signal intensities show their highest responses at a pH value of 1, the UO_2Ac species at pH = 2, and UO_2Ac_2-related species' response is maximized at the highest pH value, 3.5. Thus, the trends within the ion families do indeed follow those depicted in Fig. 3.1. The lack of a precipitous drop in the inorganic uranyl response at pH 2 suggests that the thermal energy of the microplasma results in some of the ligated species being decomposed down to the bare uranyl ion or its related solvated ions, resulting in an overestimation of the UO_2^{2+} content in solutions above pH = 1. As shown in Fig. 3.1, chemical equilibrium calculations suggest that the dominant solution species at the highest pH is the tri-acetate anion ($UO_2Ac_3^-$). That ion would not be observed in the present positive-ion sampling mode, unless it had been cationized by some means (e.g., protonation). No such species were observed. By the same token, that species could be thermally-activated and lose ligands to yield di- and mono-acetates and free uranyl ions.

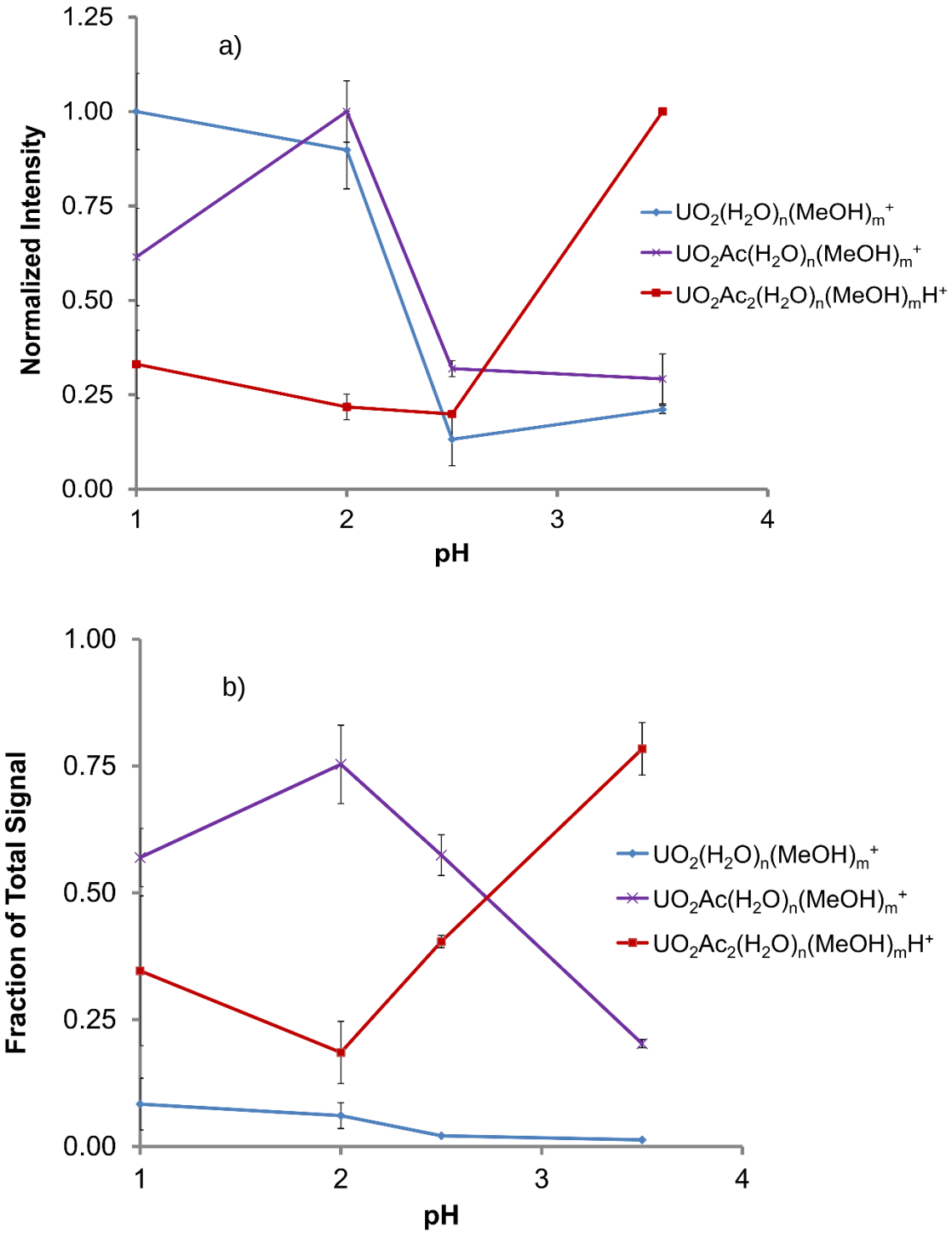

Figure 3.7 A comparison of the a) normalized intensities of the various uranyl species and the b) mole fractions of those species as a function of pH value

Plotting the species'-related ion signals relative to the total uranyl acetate-related ion signals presents the MS data in a format that more closely represents the equilibrium-based distributions shown in Fig. 3.1. The responses shown in Fig. 3.7b resemble the trends that might be expected, with the mono-acetate being the most abundant species at pH = 2, and the di-acetate dominating the positive ion mass spectra at pH = 3.5. Clearly seen, and reflective of the responses presented in Fig. 3.2b, is an under representation of the inorganic uranyl species. Here the vaporization and ionization processes affecting the different species within the plasma must be considered. Indeed, uranyl ion is highly refractory in nature and may be poorly vaporized to the form of free molecules/ions in the mixed-solvent case. This differs from the case of the organo-forms, which likely have some greater level of volatility. It must also be considered that the change in solvent composition translates to very different ionization processes taking place. It would not be unreasonable that the plasma transitions from an electron ionization to a chemical ionization environment. Clearly, these aspects much be confirmed in future studies. Based on the inorganic uranyl ion responses at pH 2 and higher (where these species are not present in solution) it is believed that the plasma's thermal properties are sufficient to remove acetate groups from the ligated complexes, but as seen in lack of UO_2^{2+}-related response for the pH = 3.5 fraction, loss of multiple acetates does not seem to be favorable.

At this point, the predominant cation species projected as a function of pH are generally followed at moderate and high pH values for the ligated uranyl ion.

In the case of the U(VI):acetate complexes, a charge reduction is seen relative to the solution state (+2 to +1), the mono-acetates "retain" their net charge (+1), and the di-acetate-related ions are the product of proton donation reactions (neutral-to-+1). It must be pointed out that there are a wide number of reactive species present in the LS-APGD that are very different from ESI- or APCI sources. Specifically, there are high densities of low energy electrons (~10^{15} cm^{-3})[40], excited state helium and nitrogen atoms, and proton donors (BrØnsted acids) that are present in the microplasma volume. In many respects the device is more like an APCI variant; though much work remains to elucidate the overall ionization scheme. To be clear, the applied field potentials here (<500 V cm^{-1}) are insufficient to affect the formation of a Taylor cone and ESI-like processes [28].

3.4 Conclusions

The LS-APGD ionization source had previously been demonstrated to provide sensitive elemental analysis of metal species in aqueous media. Simple changes in geometry and the electrolyte composition allow for sensitive probing of molecular species. Demonstrated here is the use of the same ionization source to derive molecular mass spectra of uranyl acetate. The ability for an otherwise "atomic" plasma source to produce "molecular" mass spectra from solution-phase species is totally unique. The experimental conditions were evaluated through a detailed variation of the plasma operating parameters. This series of measurements allowed for the determination of conditions providing the greatest

ionization yields, while also proving that the resultant mass spectra were fairly immune to changes in plasma conditions. This is a key point in obtaining reproducible speciation information, without experimental bias.

A study of uranyl:acetate speciation as a function of pH value was performed under the optimized operating conditions. The general spectral trends observed follow the solution chemistry as predicted by equilibrium calculations. The primary discrepancies lie in the poor ionization yield for inorganic uranyl ions and the potential degradation of the multi-ligated species. In the first case, the non-ligated species appear to be underrepresented at the lowest pH values, and in the latter case somewhat overrepresented at modest pH. Whilst direct conversion from spectral composition to accurate solution-phase speciation cannot be established at this point, the fact that the ligated species can be readily identified and that variations in discharge conditions do not directly impact the species distribution bode very well for future use of the microplasma for metal speciation in general.

Future work will concentrate on the improvement and fine-tuning of the LS-APGD source for the quantitative evaluation of metal-ligand speciation in aqueous (and perhaps non-aqueous) solution. While not applied here, the use of cooler plasma conditions could be offset by CID strategies in the MS sampling orifice or gentle “heating” within the ion trap environment. Of greater scientific importance will be well-controlled studies directed at elucidating the underlying vaporization/ionization processes occurring within the microplasma. Only after

developing such an understanding can the broader use of the device for widely-varying speciation challenges be fully realized.

3.5 Acknowledgement

This work was supported by the Defense Threat Reduction Agency, Basic Research Award # HDTRA1-14-1-0010, to Clemson University.

3.6 References

1. Haraguchi, H. *J. Anal. At. Spectrom.* **2004**, *19*, 5-14.

2. Mounicou, S.; Szpunar, J.; Lobinski, R. *Chem. Soc. Rev.* **2009**, *38*, 1119-1138.

3. Szpunar, J. *Analyst* **2005**, *130*, 442-465.

4. Fein, J. B.; Powell, B. A. In *Uranium: Cradle to Grave*, Burns, P. C.; Sigmon, G. E., Eds.; Mineralogical Association of Canada: Winnipeg, Manitoba, 2013.

5. Silva, R. J.; Nitsche, H. *Radiochim. Acta* **1995**, *70-1*, 377-396.

6. Neck, V.; Kim, J. I. *Radiochim. Acta* **2001**, *89*, 1-16.

7. Wan, J.; Tokunaga, T. K.; Brodie, E.; Wang, Z.; Zheng, Z.; Herman, D.; Hazen, T. C.; Firestone, M. K.; Sutton, S. R. *Environ. Sci. Technol.* **2005**, *39*, 6162-6169.

8. Brooks, S. C.; Fredrickson, J. K.; Carroll, S. L.; Kennedy, D. W.; Zachara, J. M.; Plymale, A. E.; Kelly, S. D.; Kemner, K. M.; Fendorf, S. *Environ. Sci. & Technol.* **2003**, *37*, 1850-1858.

9. Dong, W.; Brooks, S. C. *Environ. Sci. Technol.* **2008**, *42*, 1979-1983.

10. Di Bernardo, P.; Zanonato, P.; Bismondo, A.; Jiang, H.; Garnov, A. Y.; Jiang, J.; Rao, L. *European Journal of Inorganic Chemistry* **2006**, 4533-4540.

11. Jiang, J.; Rao, L. F.; Di Bernardo, P.; Zanonato, P.; Bismondo, A. *J. Chem. Soc., Dalton Trans.* **2002**, 1832-1838.

12. Bailey, E. H.; Mosselmans, J. F. W.; Schofield, P. F. *Geochim. Cosmochim. Ac.* **2004**, *68*, 1711-1722.

13. Kim, H. Y.; Kakihana, M.; Aida, M.; Kogure, K.; Nomura, M.; Fujii, Y.; Okamoto, M. *J. Chem. Phys.* **1984**, *81*, 6266-6271.

14. Ivanova, B.; Spiteller, M. *Environ. Sci. Pollut. Res.* **2014**, *21*, 1548-1563.

15. Shundalau, M. B.; Umreiko, D. S.; Zazhogin, A. P.; Komyak, A. I. *J. Appl. Spectrosc.* **2013**, *80*, 530-535.

16. Bhandari, D.; Wells, S. M.; Retterer, S. T.; Sepaniak, M. J. *Anal. Chem.* **2009**, *81*, 8061-8067.

17. Ruan, C.; Luo, W.; Wang, W.; Gu, B. *Anal. Chim. Acta* **2007**, *605*, 80-86.

18. Crawford, C. L.; Fugate, G. A.; Cable-Dunlap, P. R.; Wall, N. A.; Siems, W. F.; Hill, H. H. *Int. J. Mass Spectrom.* **2013**, *333*, 21-26.

19. Jaison, P. G.; Kumar, P.; Telmore, V. M.; Aggarwal, S. K. *Rapid Commun. Mass Spectrom.* **2013**, *27*, 1105-1118.

20. Pasilis, S.; Somogyi, A.; Herrmann, K.; Pemberton, J. E. *J. Am. Soc. Mass Spectrom.* **2006**, *17*, 230-240.

21. Hubert, A.; Claverie, F.; Pecheyran, C.; Pointurier, F. *Spectrochim. Acta B* **2014**, *93*, 52-60.

22. Bu, W.; Zheng, J.; Guo, Q.; Aono, T.; Tagami, K.; Uchida, S.; Tazoe, H.; Yamada, M. *J. Chromatogr. A* **2014**, *1337*, 171-178.

23. Liu, C. X.; Hu, B.; Shi, J. B.; Li, J. Q.; Zhang, X. L.; Chen, H. W. *J. Anal. At. Spectrom.* **2011**, *26*, 2045-2051.

24. Duffin, A. M.; Hart, G. L.; Hanlen, R. C.; Eiden, G. C. *J. Radioanal. Nucl. Chem.* **2013**, *296*, 1031-1036.

25. Brittain, S. R.; Cox, A. G.; Tomos, A. D.; Paterson, E.; Siripinyanond, A.; McLeod, C. W. *J. Environ. Monit.* **2012**, *14*, 782-790.

26. Lechtenfeld, O. J.; Koch, B. P.; Geibert, W.; Ludwichowski, K. U.; Kattner, G. *Anal. Chem.* **2011**, *83*, 8968-8974.

27. Moser, C.; Kautenburger, R.; Philipp Beck, H. *Electrophoresis* **2012**, *33*, 1482-1487.

28. Cole, R. B. *Electrospray and MALDI Mass Spectrometry: Fundamentals, Instrumentation, Practicalities, and Biological Applications*, 2nd ed.; John Wiley & Sons: Hoboken, 2010.

29. Treager, J. C. *Int. J. Mass Spectrom.* **2000**, *200*, 387-401.

30. Agnes, G. R.; Horlick, G. *Appl. Spectrosc.* **1992**, *46*, 401-406.

31. Agnes, G. R.; Horlick, G. *Appl. Spectrosc.* **1995**, *49*, 324-334.

32. Stewart, I. I.; Horlick, G. *Anal. Chem.* **1994**, *66*, 3983-3993.

33. McDonald, L. W. t.; Campbell, J. A.; Clark, S. B. *Anal. Chem.* **2014**, *86*, 1023-1029.

34. Dion, H. M.; Ackerman, L. K.; Hill, H. H., Jr. *Talanta* **2002**, *57*, 1161-1171.

35. Somogyi, A.; Pasilis, S. P.; Pemberton, J. E. *Int. J. Mass Spectrom.* **2007**, *265*, 281-294.

36. Luo, M.; Hu, B.; Zhang, X.; Peng, D.; Chen, H.; Zhang, L.; Huan, Y. *Anal. Chem.* **2010**, *82*, 282-289.

37. Marcus, R. K.; Davis, W. C. *Anal. Chem.* **2001**, *73*, 2903-2910.

38. Cserfalvi, T.; Mezei, P. *J. Anal. At. Spectrom.* **1994**, *9*, 345-349.

39. Webb, M. R.; Chan, G. C. Y.; Andrade, F. J.; Gamez, G.; Hieftje, G. M. *J. Anal. At. Spectrom.* **2006**, *21*, 525-530.

40. Manard, B. T.; Gonzalez, J. J.; Sarkar, A.; Dong, M. R.; Chirinos, J.; Mao, X. L.; Russo, R. E.; Marcus, R. K. *Spectrochim. Acta B* **2014**, *94-95*, 39-47.

41. Konegger-Kappel, S.; Manard, B. T.; Zhang, L. X.; Konegger, T.; Marcus, R. K. *J. Anal. At. Spectrom.* **2015**, *30*, 285-295.

42. Marcus, R. K.; Quarles, C. D., Jr.; Barinaga, C. J.; Carado, A. J.; Koppenaal, D. W. *Anal. Chem.* **2011**, *83*, 2425-2429.

43. Quarles, C. D., Jr.; Carado, A. J.; Barinaga, C. J.; Koppenaal, D. W.; Marcus, R. K. *Anal. Bioanal. Chem.* **2012**, *402*, 261-268.

44. Zhang, L. X.; Manard, B. T.; Konegger-Kappel, S.; Marcus, R. K. *Anal. Bioanal. Chem.* **2014**, *406*, 7497-7509.

45. Marcus, R. K.; Burdette, C. Q.; Manard, B. T.; Zhang, L. X. *Anal. Bioanal. Chem.* **2013**, *405*, 8171-8184.

46. Davis, W. C.; Marcus, R. K. *J. Anal. At. Spectrom.* **2001**, *16*, 931-937.

47. Bykhovski, D. N.; Guilbeau, K. E.; Ibragimov, J. I. In *Progress in Plasma Processing of Materials 1999*, Fauchais, P.; Amouroux, J., Eds.; Begell House: New York, 1999.

48. Van Stipdonk, M. J.; Chien, W.; Bulleigh, K.; Wu, Q.; Groenewold, G. S. *J. Phys. Chem. A* **2006**, *110*, 959-970.

49. Davis, W. C.; Marcus, R. K. *Spectrochimica Acta Part B-Atomic Spectroscopy* **2002**, *57*, 1473-1486.

CHAPTER FOUR

MASS SPECTRA OF DIVERSE ORGANIC SPECIES UTILIZING THE LIQUID SAMPLING-ATMOSPHERIC PRESSURE GLOW DISCHARGE (LS-APGD) MICROPLASMA IONIZATION SOURCE

4.1 Introduction

The use of electrical discharges (plasmas) as ionization sources is as old as the field of mass spectrometry (MS). Two of the most common ionization sources are the inductively coupled plasma (ICP) and the atmospheric pressure chemical ionization (APCI) devices. The ICP has been the benchmark method for performing elemental/ isotopic analysis across solid, liquid, and gaseous samples for over 30 years.[1,2] The 1-2 kW rf argon plasmas generate an intense ionization environment that efficient vaporizes and dissociates aerosol-introduced species to the atomic ion form. APCI is often the method of choice for MS analysis of small, polar, organic molecules, most often used as a detector for liquid chromatography separations.[3,4] In this case, a low current, high voltage dc potential creates a corona discharge that efficiently converts mobile phase species into CI agents in the gas phase. These discharge/plasma sources operate on very different physical mechanisms and surely have two very different fields of application.

More recently, low power plasma sources have been introduced for the probing of surfaces to affect ambient desorption ionization (ADI) MS analysis. Originating with the low current, atmospheric pressure helium glow discharge described as the DART (direct analysis in real time),[5] there are more than a dozen plasma sources and geometries which have been applied in ADI-MS.[6-12] While the mechanisms for creating these discharges are varied, thermal energy within the plasma or through heating of the gas is often used as the means of vaporizing molecular species from the sample surface. Beyond the vaporization step, ionization of volatilized species can occur via a variety of mechanisms, though predominately attributed to a CI event with agents created in the plasma.[12,13]

In an effort toward delivering a miniaturized plasma source alternative for elemental analysis, Marcus and co-workers developed the liquid sampling atmospheric pressure glow discharge (LS-APGD) source, first for optical emission (OES)[14] and then MS elemental analysis.[15,16] The LS-APGD operates at a low power (<50 W dc) with very low sample flow rates (<100 µL min^{-1}) and small sample volumes (10 µL), wherein the microplasma is sustained between the surface of the electrolyte carrier solution and a metallic counter electrode. The gap between the electrodes (0.5 – 2 mm) effectively controls the power density of the discharge. In concept, this device is related to the electrolyte cathode discharge (ELCAD), designed by Cserfalvi and co-workers,[17] and further characterized and improved by Hieftje and co-workers under the name of solution cathode glow discharge (SCGD).[18,19] The distinction is that the size of LS-APGD

yields much higher power densities (>10 W mm^{-3}) providing sufficient energy for operation in a total-consumption mode as well as serve as a source for the elemental analysis of particles generated via laser ablation (LA).[20-22]

Implementation of the device as an elemental ionization source was first undertaken on a high resolution Thermo Scientific LTQ Orbitrap mass spectrometer.[15,23] Further characterization took place on a Thermo Scientific LCQ, ion trap spectrometer.[16] In both instances, the microplasma was simply mounted in the place of the commercial ESI source. A detailed parametric evaluation was performed to better understand factors affecting overall spectral composition, target analyte (metals) signal intensities and signal-to-background ratios (S/B), and the limits of detection (LODs).[16] Of relevance to the work described here, the LS-APGD has been demonstrated to operate effectively in an ADI-MS mode, yielding high quality "molecular" mass spectra.[11] More recently, the use of the microplasma to assess the metal-ligand speciation of uranyl acetate has been presented.[24] In that work, use of a mixed solvent electrolyte solution was found to "cool" the plasma such that complete dissociation of solutes (required in elemental MS) did not occur. Operation in a 70:30 MeOH:H_2O electrolyte flow allowed direct injection of the metal acetates, with the product mass spectra readily revealing the changes in ligation as a function of pH. Based on that work, it is obvious to ask the question as to whether this microplasma ionization source could generate high quality mass spectra from organic compounds injected in the solution phase. In

short, can the same ionization source be employed for both “atomic” and “molecular” mass spectrometry, in fact on the same mass analyzer system?

We present here preliminary efforts in the use of the LS-APGD microplasma as an ionization source for a variety of organic molecules. As reflected in the previous ADI-MS and metallo-organic speciation reports,[11,24] the predominately-water vapor microplasma environment is rich in active species such as H^+ and protonated solvent clusters which act as BrØnsted acid CI agents. Use of a 70:30 MeOH:H_2O electrolyte yields a “softer” environment versus the 1M HNO_3 used in elemental MS, and therefore can be expected to generate molecular ions from organic compounds. The LS-APGD mass spectra for a diverse set of organic compounds are presented here, demonstrating the basic characteristics that might be achieved. Caffeine is used as a test compound to initially assess the role of microplasma operation conditions on the total ion response as well as levels of fragmentation. The ability of the LS-APGD to produce molecular ions directly from organic compounds in solution, places the device in a very unique position among the myriad of MS ionization sources. These multiple functions (elemental/isotopic/molecular) on a single platform, that can be easily interfaced with the existing commercial mass spectrometry systems, suggest a good deal of potential.

4.2 Experimental Section

4.2.1 Sample preparation.

Test samples were made as 10^{-5} M solutions of the selected compounds in 70:30 MeOH:H_2O solution (matching the carrier electrolye composition). The compounds were selected to represent a range in molecular weights, chemical stability, and chemical function. Caffeine (99.7%) and the common MS standard Ultramark® 1621 (95%) were purchased from Alfa Aesar (Ward Hill, MA); sinapic acid (99%) and myoglobin (>95%) were obtained from Sigma-Aldrich, Co. LLC (St. Louis, MO, USA), daidzin (>99%) was purchased from BIOTANG Inc. (Lexington, MA), and the fluorescein isothiocyanate-labelled lipid tethered ligand (FITC-LTL) was synthesized in this laboratory.[25] Methanol (HPLC grade) was purchased from Burdick & Jackson, Honeywell International (Morristown, NJ), and mixed with deionized water (DI-H_2O) that prepared by a NANOpure Diamond Barnstead/Thermolyne Water System (18.2 MΩ cm^{-1}) (Dubuque, IA). 1 M HNO_3 was diluted from concentrated nitric acid (trace grade) purchased from BDH Chemicals (Poole Dorset, UK).

4.2.2 LS-APGD ionization source.

The basic LS-APGD ionization source design and operation principles as they apply to elemental MS have been described in detail previously.[16] In fact, no changes have been made in moving to molecular MS except the change in electrolyte composition from 1 M HNO_3 to 70:30 MeOH:H_2O. Power was provided

to the counter electrode by a direct current (d.c.) Bertan Model 915 series positive polarity power supply (Hickville, NY, USA); 0-100 mA, 0-1 kV, through a 10 kΩ, 50 W resistor (HS50, Arcol UK Ltd, Truro Cornwall, UK). Helium (99.99%) was introduced between the surrounding stainless steel capillary and the glass capillary to serve as sheath/cooling gas (0.1-1. L min^{-1}), while the electrolyte flow (5-50 µL min^{-1}) was pumped through the glass capillary using a syringe pump (NE-1000, New Era Pump Systems, Farmingdale NY, USA). Four operation parameters were studied in terms of the spectral response of the caffeine test compound: liquid/sampling flow rate (5-30 µL min^{-1}), He gas flow rate (0.1-1.1 L min^{-1}), discharge current (5-30 mA), and plasma sampling distance (0.25-1.25 cm). In all cases, triplicate 20 µL samples were introduced using a manual six-port injector. The repeatability of these measurements generally displayed precision of better than 8% RSD.

Mass spectrometer system. A LCQ Advantage Max™ ion trap mass analyzer from Thermo Scientific (Waltham, MA, USA) was used to detect the ions produced in the glow discharge, and the accompanying Xcalibur™ data acquisition software were used for further data processing (i.e. background subtraction). As in the previous report,[16] the LS-APGD stage is mounted directly in the place of the equipped ESI source; with no changes to the ion sampling interface. The system *auto-tune* function was employed based on the signal intensity of the molecular ion for each compound, with no form of collisional activation (e.g., CID) employed.

4.3 Results and Discussion

4.3.1 Parametric Evaluation using Caffeine as the Test Compound.

Investigations into the behavior of the metallo-organic compound uranyl acetate pointed to the need to operate the plasma in less kinetically energetic conditions to preserve molecular information in the product mass spectra.[24] Key in that work was the realization that use of a mixed-solvent electrolyte provided the desired spectral features. This concept is demonstrated for the test compound caffeine, with the mass spectra (Fig. 4.1) derived from the normal a) 1 M HNO_3 solvent and the b) 70:30 MeOH:H_2O found optimal in the uranyl acetate studies.[24] Clearly seen is the shift from a spectrum that reflects electron ionization (EI)-type fragmentation where the 138 Da fragment dominates, to one which provides an $(M+H)^+$ base peak at 195 Da and far higher analyte ion counts. This response is interpreted as the mixed-solvent plasma having a lower kinetic temperature (though this must be proven spectroscopically). The fused-ring caffeine molecule is structurally robust in comparison to uranyl acetate, which yielded virtually no molecular ion peak in the pure nitric acid solvent. It should be stated, while the 70:30 MeOH:H_2O solvent had indeed been chosen through a variation of compositions in the case of the uranyl acetate studies, the same will need to be validated in the future across other "molecular" analyte systems.

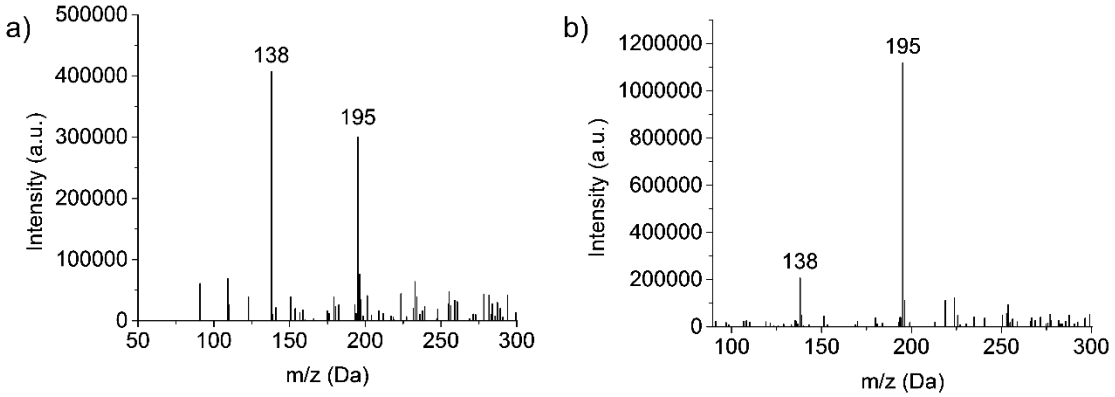

Figure 4.1 Caffeine spectral composition based on use of "elemental" and "molecular" electrolyte solutions, respectively: a) 1 M HNO_3 and b) 70:30 MeOH:H_2O. Discharge conditions: discharge current = 20 mA, solution flow rate = 10 µL min^{-1}, sheath gas flow rate = 0.9 L min^{-1}, and plasma sampling distance = 0.75 cm

Previous LS-APGD-MS studies demonstrated that changes in the individual parameters' effect, as well as inter-parametric co-effects, on the observed metal ion intensities, metal oxide fractions, and signal-to-background (S/B) ratios for elemental analysis.[16] Likewise, detailed parametric evaluations showed that the product mass spectra could be affected by the operation and ion sampling conditions. Figure 2 presents the responses of the caffeine psuedomolecular ion ($(M+H)^+$) at m/z = 195 Da and the ratio of the 138 Da/195 Da signals (reflective of the fragmentation of the molecule) as a function of the microplasma operation parameters. The responses reflect the peak height of the signal transient of the two species for triplicate 20 µL injections of 10^{-5} M caffeine in the 70:30 MeOH:H_2O carrier. The investigated parameter space was based on the previous uranyl acetate work.

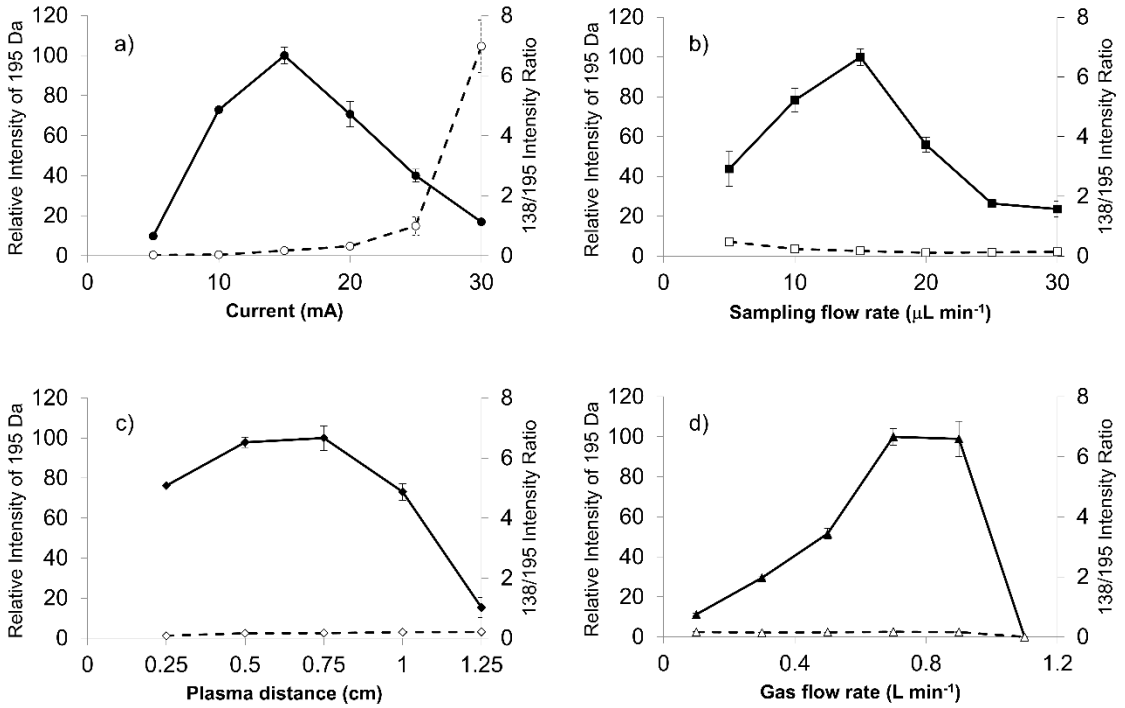

Figure 4.2 Evaluation of LS-APGD operating parameters on the response of the 195 Da (M+H) psuedomolecular ion and the ratio of the 138 Da/195 Da responses utilizing triplicate 20 µL injections of 10^{-5} M caffeine in 70:30 MeOH:H_2O. a) Role of discharge current (solution flow rate = 15 µL min^{-1}, plasma sampling distance = 0.75 cm, sheath gas flow rate = 0.7 L min^{-1}), b) Role of solution flow rate (discharge current = 15 mA, plasma sampling distance = 0.75 cm, sheath gas flow rate = 0.7 L min^{-1}), Role of plasma sampling distance (discharge current = 15 mA, solution flow rate = 15 µL min^{-1}, sheath gas flow rate = 0.7 L min^{-1}), and c) Role of sheath gas flow rate (discharge current = 15 mA, solution flow rate = 15 µL min^{-1}, plasma sampling distance = 0.75 cm).

The current at which the microplasma operates directly controls the energy available for solution vaporization and the subsequent gas phase processes including desolvation and ionization. As in seen in Fig. 4.2a, the initial increase in current yields greater M+H response, as the added energy is used to advantage. Previous optical emission studies suggest that the kinetic temperature of the

microplasma does increase as a function of discharge,[22] and so one would expect greater levels of gas phase desolvation will occur, likely yielding greater ion responses. Beyond a discharge current of 15 mA, there is a dramatic decrease in the psuedomolecular ion response, that is complemented by an increase in the 138/195 ratio. This pair of effects suggests increased collisional dissociation (fragmentation) as the discharge current increases. As the total response for the caffeine analyte remains fairly constant across this range, it seems clear that the added energy (via current) is channel into dissociation of previously protonated molecular species. It is important to note throughout this set of studies that the microplasma operates quite stably for the triplicate, 20 µL (~40 ng mass) caffeine injections. While not the focus of the present work, preliminary evaluation of the limits of detection based on triplicate injections at the 10^{-5} M caffeine level yield a value of 5.9×10^{-9} M (43 pg) using the SNR-RSDB method.[16] This value, as a single point measurement, is biased high. A more thorough analytical characterization will be the focus of future reports.

The solution flow rate into the microplasma will affect the total solvent load on the discharge, and thus the amount of work that must be done to vaporize and desolvate the solute molecules. Energy consumed to affect these processes is lost towards affecting the remainder of necessary ionization events, etc. The higher flow rate should be reflected in higher analyte delivery rates per unit time to the glow discharge, which explains the intensity increases seen in Fig. 4.2b for the M+H species as the electrolyte (carrier) flow rate increases from 5 µL min^{-1} to 15

μL min^{-1}. Depending upon the available energy in the microplasma (set principally by the discharge current), the solvent vaporization and subsequent gas-phase desolvation consume greater proportions of the total, and so the net result is fewer observed analyte ions. This response is generally classified under the umbrella of "solvent loading" with respect to other flame and plasma sources. These same effects are seen in both the OES and MS elemental analysis modes for the LS-APGD source.[23,24,26] In fact, in those works it is clear that higher flow rates, even with higher discharge currents, simply generate more solvent-related signals. For the 15 mA discharge current here, the onset of this set of effects is quite clear. Indeed, the lower energy for the downstream gas-phase processes (i.e., ionization and fragmentation) is reflected in the decreasing 138/195 ratio as a function of increasing solvent flow rate.

The roles played by the plasma sampling distance and gas flow rate are manifest in the ion delivery to the mass spectrometer ion sampling orifice, with their net effects being inter-related as seen in previous elemental MS studies.[16] Longer sampling distances at a given gas flow rate result in longer residence times and lower collection efficiency due to increased solid angles of acceptance. Likewise, higher gas flow rates should reduce residence times and provide a greater exclusion of ambient species. (At this point it is not clear what, if any, role the helium atoms play in the plasma ionization processes.) Assuming that the M+H ions are formed in the gas phase following solute desolvation, there is some required residence time to effect the most efficient ionization (interaction with the

BrØnsted acid CI agent and proton transfer). Beyond this time (distance), the propensity for ion-neutral interactions increases. These reactions could be chemical in nature causing the loss of the desired analyte ions (either through further proton transfer or adduct formation) or result in greater amounts of collisional fragmentation.

As presented in Fig. 4.2c, there are indeed trade-offs in the M+H response as a function of the sampling distance. The trends here are in agreement from the simple picture presented above. For example, the amounts of solvent-adduct species are most pronounced (albeit at low levels (<10%)) at sampling distances ≤0.5 cm, decreasing substantially with increasing separation. The previous studies showed that longer sampling distances greatly increased the proportion of metal oxide formation versus atomic ions.[16] Different here, spectral interrogation for the formation of caffeine adduct ions provided no evidence that secondary gas-phase reactions was a loss mechanism. Finally, it is clear through the invariance in the 138/195 ratio that the increased distance/residence time does not add appreciably to the amount of collision dissociation observed. This makes sense as these further distances are removed from the energetic regions of the plasma, in fact they are likely at temperatures approaching ambient conditions.[27] Thus, in lieu of more detailed optical and mass spectrometric mapping, it seems reasonable that the loss in signal as a function of sampling distance is dominated by dispersion effects.

For a fixed sampling distance, the role of the sheath gas flow is to improve ion transport and exclude ambient gases. As shown in Fig. 4.2d for a 0.75 cm sampling distance, the gas flow rate operates as projected above. At low flow rates, increases result in much improved transport as evidenced in the m/z = 195 Da response. At the highest flow rates, though, there is a dramatic drop in that signal and the onset of plasma instability. In this case, analogous to short sampling distances, the residence time in the microplasma is reduced, perhaps to levels wherein solute vaporization and ionization are not kinetically favorable prior to ion acceptance. As in the case of the sampling distance, there is little effect of gas flow rate on the observed degree of fragmentation nor is there any indication that the extent of adduct formation is influenced by the sheath gas flow.

The responses for both the psuedomolecular ion of caffeine and the relative extent of fragmentation ((i.e., 138 Da/195 Da) presented in Fig. 4.2 yield no particular surprises. The trends here build upon insights gained in the corresponding parametric evaluation towards elemental MS use of the LS-APGD. The monitoring of the degree of fragmentation as a function of discharge conditions clearly pointed to the critical aspects that affect the energy (kinetic temperature) within the discharge region, discharge current and solvent loading. While no single molecular species can be used as a comprehensive model for the processes relevant to ionization of every potential analyte, the lessons learned here are carried over to the initial spectral characterization of diverse organic molecules. As such, a generalized set of glow discharge conditions is identified: discharge

current of 15 mA, liquid sampling flow rate of 15 µL min^{-1}, the sampling distance of 0.75 cm and the helium gas flow rate of 0.7 L min^{-1}.

4.3.2 Spectral Characteristics of Diverse Organic Compounds.

As described in the experimental section, six different organic compounds were selected as test samples. As there is a range of chemistries and molecular weights/structures, To be sure, the range of solutes investigated here is immense when one projects what might be expected from an energetic *atomic* ion source. All sample solutions were injected into the plasma at the uniform operating conditions, and the obtained spectra presented in Fig. 4.3. In each case, we make qualitative spectral comparisons with the most common organic, molecular ionization sources; ESI and APCI (where they are available). It must be emphasized that even for these two established methods, there will be differences in spectral features among laboratories that are attributable to specific source operation conditions, solvent composition, and MS operation parameters. As such, the comparisons are only provided for general perspective.

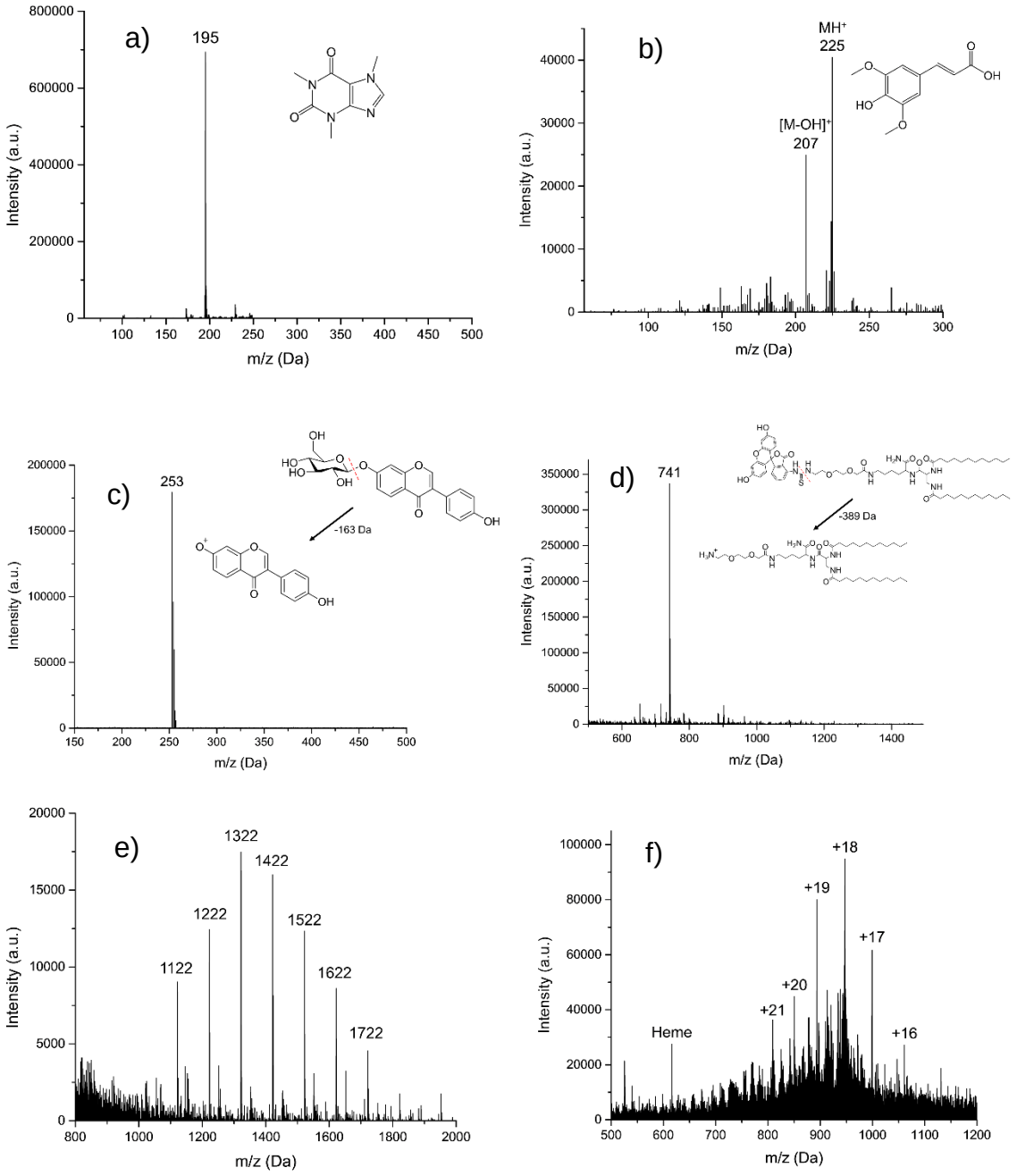

Figure 4.3 Spectral patterns for the representative organic molecule classes: a) caffeine, b) sinapinic acid, c) daidzin, d) FITC-LTL, e) Ultramark 1621, and f) myoglobin. Solutes introduced as 20 µL aliquots of 10^{-5} M dilutions in 70:30 MeOH:H_2O solution flow. Discharge conditions: current = 15 mA, solution flow rate = 15 µL min^{-1}, plasma sampling distance = 0.75 cm, and sheath gas flow rate = 0.7 L min^{-1}. In each case, no signals above 5% relative intensity to the base peak are seen outside of the displayed mass range.

For small polar molecules such as caffeine (Fig. 4.3a) and sinapinic acid (Fig. 4.3b), the base peak in the LS-APGD mass spectrum is the protonated, psuedomolecular ion $(M+H)^+$. Different from the conditions employed in Fig. 4.1, the microplasma here generates this ion almost exclusively, with almost no fragmentation observed. Given the fused ring structure of caffeine, the lack of appreciable fragmentation is not surprising. This spectrum is virtually identical to what is seen in APCI-MS,[28] while for ESI-MS there is a small amount of fragmentation,[29] with the 79 Da fragment being the most prominent.

In the case of sinapinic acid (Fig. 4.3b), a common matrix employed in MALDI-MS, the BrØnsted acid CI product is the primary ion, but there is appreciable response related to the loss of the hydroxyl group, most likely the one related to the carboxylic acid moiety. Given the structure of that molecule, and its added degrees of freedom, collisional/thermal activation is not unexpected, and thus more low-intensity fragments are seen versus caffeine. The corresponding ESI mass spectrum is composed of the same two ions (M+H and M-OH), though with the fragment ion being the base peak of the spectrum.[30]

Certain compounds are thermally unstable, thus no molecular ions are detected in the LS-APGD spectra. As an example of daidzin (Fig. 4.3c), a common flavonoid compound, the glycoside (sugar) moiety is lost (as depicted) in post-ionization degradation, resulting in highest abundance from the base aglycone fragments. Here again, such fragmentation is not unexpected, though the non-existence of any sort of molecule ion is surprising. In the case of both APCI and

ESI-MS, the protonated psuedomolecular ion is the base peak, with the sole fragment being the aglycone unit.[31,32] In both cases the compounds exist as a pronated ions.

The microplasma-produced mass spectrum for the laboratory-synthesized, FITC-labeled ligand tethered ligand (FITC-LTL) (Fig. 4.3d) also reflects the more energetic (higher kinetic temperature) environment versus ESI-MS. In this case, the otherwise stable FITC unit is lost, as illustrated in the diagram. What is surprising in this case is the minimal amount of overall fragmentation, as certainly its structure would suggest that would be the case. The ESI mass spectrum obtained in this laboratory,[25] on the other hand, is composed solely of the protonated molecular ion at m/z = 1130 Da, with an added solvent adduct ion. In both the cases of the natural project and the lipid, the observed fragmentation is far less than might be inferred based on optical emission-based temperature measurements on the order of 800-1200 K.[22]

The final two compounds, Ultramark 1621 (a commercially available mixture of fluorinated phosphazines) and the protein myoglobin, present a totally different set of challenges and potential ionization pathways to the other test compounds. The Ultramark spectrum in Fig. 4.3e depicts the expected distribution of different molecular weight species, with the specific singly-protonated mass marker appearing at 1621.9 Da. There is appreciable spectral background below 1000 Da, which could be from fragmentation of these molecules, composed of fluorocarbon chains emanating from a cyclic phosphazine core. However, the

spectrum range from 1000-2000 Da is clean. ESI-MS yields a similarly-composed spectrum,[33] reflective of the protonation of basic sites of the molecules in the course of the electrospray process. The mass spectrum for myoglobin (Fig. 4.3f) displays a range of peaks representing different degrees of protonation. As in the case of ESI-MS, it is clear that the ionization takes the form of multiple proton additions.[34] As noted previously, the precise charge state distributions for ESI mass spectra are a function of many parameters, and so there is little to be gained at this stage in direct comparisons. What is decidedly different in the LS-APGD spectrum, is the clear presence of a signal corresponding to the heme group in the protein, which is not present in most ESI spectra.

Based on the ionization behavior/spectral pattern of the molecules tested, and in comparison to the literature, it is reasonable to say the collisional energetics of the LS-APGD ionization source is somewhere between an APCI source and an ESI source. With thermally stable and smaller molecules, the spectra are much cleaner and the signal intensity is strong, the spectra pattern is very similar with ones obtained from APCI. On the other hand, the LS-APGD produces mass spectra for macromolecules for which APCI is not applicable, such as the Ultramark compound. In the case of the protein, the ionization source yields spectra that composed similar to those of ESI-MS, but it would seem unlikely that in-solution/droplet ionization processes are occurring in the LS-APGD system. Indeed, based on a first-principles analysis, any sort of aerosol generation mechanism based on the formation of a Taylor cone and subsequent coulombic

fission[35] are not going to occur at the fields strengths used to create the LS-APGD microplasma.

4.4 Conclusions

The liquid sampling-atmospheric pressure glow discharge (LS-APGD) ionization source had previously been demonstrated to provide sensitive elemental analysis in aqueous electrolytic solution. Modification of the electrolytic solution composition provides the capacity for organic compounds analysis, yielding molecular mass spectra of high information content. The roles of the microplasma operating conditions on the basic spectral responses were evaluated for the test compound, caffeine. It was observed, that the relative extent of fragment ions corresponded to the energy input; with greater extents seen at higher discharge currents and lower liquid flow rates. The spatial profiling of the plasma suggests that a succession of processes occurs. The resultant mass spectra for the various test compounds are very much in line with a process where solution-phase solutes are vaporized and subsequently cationized via a proton transfer step, with spectral features very much like seen for ESI- and APCI-MS.

Future work will concentrate on the improvement and fine-tuning of the LS-APGD source and developing a deeper level of understanding of the fundamental processes occurring the microplasma with regards to organic molecule analysis. There is a wealth of quantitative characterization that must also occur. During such studies, a wide range of compounds having different chemical/physical

properties should be used to allow well-controlled, multi-parameter studies. It is believed that the LS-APGD ionization source, having multiple functions in one device, holds a unique position among atmospheric pressure discharges and has great potential to be utilized in many fields of analysis; from elemental/isotopic analysis to perhaps proteomics.

4.5 Acknowledgement

This work was supported by the Defense Threat Reduction Agency, Basic Research Award # HDTRA1-14-1-0010, to Clemson University. LXZ wishes to thank Liuwei (Jerry) Jiang for supplying the lipid test compound and many helpful discussions.

4.6 References

1. Houk, R. S.; Fassel, V. A.; Flesch, G. D.; Svec, H. J.; Gray, A. L.; Taylor, C. E. *Anal. Chem.* **1980**, *52*, 2283-2289.

2. Montaser, A.; Wiley-VCH: Weinheim, 1998.

3. Bruins, A. P.; Covey, T. R.; Henion, J. D. *Anal. Chem.* **1987**, *59*, 2642-2646.

4. Rosenberg, E. *J. Chromatogr. A* **2003**, *1000*, 841-849.

5. Cody, R. B.; Laramee, J. A.; Durst, H. D. *Anal. Chem.* **2005**, *77*, 2297-2302.

6. Harris, G. A.; Galhena, A. S.; Fernandez, F. M. *Anal. Chem.* **2011**, *83*, 4508-4538.

7. Harper, J. D.; Charipar, N. A.; Mulligan, C. C.; Zhang, X. R.; Cooks, R. G.; Ouyang, Z. *Anal. Chem.* **2008**, *80*, 9097-9104.

8. Salter, T. L.; Gilmore, I. S.; Bowfield, A.; Olanbanji, O. T.; Bradley, J. W. *Anal. Chem.* **2013**, *85*, 1675-1682.

9. Nyadong, L.; Galhena, A. S.; Fernandez, F. M. *Anal. Chem.* **2009**, *81*, 7788-7794.

10. Shelley, J. T.; Wiley, J. S.; Chan, G. C. Y.; Schilling, G. D.; Ray, S. J.; Hieftje, G. M. *J. Am. Soc. Mass Spectrom.* **2009**, *20*, 837-844.

11. Marcus, R. K.; Burdette, C. Q.; Manard, B. T.; Zhang, L. X. *Anal. Bioanal. Chem.* **2013**, *405*, 8171-8184.

12. Albert, A.; Shelley, J. T.; Engelhardt, C. *Anal. Bioanal. Chem.* **2014**, *406*, 6111-6127.

13. Andrade, F. J.; Shelley, J. T.; Wetzel, W. C.; Webb, M. R.; Gamez, G.; Ray, S. J.; Hieftje, G. M. *Anal. Chem.* **2008**, *80*, 2646-2653.

14. Marcus, R. K.; Davis, W. C. *Anal. Chem.* **2001**, *73*, 2903-2910.

15. Marcus, R. K.; Quarles, C. D., Jr.; Barinaga, C. J.; Carado, A. J.; Koppenaal, D. W. *Anal. Chem.* **2011**, *83*, 2425-2429.

16. Zhang, L. X.; Manard, B. T.; Konegger-Kappel, S.; Marcus, R. K. *Anal. Bioanal. Chem.* **2014**, *406*, 7497-7509.

17. Cserfalvi, T.; Mezei, P. *J. Anal. At. Spectrom.* **1994**, *9*, 345-349.

18. Webb, M. R.; Andrade, F. J.; Gamez, G.; McCrindle, R.; Hieftje, G. M. *J. Anal. At. Spectrom.* **2005**, *20*, 1218-1225.

19. Webb, M. R.; Chan, G. C. Y.; Andrade, F. J.; Gamez, G.; Hieftje, G. M. *J. Anal. At. Spectrom.* **2006**, *21*, 525-530.

20. Carado, A. J.; Quarles, C. D., Jr.; Duffin, A. M.; Barinaga, C. J.; Russo, R. E.; Marcus, R. K.; Koppenaal, D. W. *J. Anal. At. Spectrom.* **2012**, *27*, 385-389.

21. Quarles, C. D.; Gonzalez, J.; Choi, I.; Ruiz, J.; Mao, X.; Marcus, R. K.; Russo, R. E. *Spectrochim. Acta B* **2012**, *76*, 190-196.

22. Manard, B. T.; Gonzalez, J. J.; Sarkar, A.; Dong, M.; Chirinos, J.; Mao, X.; Russo, R. E.; Marcus, R. K. *Spectrochim. Acta Part B* **2014**, *94*, 39-47.

23. Quarles, C. D., Jr.; Carado, A. J.; Barinaga, C. J.; Koppenaal, D. W.; Marcus, R. K. *Anal. Bioanal. Chem.* **2012**, *402*, 261-268.

24. Zhang, L. X.; Manard, B. T.; Powell, B. A.; Marcus, R. K. *Anal. Chem.* **2015**, *87*, 7218-7225.

25. Jiang, L.; Schadock-Hewitt, A. J.; Zhang, L. X.; Marcus, R. K. *Analyst* **2015**, *140*, 1523-1534.

26. Quarles, C. D.; Manard, B. T.; Burdette, C. Q.; Marcus, R. K. *Microchem. J.* **2012**, *105*, 48-55.

27. Davis, W. C.; Marcus, R. K. *Journal of Analytical Atomic Spectrometry* **2001**, *16*, 931-937.

28. Arinobu, T.; Hattori, H.; Kumazawa, T.; Lee, X. P.; Mizutani, Y.; Katase, T.; Kojima, S.; Omori, T.; Kaneko, R.; Ishii, A.; Seno, H. *Forensic Toxicology* **2009**, *27*, 1-6.

29. Dalmazio, I.; Santos, L. S.; Lopes, R. P.; Eberlin, M. N.; Augusti, R. *Environmental Science & Technology* **2005**, *39*, 5982-5988.

30. Wada, Y.; Mass Spectrometry Society of Japan, 2011.

31. Rong, H. J.; Stevens, J. F.; Deinzer, M. L.; De Cooman, L.; De Keukeleire, D. *Planta Medica* **1998**, *64*, 620-627.

32. Tohge, T.; Massbank, 2011.

33. Moini, M. *Rapid Communications in Mass Spectrometry* **1994**, *8*, 711-714.

34. M. J. Powell, T. T. R., A. D. Biddle, and G. R. Asbury. *BioTechniques Special Issue* **2009**, *46*, 2.

35. Cole, R. B.; John Wiley & Sons: Hoboken, 2010.

CHAPTER FIVE

SUMMARY

The aim of this dissertation was to emphasize the importance of the development of the liquid sampling-atmospheric glow discharge (LS-APGD) as a multi-functional ionization source for mass spectrometry. Chapter 1 outlined different types of ionization sources along with their ionization mechanism and highlighted the advantages of LS-APGD as ionization source to obtain both atomic and molecular information. Chapter 2 has been published by *Analytical and Bioanalytical Chemistry* (doi: 10.1007/s00216-014-7990-6), which is a detailed study of the operating parameters, including the individual effect of each parameter onto the mass spectra, and the inter-parametric relationships. The parametric evaluation lead to a better fundamental understanding of the LS-APGD operating and plasma physics and chemistry. Such knowledge is then further employed into the improvement of the LS-APGD, to solve challenged analytical problem. Chapter 3 (published by *Analytical Chemistry*, doi: 10.1021/acs.analchem.5b01637) and 4 (published by *Journal of Analytical Atomic Spectrometry*, doi: 10.1039/C5JA00376H) are the further development of the LS-APGD to a softer ionization source, using a different mobile phase (70:30 MeOH:H_2O) as electrolytic solution to operate the plasma. This modification allows for the ability of obtain metal-ligand speciation information and molecular information of the analyte directly from aqueous phase

sampling. Uranyl –acetate aqueous system was studied in details, as the uranyl –acetate speciation as a function of pH values of the solution, after the optimization of the operating parameters. The general spectral trends observed follow the solution chemistry as predicted by equilibrium calculations. Chapter 4 presented the analysis of organic compounds utilizing LS-APGD, with resultant mass spectra very much likely following a process where solution-phase solutes are vaporized and subsequently cationized via proton transfer step, with spectral features very similar to ESI- and APCI-MS.

The research presented here has established the base knowledge necessary to continue the work on the improvement of the LS-APGD in this laboratory. Future studies will continue to on fundamental understanding on the ionization mechanisms, determine the analytical figures of merits under various operating modes, and use it to solve the challenged analytical problem.

APPENDICES

APPENDIX A.

DETERMINATION OF ISOFLAVONE CONTENT IN SRM 3238 USING LIQUID CHROMATOGRAPHY-PARTICLE BEAM/ELECTRON IONIZATION MASS SPECTROMETRY

A.1 Introduction

Soy has been a regular part of the diet in many countries for centuries, and as a result, soybeans and soy-based products are among the most studied foods for their potential health benefits and risks. Epidemiologic studies over the last decade have suggested that soy-containing foods and supplements offer protective effects against a number of chronic diseases, including heart disease, breast cancer, and endometrial cancer [1-5]. Isoflavones, the naturally occurring phytoestrogen components of soy, have gained considerable attention for their potential role in reducing risk factors for these diseases [2,3]. This interest, in turn, has led to more commercially available dietary supplements and functional foods containing isoflavones [1,2,6]. Not coincidently, the use of dietary supplements continues to increase as the public becomes more concerned about lifestyle and health. The 2013 HerbalGram *Herb Market Report* released by the American Botanical Council estimated the total retail sales of herbal and botanical dietary supplements in the United States at 6 billion USD, which is an increase of an estimated 7.9 % from the previous year and the highest observed growth

percentage since the late 1990s [7]. Isoflavone supplement total sales were 8.7 million USD in 2013, ranking 21st of the top-selling herbal dietary supplements.

The considerable level of herbal supplement use has brought increased awareness for consumer safety and regulations on supplement products. In 1994, the Dietary Supplement Health and Education Act (DSHEA) defined and described in detail terminology concerning dietary supplements. Included were regulations concerning the identity, purity, and biological function of the active ingredients and accurate presentation on the labels of supplement products. Additional complications exist as there may be variations in the chemical content of similar botanicals due to differences in growth locations, seasons, production years, and other environmental conditions, making it nearly impossible to have a single chemical-content fingerprint matched to every product. In order to achieve sufficient accuracy in herbal product analyses, the availability of matrix-matched materials for validation of measurements is essential. The Chemical Sciences Division of the National Institute of Standards and Technology (NIST, Gaithersburg, MD), in collaboration with the Office of Dietary Supplements (ODS) at the National Institutes of Health (NIH), has developed dietary supplement Standard Reference Materials (SRMs) with certified values reported for specific analytes across various representative matrices [8]. These materials are used to assess the accuracy and precision of analytical methods used by the manufacturers to determine the content of their products. The SRMs are characterized using multiple, orthogonal analytical methods, often in different laboratories, to evaluate sources of

measurement bias and establish certified values. NIST has recently developed a suite of soy-based SRMs with certified and reference values for isoflavones, including soy flour, soy protein isolate, soy protein concentrate, and a soy-containing solid oral dosage form.

The analysis of botanical materials requires extensive sample pretreatment steps to achieve complete extraction of the analytes of interest, and sample pretreatment can lead to sample degradation, contamination, and loss. An appropriate extraction procedure should isolate all analytes of interest from the sample matrix in the smallest volume of solvent compatible with subsequent analysis techniques [9]. Maintaining the original chemical profile is a consideration, meaning that all the target compounds are detected in the same chemical/structural form as present in the original botanical material. Isoflavones in particular are sensitive to UV photodegradation, high temperatures, and pH extremes, which need to be taken into account when choosing an extraction method, paired with adequate storage conditions. In the case of isoflavones, the chemically similar compounds must be separated prior to spectrometric detection. Methods providing high information content (i.e., MS vs absorbance detection) help to ensure selective determinations.

A variety of approaches have been reported for the extraction of isoflavones from soy bean matrices that utilize soaking, physical agitation, sonication, or maceration with various solvents [10-13]. More recently, extraction procedures such as pressurized liquid extraction (PLE) [14,15], supercritical fluid

extraction (SFE) [16-18], and microwave-assisted extraction (MAE) [19-21] have been reported for isoflavone extraction from botanical materials. The common solvents for the extraction of isoflavones are aqueous solutions containing a high percentage of organic solvents (50 % to 90 %, v/v), including methanol, ethanol, acetonitrile, and/or acetone. Additives, such as acids, have also been used to accelerate extraction and inhibit precipitation [22]. Extraction times vary from 30 min to 24 h, and temperatures used range from 4 °C to 80 °C. Most of these methods do not achieve full extraction of target analytes, and so the combination of several methods is common [10,13,21]. A review of the literature shows that laboratories employ some combination of sonication and/or agitation with centrifugation, filtration, and/or dilution steps following the initial chemical extraction due to ease and availability of the procedures [13]. Other steps, such as pre-concentration, hydrolysis, and/or filtration, may also be necessary depending on the composition of the resulting extract and the stability of extracted compounds [23-25].

The final steps, essential for achieving accurate quantitation, are the separation and detection of target compounds. The most widely used analytical technique for the characterization of isoflavones is reversed phase (RP) LC in combination with absorbance detection [26-28], due to its simplicity, general sensitivity, stability, and relatively low instrumentation costs. This method is highly efficient and reproducible, however, the use of absorbance detection has limitations related to the lack of analyte specificity. Isoflavones generally absorb

UV light optimally in the wavelength range of 250 nm to 270 nm, coincident with other compound classes commonly seen in botanical materials. Species-specific spikes of suspected components aids in the identification of eluting compounds as they yield increased absorbance values for the coincident peak in the analytical chromatogram. Alternatively, reports have described the use of LC coupled with electrospray ionization mass spectrometry (ESI-MS) to provide more specific identification of the isoflavones [29-31]. The approach described here involves use of LC in tandem with electron ionization (EI) MS to fully separate the analytes and provide single-charged molecular ions with an appreciable amount of predictable fragmentation. The major challenge of coupling LC with EIMS is that LC solvents/vapors must be removed before the analytes arrive in the ionization chamber. Marcus et al. have employed a particle beam (PB) interface to remove solvents between LC and the low-pressure environment of an EI source for the analysis of botanical products and for metal speciation studies [32-36]. The PB has two major components (Figure A1): a thermoconcentric nebulizer and a two-stage momentum separator. The function of each component is described in the Experimental Section.

The work presented demonstrates the development of a method using the PB interface to couple LC to the EIMS for the determination of the isoflavone content in NIST SRM 3238 Soy-Containing Solid Oral Dosage Form. Five target isoflavones (daidzein, genistein, genistin, daidzin, and glycitin) were characterized using LC-PB/EIMS, with the quantitative results compared with the values from the

NIST Certificate of Analysis. In this study, a chemically similar, but non-isoflavone compound, 7-hydroxy-4-chromone is employed as the internal standard (IS) [34]. Studies that use IS quantitation select either an isoflavone compound *not believed* to be present in the specific matrix (for absorbance detection) or stable isotope labeled (e.g., deuterium, ^{13}C) isoflavone compounds for each analyte of interest (for MS detection). As shown in Figure A2, the chemical structure of 7-hydroxy-4-chromone is in fact similar to the base structure of all of the target isoflavones, leading to similar behavior in the absorbance and MS ionization modes. The general strategy employed here provides a very useful alternative for botanical product characterization in terms of the simplicity of the extraction, use of the simple IS compound, and the use of EIMS as a detection tool.

A.2 Experimental

A.2.1. Reagents

a) Water- High purity, deionized using a NANOpure Diamond water system (18.2 MΩ-cm, Barnstead International, Dubuque, IA).

b) Methanol (MeOH)- HPLC grade. (Merck KGaA, Darmstadt, Germany).

c) Acetic acid- 70 % HPLC grade. (ThermoFisher Scientific Inc., Waltham, MA).

d) Dimethylsulfoxide (DMSO)- > 99.9 % purity (Sigma-Aldrich, St. Louis, MO).

e) Reference Standards- soy isoflavone glycosides: daidzin, glycitin,

genistin (BIOTANG Inc., Lexington, MA); aglycones: daidzein, genistein (BIOTANG Inc.); and the internal standard (IS) 7-hydroxy-4-chromone (Sigma-Aldrich). The purity of each compound as stated in Certificate of Analysis was used for purity correction in the determination of the concentration of the calibrant solutions.

A.2.2. Solutions

a) Dilution solvent- 30:70 (v:v) methanol:water. Also used as syringe wash.
b) Extraction solvent- 74.5:20:5.5 (v:v:v) methanol:water:DMSO.
c) IS stock solution- 2 mg/mL in 80:20 (v:v) methanol:water. Weigh 3 mg of 7-hydroxy-4-chromone, then add 15 mL pre-mixed 80:20 (v:v) methanol:water to dissolve. Solution was determined to be stable for at least 6 months when stored in a freezer.
d) Stock solution containing isoflavone standards- Accurately weigh the following into individual 10 mL volumetric flasks: 1.7 mg daidzin, 1.0 mg glycitin, 0.7 mg daidzein, 1.7 mg genistin, and 0.6 mg genistein. Dilute to volume using pre-mixed extraction solution. LC stock standard solutions were stored in the refrigerator (5 °C) prior to use.

A.2.3. Extraction method

Approximately 0.4 g of as-received sample was weighed, spiked with ~0.4 g of IS solution, and then extracted at room temperature for 4 h in 6 g of the extraction solvent in a 15 mL polypropylene centrifuge tube, with agitation provided

by a homemade rotary mixer adapted from a commercially available rotovap setup (Buchi rotavapor R-144, Buchi Corp., New Castle, DE). The samples were then centrifuged (VWR, West Chester, PA) for 30 min at a speed of 4000 RPM (1914 x g centrifugal force) to remove any insoluble materials, and the supernatant was removed, filtered (by 0.45 µm PTFE syringe filter; VWR), and stored at 5 °C. Sample solutions were diluted for LC separation and absorbance detection.

A.2.4. Instrumentation

Waters Corp. (Milford, MA) Model Series 1500 liquid chromatograph, with a binary gradient pump, gradient mixer, and a 20 µL injection loop. A C_{18} column (250 X 4.6 mm, 5 µm particles, Alltech, Columbia, MD) was used to separate the components of the sample. Helium sparging was used for solvent degassing. Mobile phase A was water and mobile phase B was methanol, both containing 0.1 % (v/v) acetic acid. The gradient program was set in three segments; 1) linear increase from 30 % to 50 % B over 10 min at flow rate of 1.2 mL/min, 2) increase to 60 % B over 15 min at a flow rate of 1.2 mL/min, and 3) increase to 90 % B over 15 min at flow rate of 1.1 mL/min. A Waters 2487 Dual Absorbance detector was used for absorbance detection at 254 nm. Data acquisition and analysis were performed using Waters Empower 2 software.

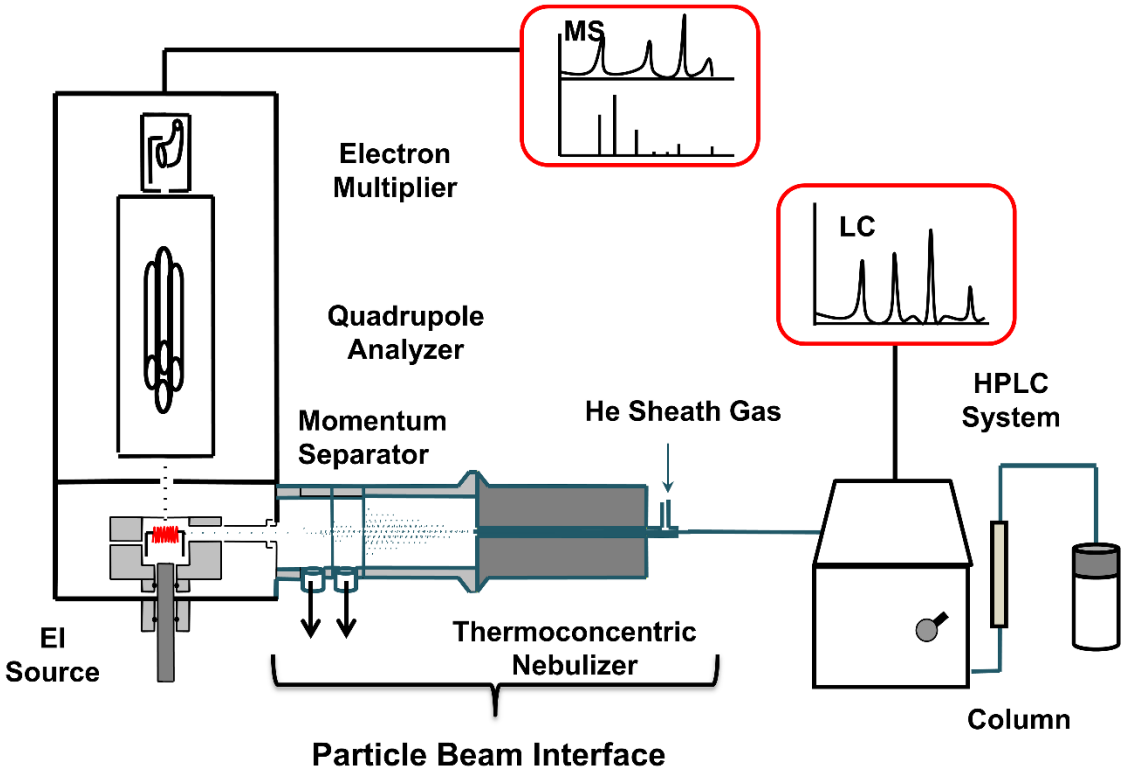

Figure A. 1 Diagrammatic representation of the LC-PB/EIMS system employed in these studies.

The LC system was coupled to an Extrel (Pittsburgh, PA) Benchmark quadrupole mass spectrometer system using a particle beam interface. As shown in Figure A.1, the PB interface (containing a thermoconcentric nebulizer and momentum separator) connects the LC and the MS detector in order to transform the liquid sample into dry analyte particles. The thermoconcentric nebulizer was heated to ≈85 ºC and helium was used to nebulize the solution into small droplets. The wet droplets then evaporate and form dry particles in the heated desolvation chamber (≈100 °C). As the particle/gas mixture passes through the momentum separator, analyte enrichment and solvent vapor removal occur simultaneously in two stages of differential pumping. The low mass solvent molecules are pumped

away because of their low momenta, while the heavier analyte-containing particles maintain their trajectory and pass through the orifices. Differential pumping not only permits solvent vapor removal but also creates pressure reduction to match the vacuum requirements of the ionization source. The resultant beam of dry analyte particles then enters the heated EI source for subsequent vaporization and ionization. The MS system was controlled by an Extrel^{TM} Merlin Automation Data System (Extrel CMS, Pittsburgh, PA). The MS system scanned masses from 100 Da to 700 Da at a rate of 1 s/scan for the collection of the total ion chromatogram (TIC), from which the mass chromatograms of the target species and their mass spectra were extracted.

A.3 Results and Discussion

The method development and validation occurred in successive steps. In the first stage, the chromatographic separation was optimized and the unique mass spectrometric signatures determined for the abundant isoflavones present in soy products. Of interest here were the aglycones daidzein and genistein, as well as the glycosides daidzin, genistin, and glycitin. The second step was the development of an efficient extraction procedure for the isoflavones in the finished product. The third step was to refine the method of quantification and compare the results with the certified and reference values from the NIST Certificate of Analysis. Calibration solutions composed of the pure isoflavones and the IS were used to determine response factors for absorbance and MS detection.

A.3.1. Separation of Soy Isoflavones and Compound Identification

a)

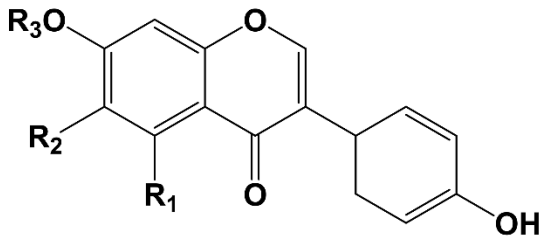

b)

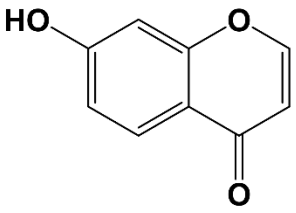

Compounds	R_1	R_2	R_3	MW (Da)
Daidzin	H	H	7-*O*-β-D-glucoside	416.4
Glycitin	H	OCH_3	7-*O*-β-D-glucoside	446.4
Genistin	OH	H	7-*O*-β-D-glucoside	432.4
Daidzein	H	H	H	254.2
Genistein	OH	H	H	270.2
7-hydroxy-4-chromone	H	H	H	162.1

Figure A. 2 Chemical structure of a) target isoflavones, and b) 7-hydroxy-4-chromone (IS) used in this study.

Previous studies in this laboratory demonstrated chromatographic separation and quantitation of a mixture of five-isoflavones containing puerarin, daidzein, genistein, formononetin, and biochanin A [34]. This solution was developed to represent the isoflavone content of several types of botanical materials, including soy, red clover, and kudzu. The separation conditions in those studies were determined to be a water and methanol gradient (30 % to 90 % (v/v) methanol containing 0.1 % trifluoroacetic acid (TFA) over 40 min at a flow rate of

1 mL/min) using a C_{18} column. These conditions were used as the starting point for the separation of the present soy isoflavone suite. Using absorbance detection at 254 nm for initial monitoring, the previously developed method did not adequately separate all the components of the soy isoflavone suite. Therefore, the gradient program variables were changed until an adequate-quality separation was achieved to with near baseline resolution of all eluent peaks.

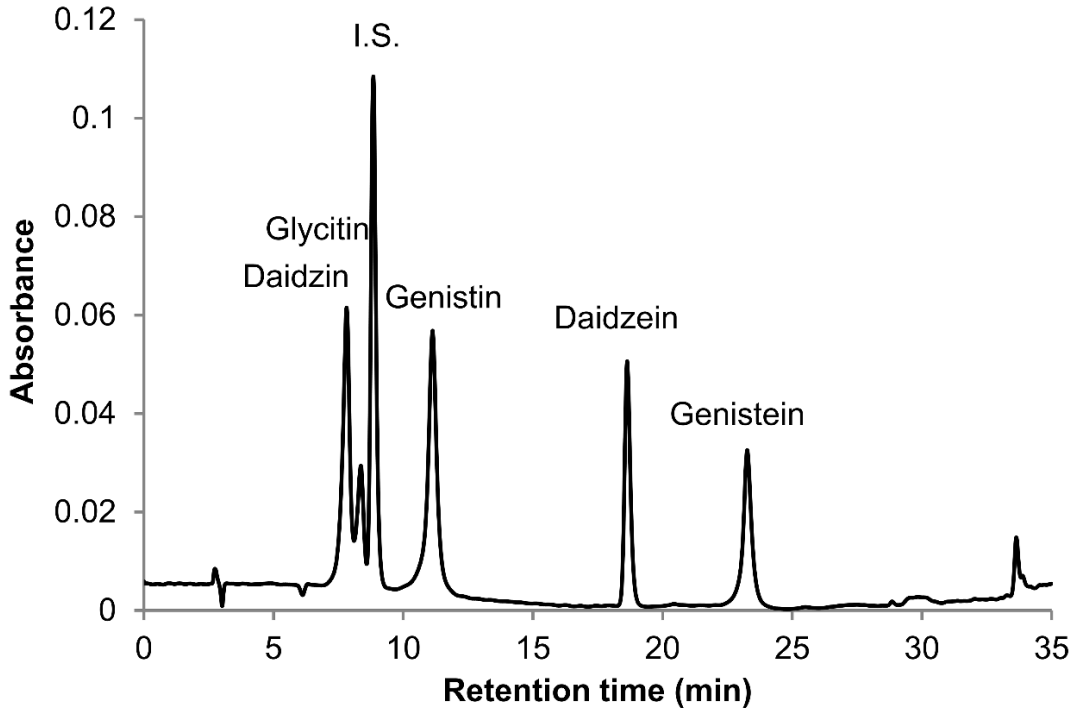

Figure A. 3 UV absorbance chromatogram obtained at 254 nm for the calibration solution containing the suite of target isoflavones and internal standard. Isoflavone standard solution separation using a C18 column and linear gradient 30 % to 50 % B over 10 min at flow rate of 1.2 mL/min, increased to 60 % B over 15 min at a flow rate of 1.2 mL/min, and to 90 % B over 15 min at flow rate of 1.1 mL/min, mobile phase A (Milli-Q water containing 0.1 % (v/v) acetic acid), and B (MeOH containing 0.1 % (v/v) acetic acid)

Interpretation of EI mass spectra, for library comparisons or identification of unknowns if needed, is facilitated by the present method, which is advantageous when analyzing complex botanical materials. Prior to the study of the complex herbal finished product material, neat solutions of single isoflavones were analyzed using LC-PB/EIMS, using the selected ion monitoring (SIM) chromatograms and resulting mass spectra to validate retention time assignments, mass spectral characteristics, and chromatographic resolution of each component. A separation of the calibration solution containing daidzin, glycitin, genistin, daidzein, genistein, and 7-hydroxy-4-chromone (IS) with absorbance detection is illustrated in Figure A.3. The first three peaks are not resolved well enough for quantitation via absorbance detection. Such an overlap may impose a burden toward MS quantification, introducing effects of cross interferences, ion enhancement, or ion suppression. Peak identification is based on their mass spectral features at the individual retention times as shown in Figure A.4. The molecular ion ($M^{+\bullet}$) is the base peak in the mass spectra for 7-hydroxy-4-chromone, daidzein, and genistein, but not so for daidzin, glycitin, and genistin. Under EI conditions, the isoflavone glycosides fragment under the EI conditions, and the spectra obtained reflect where the fragmentation occurs; specifically, the loss of the 7-*O*-β-D-glucoside moiety (*m/z* = 163 Da). Using the spectra presented in Figure A.4, base peaks were selected for daidzin (*m/z* 253), glycitin (*m/z* 283), genistin (*m/z* 269), daidzein (*m/z* 254), genistein (*m/z* 270), and 7-hydroxy-4-chromone (*m/z* 162). In the cases of daidzin, glycitin, and genistin, the glycoside moiety is likely lost in post-ionization

degradation, resulting in highest abundance from the base aglycone fragments. Quantitation was based on integration of peaks present in the extracted ion chromatograms for each isoflavone (recorded ± 1 Da) (Figure A.5).

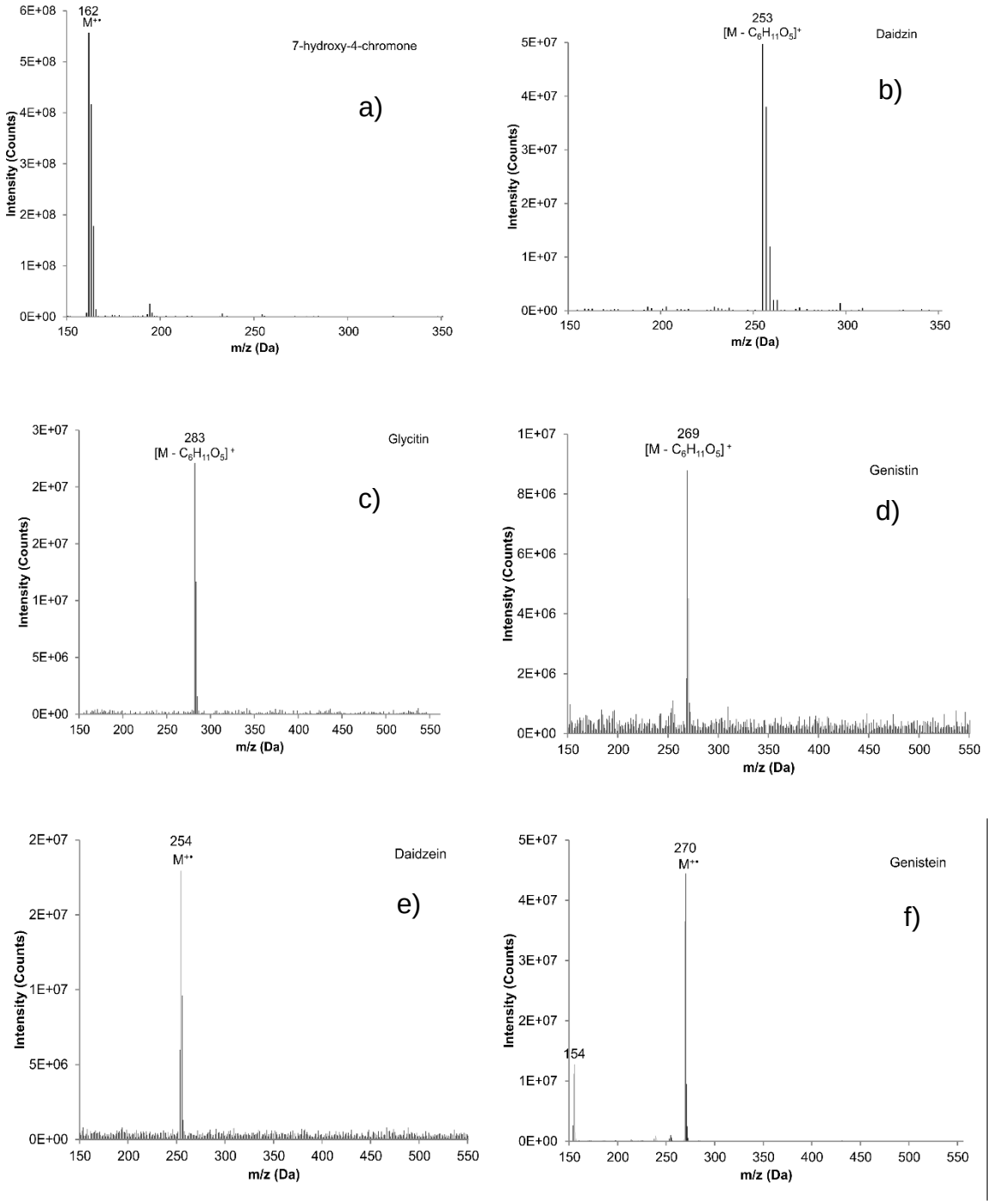

Figure A. 4 Extracted mass spectra derived from the elution of the internal standard and isoflavones in the chromatogram depicted in Figure 3: a) 7-hydroxy-4-chromone (IS), b) daidzin, c) glycitin, d) genistin, e) daidzein, f) genistein.

A.3.2. Extraction of Soy Isoflavones

A complete and accurate analysis of the active components in botanical materials is a non-trivial process that is affected by a number of factors, especially during the extraction and storage processes. Solvent composition and extraction times can affect significantly the extraction efficiency and relative yields of the individual compounds. Hydrolysis steps are often employed in isoflavone assays to cleave the acetyl and malonyl moieties on the glycoside and aglycone structures, thus reducing the chromatographic complexity [12,37-39]. The methodology used at NIST for characterizing SRM 3238 employs hydrolysis as a means of simplifying the analysis and to better meet the needs of the dietary supplement community [40]. The method of extraction used here is a 74.5:20.0:5.5 (v:v:v) MeOH:H_2O:DMSO solvent and 4 h rotary mixing at room temperature, which was developed based on the target isoflavones in SRM 3238. Methanol has been reported to yield higher recoveries for daidzin, glycitin, genistin, and genistein than acetonitrile and ethanol [13], and the DMSO additive improves the overall recoveries. Rotary mixing is a gentle method in comparison to shaking, being more comparable to stirring, which is one of the commonly used extraction techniques for isoflavones. An overt hydrolysis step was not employed, as EIMS detection was expected to yield unambiguous spectra from complex samples, including the various isoflavone glycoforms. However, the results suggest that acetyl and malonyl forms that may have been present in the extracts are ultimately reduced to the base glycosides in the course of the present method. In

addition, the extract is simply centrifuged and the supernatant transferred for storage without a sonication step, which reduces the number of sample handling steps and chemical modifications required, and in turn reduces the potential for sample degradation, contamination, or loss.

A.3.3. Method of Quantitation

Once a suitable separation had been achieved, sample extract solutions were evaluated (n = 3) using both LC-UV and LC-PB/EIMS. The internal standard compound, 7-hydroxy-4-chromone, was added to each test solution. The specific attributes of this IS compound include: 1) structural similarity to each of the target isoflavones (same base molecule without the presence of the phenyl group on the pyrone ring), 2) very similar absorbance characteristics including spectral structure and molar absorptivity at 254 nm, 3) relatively high mass spectrometric responses with very little fragmentation (minimizing potential fragmentation variability), 4) commercial availability of the product in high purity and low cost, and 5) high chemical and thermal stability.

Levels of isoflavones in SRM 3238 are listed in Table A.1 for both the absorbance and MS detection methods. An internal standard approach to quantitation was used. Because genistin and daidzin are much higher in concentration in comparison to the other isoflavones in the SRM, a 10-fold dilution prior to analysis was needed to obtain acceptable linearity. Unfortunately, the concentrations of genistein and daidzein in the diluted solution were below the limit of quantification for PB/EI-MS analysis, thus the original extract was used for

PB/EI-MS analysis and then diluted for subsequent absorbance detection. The SIM traces for the base peak produced by each isoflavone (identified in Figure A.4) were used for peak area determinations as demonstrated in Figure A.5. Note that in the SIM chromatograms for daidzein (e) and genistein (f), two peaks are observed. In both cases, the first peak in the chromatogram corresponds to another isoflavone present in the mixture as designated by the dashed lines; the 254 Da related to daidzin (a) and 270 Da associated with genistin (d). The second peak in each chromatogram (circled), associated with daidzein and genistein, respectively, was used for the quantification.

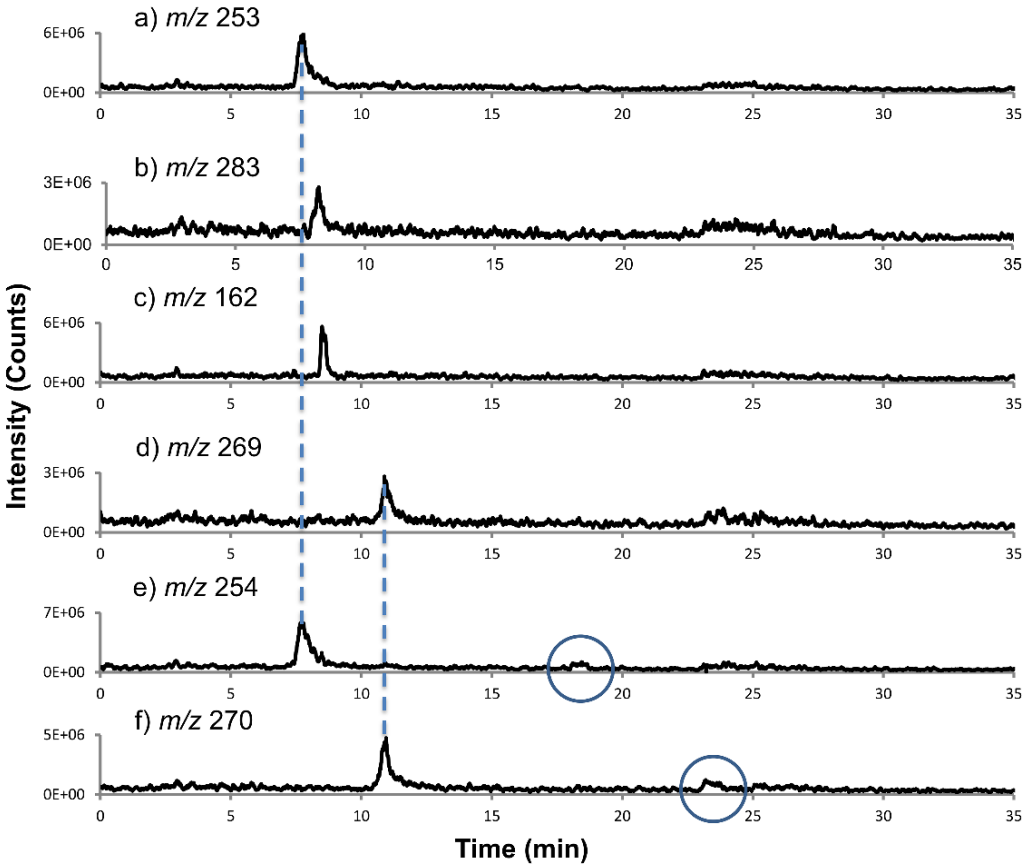

Figure A. 5 Selected ion chromatograms of the target isoflavones and internal standard: a) daidzin, b) glycitin, c) IS, d) genistin, e) daidzein, and f) genistein. In the case of e and f, the circled peak corresponds to the elution of the target analyte.

As seen in Table A.1, both detection methods provide excellent precision as expressed in the coefficients of variation (CV) for daidzin, genistin, and glycitin. In this case, the CVs refer to triplicate injections of the same extract, as the focus here was on the characterization of the instrumental method. The PB/EI-MS determinations have much higher CV values compared to those determined by absorbance detection for daidzein and genistein. The greater variability for these two compounds via MS detection is likely a result of the concentration of daidzein and genistein being much lower than the other isoflavones. Indeed their

concentrations are only a factor of three above the LOQs calculated using the previously computed LODs for those compounds based on single-component injections [34]. The absolute values presented in Table A.1 for the respective compounds determined by absorbance and MS detection are in rather good agreement; except for daidzein. In this case, the absorbance-derived concentration is almost a factor of two higher than the MS value. The difference here is directly attributed to the co-elution of a UV-absorbing compound that does not contribute to the SIM signal at 254 Da, which is possible due to the complexity of the botanical extract versus the isoflavone standard solutions from which the separation method was developed.

Table A. 1 Comparison of quantitative results for the analysis of SRM 3238 based on developed extraction and chromatography methods, using absorbance and PB/EI-MS detection.

	Absorbance Detection				
	Daidzin	**Glycitin**	**Genistin**	**Daidzein**	**Genistein**
Mass Fraction (mg/g)	13.793	3.581	12.896	0.559	0.123
SD (n=3)	0.045	0.008	0.033	0.002	0.002
CV	0.003	0.002	0.003	0.003	0.013

	MS Detection				
	Daidzin	**Glycitin**	**Genistin**	**Daidzein**	**Genistein**
Mass Fraction (mg/g)	14.012	3.913	12.684	0.310	0.104
SD (n=3)	0.144	0.032	0.129	0.069	0.084
CV	0.010	0.008	0.010	0.223	0.807

Confirmation of this is seen in the extracted mass spectrum taken from the daidzein retention time, shown in Figure A. 5, where the starred peaks confirm the presence of a co-eluting compound, which has appreciable absorbance at 254 nm. Collisional activation of these ion species (MS/MS) would be valuable in identifying the co-eluting compound(s).

Table A. 2 Comparison of quantitative results for the analysis of SRM 3238 based on developed extraction and chromatography methods using PB/EI-MS detection and those of the NIST certification.

	PB/EI-MS detection (mg/kg)	NIST-determined mass fraction (mg/kg)	Absolute percentage difference (%)
Daidzin	14012 ± 144	13400 ± 2400[1]	4.57
Glycitin	3913 ± 32	3760 ± 180[2]	4.07
Genistin	12684 ± 129	12700 ± 530[2]	0.13
Daidzein	310 ± 69	241 ± 5[2]	28.63
Genistein	104 ± 84	108 ± 10[2]	3.70

A comparison between the NIST-assigned values in SRM 3238 and those obtained by PB/EI-MS in Table A. 2 provides insight into strengths and weaknesses of the LC-PB/EI-MS method. The certified and reference mass fractions provided by NIST for each isoflavone are the mean from the combination of the means of LC/absorbance and ID-LC/MS methods developed at NIST. The

uncertainty provided for those values is an expanded uncertainty about the mean to cover the measured value with approximately 95 % confidence. The concentrations determined in this laboratory using PB/EI-MS match the NIST assigned values to within 5 % absolute difference, with the exception of daidzein. The measured values for all of the isoflavones are within the expanded uncertainty range.

The analysis performed at NIST involved a basic hydrolysis step, which breaks the ester bond of the malonyl and acetyl groups esterified to the alcoholic function of the sugar moieties of isoflavones. The hydrolysis step reduces the chemical complexity and allows the determination of the *total* of the glycosides and free aglycones. The fact that the mass fractions of daidzin, glycitin and genistin determined in this laboratory agree with the NIST certified mass fractions suggests that, even without the discrete hydrolysis step, the glycoside mass fractions obtained in this laboratory represents the total glycoside contents. In practice, there are two reasons that could lead to this result for the present method. First, hydrolysis could happen in the course of the present extraction step, converting the malonyl and acetyl derivatives into their stable glycoside forms. While the extraction takes place without acid or base addition, 4 h of processing at room temperature and in mixed solvent may cause hydrolysis of the malonyl and acetyl forms, leaving the total glycosides present in the respective chromatographic fractions. No evidence of malonyl or acetyl species was observed in any of the extracted mass spectra. Alternatively, native malonyl and acetyl forms could have

been hydrolyzed in the course of the manufacture of the dietary supplement matrix SRM. If this were occurring, the two extraction methods would indeed yield the same results; the quantification of the total glycosides.

A.4 Conclusions

Presented here is a method for the determination of isoflavone content in soy materials. The LC-PB/EIMS method developed here provides orthogonality in terms of the extraction procedure, chromatography protocol, and detection methodology to those used at NIST in the certification of SRM 3238. The LC-PB/EIMS approach provides accurate and precise measurements for the determination of the target isoflavones as well as providing simultaneous structural information. Structural information is a valuable asset, especially in the case of diagnosing the occurrence and potentially identifying co-eluting compounds. Such capabilities would clearly be advantageous in the case of characterizing natural products of ill-defined composition. The optimized method of analysis can be used in future work, such as quantifying the isoflavone content in other SRMs, or as a highly versatile tool for the characterization of herbal products in general [32-34,36]. In comparison to the use of ESI-MS following LC separation, the current method affords the ability to use MS databases and simple EI-type fragmentation rules to identify unknowns. In addition, the method places fewer constraints on the LC mobile phase as it is removed prior to the ionization event. Quantitative points of

comparison including sensitivity, linearity, reproducibility, etc. will the focus of future studies.

A.5 Acknowledgements

This work was financially supported by the National Institute for Standards and Technology under grant # 1169208 to Clemson University. LXZ would also like to thank Drs. Benjamin T. Manard and Joaudimir Castro for their help throughout the duration of this project.

A.6 References

1. Xiao, C. W. *J. Nutr.* **2008**, *138*, 1244S-1249S.

2. Isanga, J.; Zhang, G. N. *Food Rev. Int.* **2008**, *24*, 252-276.

3. Andres, S.; Abraham, K.; Appel, K. E.; Lampen, A. *Crit. Rev. Toxicol.* **2011**, *41*, 463-506.

4. Nielsen, I. L.; Williamson, G. *Nutrition and cancer* **2007**, *57*, 1-10.

5. Dewell, A.; Hollenbeck, P. L.; Hollenbeck, C. B. *The Journal of clinical endocrinology and metabolism* **2006**, *91*, 772-780.

6. Sacks, F. M.; Lichtenstein, A.; Van Horn, L.; Harris, W.; Kris-Etherton, P.; Winston, M. *Circulation* **2006**, *113*, 1034-1044.

7. Lindstrom, A.; Ooyen, C.; Lynch, M. E.; Blumenthal, M.; Kawa, K. *HerbalGram.* **2014**, 52-56.

8. Klein, M. A.; Nahin, R. L.; Messina, M. J.; Rader, J. I.; Thompson, L. U.; Badger, T. M.; Dwyer, J. T.; Kim, Y. S.; Pontzer, C. H.; Starke-Reed, P. E.; Weaver, C. M. *The Journal of nutrition* **2010**, *140*, 1192S-1204S.

9. Vacek, J.; Klejdus, B.; Lojkova, L.; Kuban, V. *Journal of separation science* **2008**, *31*, 2054-2067.

10. Achouri, A.; Boye, J. I.; Belanger, D. *Food Res. Int.* **2005**, *38*, 1199-1204.

11. Wu, Y.; Wang, X.; Fan, E. *Phytochem. Anal.* **2012**, *23*, 513-519.

12. Rostagno, M. A.; Villares, A.; Guillamon, E.; Garcia-Lafuente, A.; Martinez, J. A. *Journal of chromatography. A* **2009**, *1216*, 2-29.

13. Luthria, D. L.; Biswas, R.; Natarajan, S. *Food Chem.* **2007**, *105*, 325-333.

14. Rostagno, M. A.; Palma, M.; Barroso, C. G. *Anal. Chim. Acta.* **2004**, *522*, 169-177.

15. Zgorka, G. *J. AOAC Int.* **2011**, *94*, 22-31.

16. Klejdus, B.; Lojkova, L.; Lapcik, O.; Koblovska, R.; Moravcova, J.; Kuban, V. *J. Sep. Sci.* **2005**, *28*, 1334-1346.

17. Klejdus, B.; Lojkova, L.; Plaza, M.; Snoblova, M.; Sterbova, D. *J. Chromatogr. A* **2010**, *1217*, 7956-7965.

18. Sheng, G.; Zhou, Q. In *Sustainable Environment and Transportation*, Chu, M. J.; Xu, H. H.; Jia, Z.; Fan, Y.; Xu, J. P., Eds.; Trans Tech Publications Inc., 2012, pp 838-842.

19. Rostagno, M. A.; Palma, M.; Barroso, C. G. *Anal. Chim. Acta.* **2007**, *588*, 274-282.

20. Gong, S. Z.; Cheng, J.; Yang, Z. R. *Chin. J. Chem. Eng.* **2005**, *13*, 556-559.

21. Zeng, J.; Jiang, B.; Xiao, Z.; Li, S. In *Advanced Research on Material Engineering, Architectural Engineering and Informatization*, Zhang, H.; Jin, D., Eds., 2012, pp 486-489.

22. In *Isoflavones: Chemistry, Analysis, Function and Effects*, Preedy, V. R., Ed.; Royal Soc Chemistry, Thomas Graham House, Science Park, Cambridge Cb4 4wf, Cambs, Uk, 2013.

23. Lee, J. H.; Choung, M.-G. *Food Chem.* **2011**, *129*, 577-582.

24. Cimino, C. O.; Shelnutt, S. R.; Ronis, M. J. J.; Badger, T. M. *Clinica. Chimica. Acta* **1999**, *287*, 69-82.

25. Konar, N.; Poyrazoglu, E. S.; Demir, K.; Artik, N. *Journal of Food Composition and Analysis* **2012**, *26*, 26-35.

26. Grynkiewicz, G.; Ksycinska, H.; Ramza, J.; Zagrodzka, J. *Acta Chromatogr.* **2005**, *15*, 31-65.

27. Wang, C.-C.; Prasain, J. K.; Barnes, S. *J. Chromatogr. B* **2002**, *777*, 3-28.

28. Wilkinson, A. P.; Wahala, K.; Williamson, G. *J. Chromatogr. B* **2002**, *777*, 93-109.

29. Wu, Q. L.; Wang, M. F.; Sciarappa, W. J.; Simon, J. E. *J. Agric. Food Chem.* **2004**, *52*, 2763-2769.

30. Singh, S. P.; Wahajuddin; Ali, M. M.; Jain, G. K. *J. Sep. Sci.* **2010**, *33*, 3326-3334.

31. Borquez, J.; Kennelly, E. J.; Simirgiotis, M. J. *Food Res. Int.* **2013**, *52*, 288-297.

32. Castro, J.; Krishna, M. V. M.; Marcus, R. K. *Am Lab* **2008**, *40*, 8-10.

33. Castro, J.; Krishna, M. V. B.; Choiniere, J. R.; Marcus, R. K. *Anal. Bioanal. Chem.* **2010**, *397*, 1259-1271.

34. Burdette, C. Q.; Marcus, R. K. *J. AOAC Int.* **2013**, *96*, 925-932.

35. Krishna, M. V. B.; Castro, J.; Brewer, T. M.; Marcus, R. K. *J. Anal. At. Spectrom.* **2007**, *22*, 283-291.

36. Krishna, M. V. B.; Castro, J.; Brewer, T. M.; Marcus, R. K. *J. Anal. At. Spectrom.* **2009**, *24*, 199-208.

37. Rostagno, M. A.; Palma, M.; Barroso, C. G. *Journal of Chromatography A* **2003**, *1012*, 119-128.

38. Richelle, M.; Pridmore-Merten, S.; Bodenstab, S.; Enslen, M.; Offord, E. A. *The Journal of nutrition* **2002**, *132*, 2587-2592.

39. Chiang, W.-D.; Shih, C.-J.; Chu, Y.-H. *Food Chemistry* **2001**, *72*, 499-503.

40. , Technology, N. I. o. S., Ed.; NIST: Gaithersburg, MD, 2014, pp 1-5.

APPENDIX B.

OPEN-CHANNEL LATERAL FLOW (IMMUNO) ASSAY SUBSTRATE BASED ON CAPILLARY-CHANNELED POLYMER FILMS

B 1. Introduction

Lab-on-chip (LOC) devices focus on the miniaturization of laboratory-scale equipment to perform diagnosis on a small scale. One obvious point of development is towards low-cost, portable and disposable point of care diagnostic (POC) devices.[1-4] In virtually all POC implementations, there is a need for a multifunction matrix material onto which operations are affected. Many polymeric materials such as polyethylene, nitrocellulose (NC), Dacron, polyvinyl chloride (PVC), nylon, polyacrylonitrile (PAN) etc. have been studied as bioassay matrices, interfacing between materials and biological moieties.[5-8] A key component in the POC toolbox has been Immunochromatographic assays, also known as lateral flow (immune) assays (LFIA). These devices use capillary action (wicking) to transport the analytes to detecting zones where the immunoreaction takes place,[9-19] greatly simplifying the operational overhead. The material of choice in the vast majority of LFA systems has historically been nitrocellulose,[12] however, there have been efforts towards introducing other material types into the market. Recently, thin layer materials with wicking power, such as paper, sponge rubber and glass fiber paper, have been employed to achieve bioseparation as a function of the analytes' physical and chemical properties.[20-27]

There are future improvements expected for the existing LFA techniques, as a reduced number of applications in multi-residue analysis has been performed when using LFA analysis. Several difficulties are brought up that associated to this fact, first is the limitation to integrate the current LFAs to vary detectors with appreciate reporter. Based on the survey report by Ngom et al., seventy five percent of published reports on LFA employed colloidal gold particle as label,[14] alternative types of label (i.e. fluorescent microsphere) can potentially improve the sensitivity by at least 10 folds in comparison to the colloidal gold or colored latex beads.[28] Another limitation is the ability of handling complex samples like milk, blood/urine, soil or groundwater, as significant amount of sample treatment is required pier to/during the LFA analysis. For example, as reported by Pike et al., the existing paper-based analytical devices varies in specificity and sensitivity.[29] Especially when using for clinical applications in particularly, false-negative and false-positive results may be observed, as the stability of the LFA, the environmental temperature and humidity, the robustness of the LFA can all effect the sensitivity different. There is also a portion of the LFA analysis is detected by the naked eye observant of the end-users, especially for colorimetric detection-based LFAs. The errors/sensitivity varies as the subjective judgment from operators and the differences in the illumination setting can lead to controversial readouts, especially when the detection signal is close to threshold. To solve these difficulties, new array materials and/or new analytical detecting methods with good sensitivity and great reproducibility is the major developing direction of the future study LFA.

Capillary-channeled polymer (C-CP) fibers have been explored in this laboratory for their use in protein chromatography and solid phase extraction.[30-34] C-CP fibers are melt-extruded from commodity polymers, the ones being focused on in this laboratory are polypropylene (PP), nylon 6, and poly(ethylene terephthalate) (PET). Structure-wise, the fibers have eight capillary channels extending the entire length of the fibers, which can self-align and results in a monolith-like structure with 1-5 µm capillary channels for fluidic flow when packed into a column. It has been shown that C-CP fiber packed columns exhibit excellent fluid transport properties suitable for macromolecular separations (i.e. achieving separation without suffering from van Deemter C-term broadening) therefore enhanced mass transfer efficiencies that allow very rapid separations with high recoveries.[32,35,36] C-CP materials can also be extruded in a ~5 mm wide film format, with parallel 100 µm wide x 100 µm deep channels running the length of the film. The use of individual channels versus a network of voids is very different from other thin layer materials currently being used as matrices for LFA. We have previously demonstrated the ability to perform protein separations via wicking action, effecting doing thin layer chromatography (TLC) down the channels.[37] In that work, proteins were detected by matrix- assisted laser desorption mass spectrometry (MALDI-MS). However, during that study of the native C-CP film, the poor uniformity of the channels and the fact there were channels present on both sides of the films caused uneven solvent flow and poor reproducibility. Thus, a new PP film spinerette was designed by Specialty & Custom Fibers, LLC (Clemson,

SC). This second-generation C-CP film has four uniform, individual channels on one side of the film, with a flat surface on the opposite side for easy mounting.

C-CP films have several potential advantages as an LFA matrix; they are flexible, chemically stable, and optically transparent, thus easy to couple with various surface analyzing/detecting methods including absorbance spectroscopy, Raman/IR spectroscopy, florescence spectroscopy, and desorption/ionization mass spectrometry. A more subtle aspect is that the wicking action in the films is unidirectional, as opposed to the capillary action in a 3-dimensional matrix. As such, one might expect greater utilization of precious analyte as the movement is along a single surface as opposed to within a matrix that may not be accessed by the detection means. A final advantage of the physical platform is that the films can be constructed with any number of parallel channels, providing the possibility for multianalyte, parallel, LFA operation as depicted in Fig. B.1.

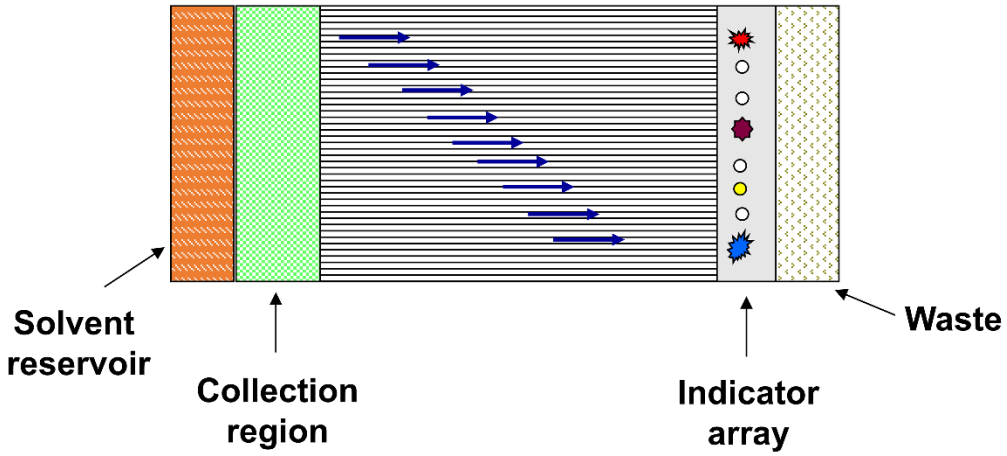

Figure. B. 1 Conceptual illustration of the use of a capillary-chanelled polymer (C-CP) film as a parallel, lateral flow (immune) assay.

While the previous protein separation on a C-CP film was performed on a native polypropylene (PP) surface to affect a reversed phase separation of proteins in Tris-HCl and phosphate buffered saline (PBS) matrices, there are a number of strategies which can be implemented to affect the selectivities desired in most LFA applications. Recently, this laboratory has focused on developing simple surface modification chemistries on C-CP fibers, which are transferable to the film format.[38-42] Of greatest relevance for the application of PP C-CP films has been the development of the lipid tethered ligand (LTL) methodology wherein the hydrophobic acyl chains actually intercalate into the polymer matrix to form an incredibly robust anchor.[43] Chemical selectivity is achieved by simple choice of the polar lipid head group. An in-house synthesized biotinylated-LTL has been used on PP C-CP fibers for capturing SAv-TR from EGFP-spiked *E. coli* cell lysate.[41]

Presented here is the proof of concept of the use of the synthesized biotinylated-LTL for the surface modification of UV-treated PP C-CP film and its use as an open-channel lateral flow (immuno) assay. Described are the simple methods for imparting greater wicking activity as well as tethering of the capture ligand. It is believed that the present C-CP film format holds a great deal of promise towards multi-analyte LFAs.

B 2. Experimental

B.2 1. Chemicals and Reagents

Streptavidin-Texas Red (SAv-TR) was purchased through Southern Biotech (Birmingham, AL) and enhanced green fluorescence protein (EGFP) (found in p3051 retrovirus vector and amplified by PCR) was provided by Dr. G. Chumanov of the Chemistry Department of Clemson University (Clemson, SC). The biotiylated-LTL was synthesized in-house, as described previously [39]. A working solution containing 0.3 μg mL^{-1} each of (SAv-TR) and EGFP was prepared in 100 mM phosphate-buffered saline tween (PBST) buffer. PBST buffer was prepared by adding 1 mL of Tween-20 into 1 L of phosphate-buffered saline (PBS) buffer that was prepared by dissolving NaCl (8.0 g), KCl (0.2 g), Na_2HPO_4 (1.44 g) and KH_2PO_4 (0.24 g) (all salts were purchased from Sigma-Aldrich, St. Louis, MO) in DI water (Milli-Q system, 18.2 MΩ cm^{-1}) to a final volume of 1 L and achieve a pH of 7.4.

Protein separations on the C-CP films were achieved using a 40:60 acetonitrile:water (ACN:H_2O) eluent. MALDI matrix solutions consisting of 10 g L^{-1} of sinapinic acid, purchased from Fisher Scientific (Pittsburgh, PA, USA), were prepared in 0.1% trifluoroacetic acid (TFA), purchased from Sigma-Aldrich. ACN was purchased from VWR (West Chester, PA). Unless specified otherwise, all reagents and solvents were used without additional purification.

B.2 2. Preparation of PP C-CP films

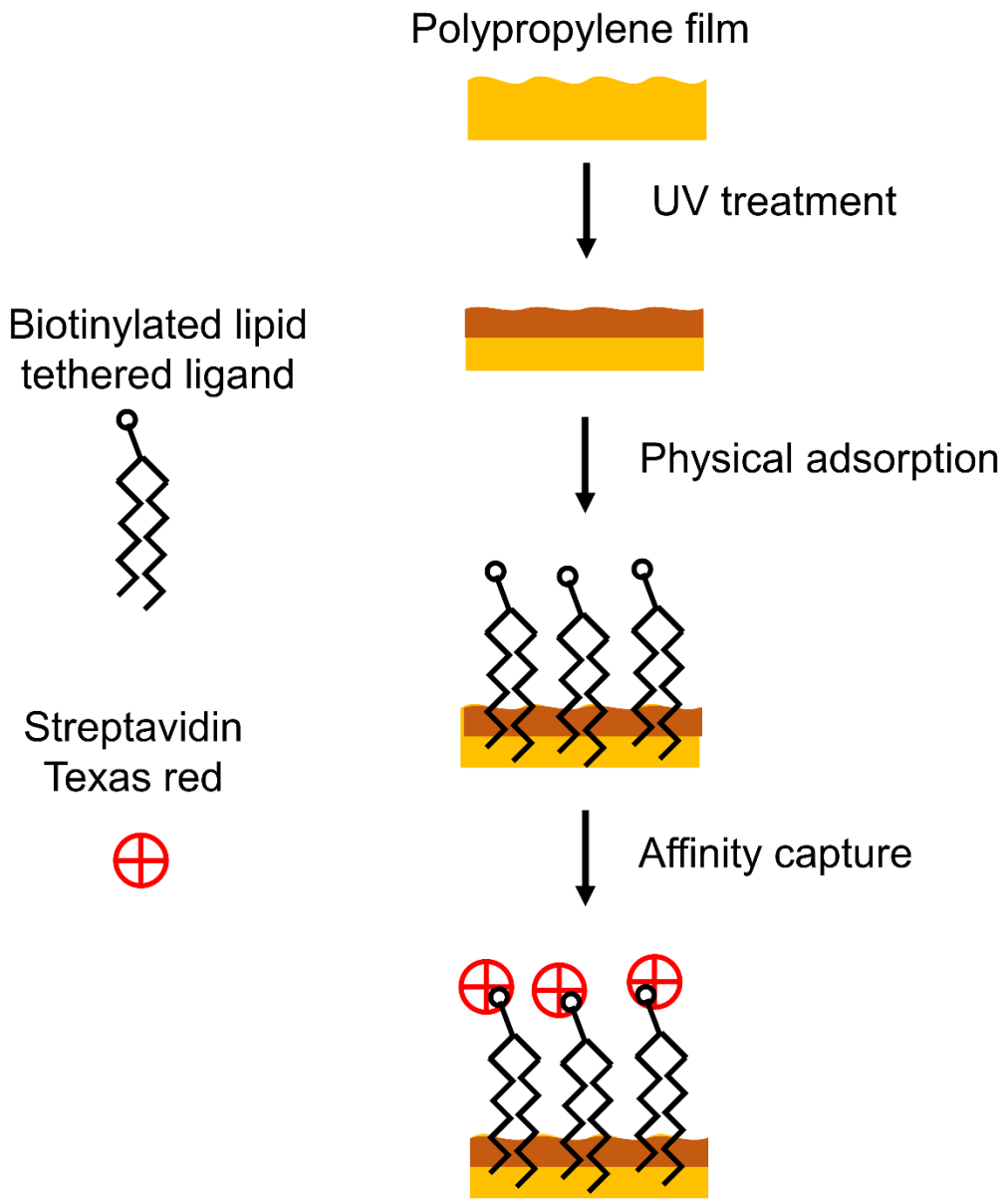

Figure. B. 2 Schematic illustration of sequential surface modification process of PP films for affinity targeting of streptavidin.

The entirety of the film preparation, surface modification, and affinity capture are depicted in Fig. B.2. Polypropylene (PP) C-CP films were melt-extruded at the Department of Materials Science and Engineering at Clemson University

(Clemson, SC, USA). If desired, films are also available from a commercial source, Specialty & Custom Fibers, LLC (Clemson, SC, USA). They contain 4 channels ~80 µm in width and height, as shown in Fig. B.2. It is important to note that the total channel volume of the C-CP film is only 0.77 µL. Film segments were washed sequentially with water, methanol, and acetonitrile, twice respectively, to remove any production residues. The films (30 mm in length) were attached via tape to a glass slide following the wash then treated in an ambient UV Irradiation chamber with a low pressure mercury grip lamp for 15 min (BioForce Nanosciences, Inc., Ames, IA). The intensity of the mercury grid lamp used was 19.4 mW cm^{-2} at a distance of 1.1 cm. The UV lamp had emission wavelengths from 185 to 450 nm (highest intensity located at 253.7 nm) and generated ozone from ambient air within the chamber. The detail of the modification is discussed later in the results section.

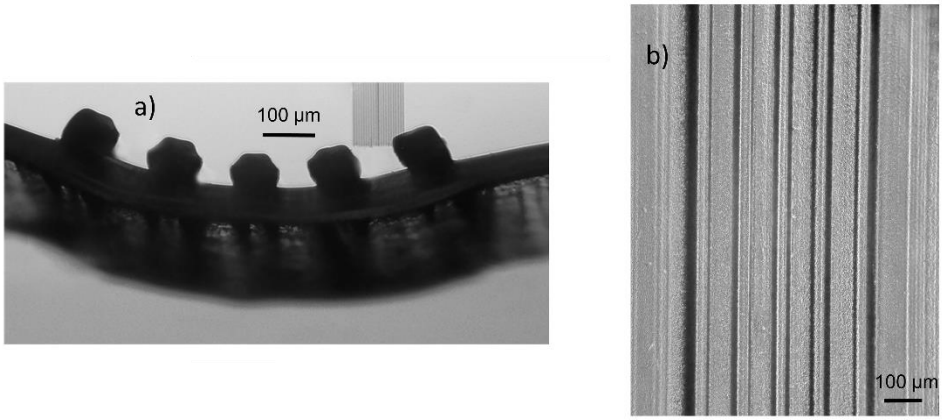

Figure. B. 3 Microscope image (4x) of the CC-P films: a) cross section, and b) the surface.

B.2 3. Biotin-LTL functionalization, Sample Spotting, and Elution Process

The application of the biotinylated-LTL test strip is complicated by the high level of spontaneous wicking in the film channels. Simply, application of a droplet will cause the solution to spread across the entire film. To mitigate the spreading, two, 1 µL drops of DI-H_2O were placed 10 mm apart, and the LTL-containing ethanolic solution deposited in between. A 50 µg mL^{-1} biotin-LTL solution was prepared in 60% ethanol to deposit the capture strip. A 3 µL droplet of the solution was applied in the mid-film region between the water droplets. Due to the higher volatility of the ethanolic solution, that portion evaporated more quickly than the water, effectively trapping the contents to a ~10 mm strip. This process was repeated five times. Following drying, a 10 µL aliquot of 60% ethanol was applied to one end of the film and wicked across the region to wash off any un-adsorbed biotin-LTL. For all on-film analysis, 2 µL of the protein test solution was spotted at one end, then washed by applying 10 µL DI-H_2O to the loaded protein. After 5 s, the wash solution was pipetted back off of the film. In both of these cases, the film's liquid capacity was overloaded, as such a small fraction wicks down the structure, with the majority left beaded on the end. The analytical elution was affected by applying 10 µL of 40:60 ACN:H_2O at the sample end of the film. In this case, a bundle of C-CP fibers loosely packed into 0.8 mm i.d. fluorinated ethylene propylene tubing (Cole Palmer, Vernon Hills, IL) placed at the far end acted as a sink to draw the entire volume across the film. In this way, the mixture was drawn across the biotinylated-LTL capture region.

B.2 4. Fluorescence Imaging of PP C-CP Films

Fluorescence imagine was achieved using a home-built spectrofluorometer system. A Xe arc lamp purchased from Chroma Technology Corporation (Bellows Falls, VT) with excitation filters set at 488 nm for EGFP, and 575 nm for SAv-TR. Fluorescence images were captured by an Ocra-ER (Hamamatsu) CCD camera, through an Olympus IX71, 2X /0.08 UPlanFI (infinity corrected) objective (Olympus, Center Valley, PA) with the emission filters set on 509 and 624 nm for EGFP and SAv-TR, respectively. The fluorescence data was processed using Micromanager 1.4 developed by Vale Lab (San Francisco, CA).

B.2 5. MALDI-MS Analysis

Films, after fluorescence imaging, were allowed to dry overnight in a dark environment and then double taped onto a MALDI target. The aforementioned MALDI matrix was sprayed onto the entire film at a low rate to limit analyte movement via wicking[37]. All analyte spectra were obtained on a Bruker Daltonics (Billerica, MA, USA) microflex LRF, a MALDI-TOF mass spectrometer, operating as linear, and positive ion detection mode. Instrument control and data processing were through Compass, a Bruker Daltonics software. The microflex is equipped with a nitrogen laser (337 nm) operating at a pulse rate of 60 Hz. Mass spectral acquisitions occurred using 100 laser shots at 35% laser power.

B 3. Result and Discussion

B.3 1. UV Surface treatment of the PP C-CP fiber

Ozone-generating UV light has been used for many years to clean organic contaminants from various surfaces.[44-47] It also has been used as one of the many surface treatment techniques for polymer films.[48] The purpose of the surface treatment in this study is to reduce the hydrophobicity of the PP film by introducing more functional groups such as –OH, =O, –OOH through UV-induced oxidation. Pure polypropylene does not absorb UV light at wavelengths < 200 nm. However, with the trace amounts of hydroperoxides and ketone chromophore/catalysts that exist in the PP films, the absorption range is extended below 200 nm through the processes depicted below.[48,49]

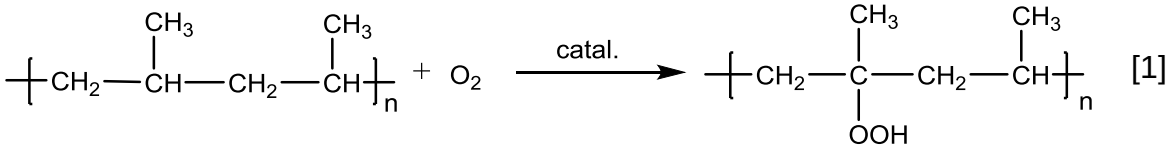

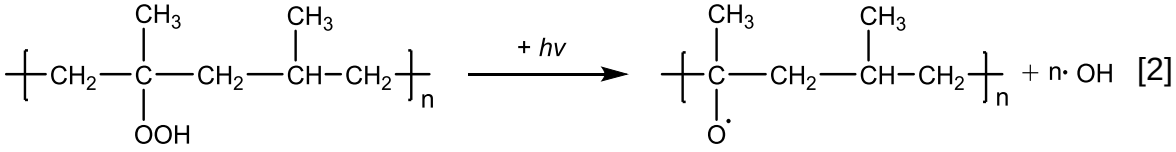

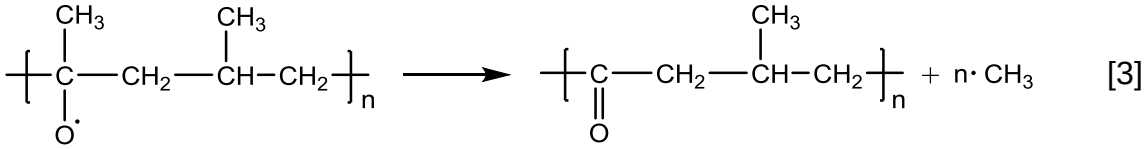

The effects of treatment time on the ozone level generated over time and the oxygen uptake on PP were reported in detail by Walzak and co-workers.[50] In that work, the O:C ratio on the PP surface was found to increase linearly with the treatment time for up to 15 min, however no significant change occurred between

15-30 min of treatment. The contact angle was tested in air and results showed a decrease in the contact angle with increasing oxygen uptake, as anticipated. This treatment method was reproduced closely for the PP C-CP films, yielding appreciably higher wicking rates for both aqueous and mixed solvents.

B.3 2. Biotin-LTL-functionalized PP C-CP films for the affinity capture of streptavidin-Texas Red

While the present protocol for depositing both the capture ligand and analytical sample are relatively crude, the concept is easily demonstrated. Figure B.4 presents the fluorescent images obtained for SAv-TR and EGFP at three locations along the C-CP film. Figure B.4a consists of images of the two proteins as-applied to the film prior to elution. As seen, both proteins are concentrated at the end, spreading down-film over distance of ~4 mm. Note that application of the relatively large droplet causes some protein buildup on the tops of the walls between the channels. Application of the eluting solvent causes transport of the proteins along the solvent front with post-elution imaging clearly showing selective capture of the SAv-TR target. Figure B.4b shows that the SAv-TR is indeed located within the channels, where expected, with no indication of the much more strongly fluorescing EGFP, which would reflect non-specific binding. While no assumption of the quantitative correctness of the fluorescent images is made here (though they were taken under the same conditions), the images taken at the end of the films (Fig. B.4c) reflect a depletion of the SAv-TR and a loss in EGFP response, likely due to dilution.

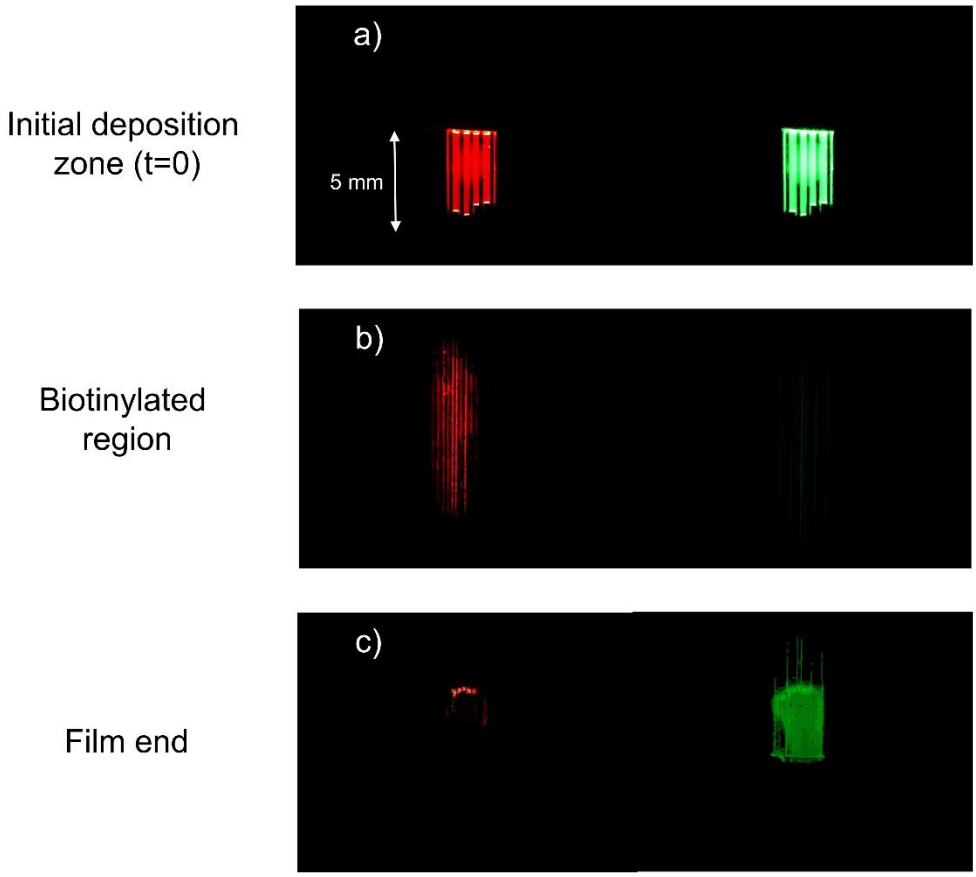

Figure. B. 4 Fluorescence image of the PP C-CP films after surface treatment of UV light, and modification with biotin-LTL in the middle of the film, and application of the protein mixture of SAv-TR and EGFP. a) Before applying the 40:60 ACN:H_2O eluting solution at initial sample deposition zone, b) after elution at biotinylated region and c) after elution at the end of the film. Presence of SAv-TR indicated in red and EGFP in green.

As in any sort of selective bioassay, the question of non-specific binding is crucial. Previous studies have clearly shown that proteins have a very high affinity for PP fiber surfaces. The initial driving force for the UV oxidation was to increase the hydrophilicity of the PP surface, and thus the propensity for wicking of aqueous phases. Perhaps an equally important effect should be a reduced tendency for non-specific binding of proteins, which would occur through hydrophobic surface

interactions. Previous studies with PP C-CP fibers dealt with the issue of non-specific binding by effecting the separations in the presence of the detergent Tween. As shown in Fig. B.5 for the case of a film not subjected to the biotin-LTL deposition, the UV modification of the PP C-CP films results in a surface that appears to be immune to non-specific binding. As seen in Fig. B.4a, the image of the initial deposition zone (Fig. B.5a) shows the proteins concentrated at the film head. Images taken post-elution at the mid-film region (Fig. B.5b) reflect no accumulation of either protein along the elution channels, with the film-end images (Fig. B.5c) showing accumulation of both. Thus, at this preliminary stage, it appears that the UV-treatment does indeed impart sufficient hydrophilicity to inhibit non-specific protein binding to a large extent.

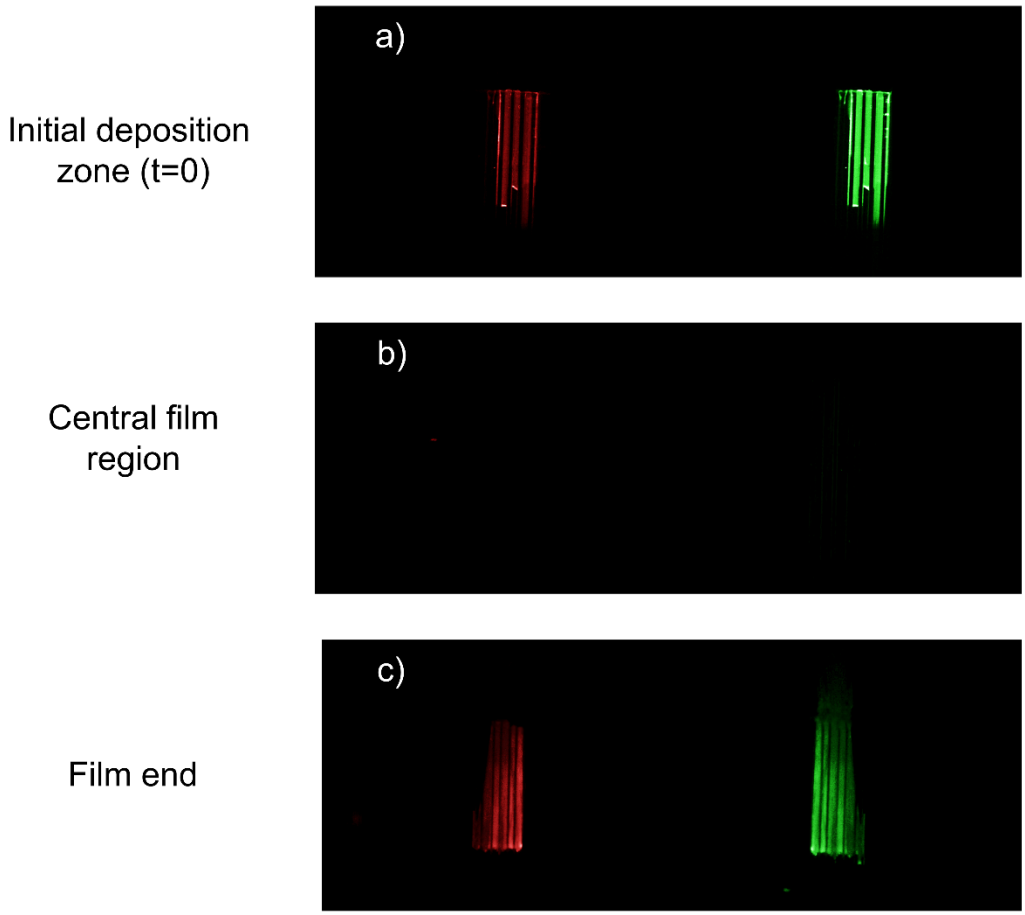

Figure. B. 5 Fluorescence image of the PP C-CP films following exposure to UV light and application of the protein mixture of SAv-TR and EGFP, a) before applying the 40:60 ACN:H_2O eluting solution at initial sample deposition zone, b) after elution at the body region and c) after elution at the end of the film. Presence of SAv-TR indicated in red and EGFP in green.

B.3 3. Using the C-CP PP film as MALDI Target for Direct Analysis of Analyte on Film

In the case that the target of an immunoassay does not have a fluorescence tag, MALDI-MS is an opportunity for identification and perhaps quantification of the captured molecule. Certainly this capability is more relevant in the case of class-specific captures, such as glycoproteins on a lectin capture surface. As

demonstrated previously, C-CP films can be used as separation media with subsequent detection using the imaging capabilities of most MALDI-MS systems. Figure B.6 demonstrates sequential use of MALDI imaging for the capture/separation of the SAv-TR/EGPF mixture. As described in the experimental section, the C-CP film was sprayed with MALDI matrix solution, allowed to dry again, then taped onto a MALDI target. Figs. B6a and b are the MALDI-MS spectra taken from the head (starting end) of the film, before and after the elusion step. In the first case (Fig. B.6a), the proteins show very strong responses. Following elution with the 40:60 ACN:H_2O solvent, the region is depleted of the SAv, with a small amount of EGFP appearing to remain. MALDI-MS imaging of the central portion of the film (Fig. B.6c), in the region of the biotin-LTL capture zone, reflects the capture of the SAv-TR as was demonstrated in the fluorescent images, with no indication of non-specifically bound EGFP. Finally, the MALDI spectrum acquired at the film end (Fig. B.6d) reflects the accumulation of the non-retained proteins. In this case, it is clear from the relative spectral responses that the SAv-TR was selectively captured in preference to the EGFP. The presence of the SAv at the end reflective of an overload situation versus the amount of adsorbed capture ligand. Utilizing the PP film as a MALDI substrate would appear to be an exemplary benefit in comparison to other thin layer film/membranes.[51,52] In this case, the fact that the solute exists on the film surface and not within a permeable structure should provide greater analytical sensitivity and less spectral background.

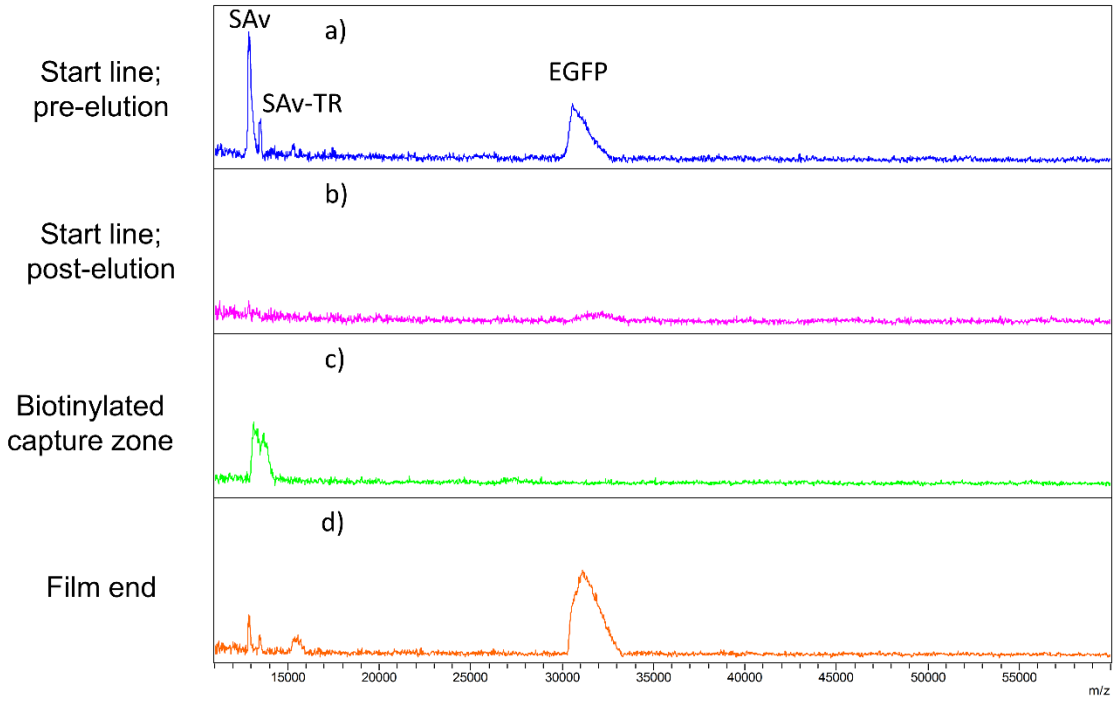

Figure. B. 6 MALDI-TOF mass spectra of the PP C-CP films after surface treatment by UV light and modification with biotin-LTL and application of the protein mixture of SAv-TR and EGFP. a) Before applying the 40:60 ACN:H_2O eluting solution at initial sample deposition zone, b) after elution at the initial sample deposition zone, c) after elution, in the biotinylated region, and d) after elution, at the end of the film**.**

B 4. Conclusions

In the present study, we developed a surface modification method for polypropylene C-CP films to be used as an open-channel lateral flow (immuno) assay substrate. The entire process, including the UV-light surface treatment and the physical adsorption of the biotin-LTL, was achieved under ambient conditions. The general methodology was illustrated for the cases of optical (fluorescent) and MALDI-MS detection. The ability of protein separation on film opens a wealth of

opportunities in the realm of protein solution processing for MALDI-MS, including simply reducing matrix effects (desalting) for the bio-molecules by using an on-film wash. Such concepts open many opportunities for bio-recognition and affinity separation when appropriate functional LTLs are attached utilizing the proposed method. The proposed method is predicted to be effective not only for the polypropylene films, but also for other types of film materials laboratory including poly(ethylene terephthalate), and polyamide (nylon 6).

A couple of issues need to be addressed in future work to reduced this concept to practice. First, the method of application of the the capture ligand must be improved. In future studies, a molecular printing system (e.g.,) should be utilized as the application technique, to insure a uniformed surface on the desired regions. A potential extension is that different affinity functional groups could be applied onto separate channels, generating a multi-analyte, parallel LFA. Second, the method of applying the initial sample in a more uniform way would ultimately help the quantification. In this case, not performing the UV treatment at the film head would restrict the movement of the initial sample, concentrating the solute species to a more-narrow region. This could be used in concert with much lower sample volumes. Finally, the versatility for a variety of C-CP film compounds will be investigated in the near future along with the detailed study of role UV light treatment conditions on both the wetting and non-specific binding.

The presented study also demonstrated the principle of using C-CP films as processing platforms and MALDI targets for proteins analysis/identification. We have encountered problems and there are challenges remaining, but the overall

simplicity, flexibility, and practicality of the approach showed its worthy of further development. In conclusion, The C-CP films as biosensor platforms, have a high potential path for lab-on-chip device applications.

B 5. Acknowledgement

The authors appreciate the EGFP provided to us by Dr. George Chumanov from the Department of Chemistry of Clemson University and the support from the National Science Foundation, Division of Chemistry, under Grant # 1307078.

B 6. References

1. Ho, H.; Lau, P.; Kwok, H.; Wu, S.; Gao, M.; Cheung, A.; Chen, Q.; Wang, G.; Kwan, Y.; Wong, C.; Kong, S. *Bioanalysis* **2014**, *6*, 2005-2018.

2. Jung, W.; Han, J.; Choi, J.; Ahn, C. *Microelectron. Eng.* **2015**, *132*, 46-57.

3. Pires, N.; Dong, T.; Hanke, U.; Hoivik, N. *Sensors* **2014**, *14*, 15458-15479.

4. Foudeh, A.; Didar, T.; Veres, T.; Tabrizian, M. *Lab Chip* **2012**, *12*, 3249-3266.

5. Charles, P.; Velez, F.; Soto, C.; Goldman, E.; Martin, B.; Ray, R.; Taitt, C. *Anal. Chim. Acta* **2006**, *578*, 2-10.

6. Jackeray, R.; Jain, S.; Chattopadhyay, S.; Yadav, M.; Shrivastav, T.; Singh, H. *J. Appl. Polym. Sci.* **2010**, *116*, 1700-1709.

7. Iole, V.; Ilaria, F.; Maria Vittoria, R.; Stefano, B.; Roberta, C.; Luisa, I.; Maria, S.; Vincenzo, A.; Antonio, V.; Mosè, R.; Sabato, D. *J. Phys.: Condens. Matter* **2008**, *20*, 474202.

8. Jain, S.; Chattopadhyay, S.; Jackeray, R.; Zainul Abid, C.; Kumar, M.; Singh, H. *Talanta* **2010**, *82*, 1876-1883.

9. Chen, A.; Yang, S. *Biosens. Bioelectron.* **2015**, *71*, 230-242.

10. Xie, Y.; Yang, Y.; Kong, W.; Yang, S.; Yang, M. *Chinese J. Anal. Chem.* **2015**, *43*, 617-628.

11. Goeselova, S.; Blazkova, M.; Holubova, B.; Karamonova, L.; Rauch, P. *Chem. Listy* **2014**, *108*, 114-119.

12. Mansfield, M. In *Lateral Flow Immunoassay*, Wong, R.; Tse, H., Eds.; Humana Press, 2009, pp 1-19.

13. Akanda, M.; Joung, H.; Tamilavan, V.; Park, S.; Kim, S.; Hyun, M.; Kim, M.; Yang, H. *Analyst* **2014**, *139*, 1420-1425.

14. Ngom, B.; Guo, Y.; Wang, X.; Bi, D. *Anal. Bioanal. Chem* **2010**, *397*, 1113-1135.

15. Maiolini, E.; Ferri, E.; Pitasi, A.; Montoya, A.; Di Giovanni, M.; Errani, E.; Girotti, S. *Analyst* **2014**, *139*, 318-324.

16. Shan, S.; Lai, W.; Xiong, Y.; Wei, H.; Xu, H. *J. Agric. Food Chem.* **2015**, *63*, 745-753.

17. Pohlmann, C.; Dieser, I.; Sprinzl, M. *Analyst* **2014**, *139*, 1063-1071.

18. Huang, H.; Fan, L.; Rajbanshi, B.; Xu, J. *Plos One* **2015**, *10*.

19. Nagatani, N.; Yamanaka, K.; Ushijima, H.; Koketsu, R.; Sasaki, T.; Ikuta, K.; Saito, M.; Miyahara, T.; Tamiya, E. *Analyst* **2012**, *137*, 3422-3426.

20. Lan, T.; Shao, Z.; Gu, M.; Zhou, Z.; Wang, Y.; Wang, W.; Wang, F.; Wang, J. *J Membrane Sci* **2015**, *489*, 204-211.

21. Situ, F.; Tan, R.; Gong, L.; Zha, Z.; Tu, M.; Zeng, R.; Wu, H.; Zhang, J.; Zheng, L. *J. Wuhan Univ. Technol.* **2015**, *30*, 416-422.

22. Miyoshi, T.; Yuasa, K.; Ishigami, T.; Rajabzadeh, S.; Kamio, E.; Ohmukai, Y.; Saeki, D.; Ni, J.; Matsuyama, H. *Appl Surf Sci* **2015**, *330*, 351-357.

23. Astaraee, R. S.; Mohammadi, T.; Kasiri, N. *Food Bioprod Process* **2015**, *94*, 331-341.

24. Grancaric, A. M.; Chibowski, E.; Pusic, T.; Soljacic, I.; Plantic, L.; Itc; Dc, I. T. C.; Dc. *Surface free energy of conventional and enzymatically scoured cotton fabrics*, 2002, p 267-273.

25. Cheung, S.; Cheng, S.; Kamei, D. *J. Lab Autom.* **2015**, *20*, 316-333.

26. Yetisen, A.; Akram, M.; Lowe, C. *Lab Chip* **2013**, *13*, 2210-2251.

27. Abe, K.; Kotera, K.; Suzuki, K.; Citterio, D. *Anal. Bioanal. Chem.* **2010**, *398*, 885-893.

28. Hampl, J.; Hall, M.; Mufti, N. A.; Yao, Y. M.; MacQueen, D. B.; Wright, W. H.; Cooper, D. E. *Analytical biochemistry* **2001**, *288*, 176-187.

29. Pike, J.; Godbert, S.; Johnson, S. *Expert opinion on medical diagnostics* **2013**, *7*, 435-441.

30. Marcus, R. K.; Davis, W. C.; Knippel, B. C.; LaMotte, L.; Hill, T. A.; Perahia, D.; Jenkins, J. D. *J. Chromatogr. A* **2003**, *986*, 17-31.

31. Nelson, D. M.; Marcus, R. K. *Protein Peptide Letts.* **2006**, *13*, 95-99.

32. Randunu, J. M.; Marcus, R. K. *Anal. Bioanal. Chem.* **2012**, *404*, 721-729.

33. Fornea, D. S.; Wu, Y.; Marcus, R. K. *Analytical Chemistry* **2006**, *78*, 5617-5621.

34. Manard, B. T.; Jones, S. M. H.; Marcus, R. K. *Proteomics Clin. Appl.* **2015**, *9*, 522-530.

35. Randunu, J. M.; Dimartino, S.; Marcus, R. K. *J. Sep. Sci.* **2012**, *35*, 3270-3280.

36. Randunu, K. M.; Marcus, R. K. *Biotechnol. Prog.* **2013**, *29*, 1222-1229.

37. Pittman, J.; Manard, B.; Kowalski, P.; Marcus, R. *J. Am. Soc. Mass Spectrom.* **2012**, *23*, 102-107.

38. Schadock-Hewitt, A. J.; Marcus, R. K. *J Sep Sci* **2014**, *37*, 495-504.

39. Jiang, L.; Marcus, R. *Anal. Bioanal. Chem.* **2015**, *407*, 939-951.

40. Schadock-Hewitt, A.; Pittman, J.; Christensen, K.; Marcus, R. *Analyst* **2014**, *139*, 2108-2113.

41. Jiang, L.; Schadock-Hewitt, A.; Zhang, L.; Marcus, R. *Analyst* **2015**, *140*, 1523-1534.

42. Jiang, L.; Marcus, R. K. *J. Chromatogr. A* **2015**, *1410*, 200-209.

43. Schadock-Hewitt, A. J.; Bruce, T.; Marcus, R. K. *Langmuir*, *in press*.

44. Vig, J. *J. Vac. Sci. Technol., A* **1985**, *3*, 1027-1034.

45. Fuchs, P.; Marti, K.; Grgic, G.; Russi, S. *Metrologia* **2014**, *51*, 387-393.

46. Moldovan, A.; Feldmann, F.; Krugel, G.; Zimmer, M.; Rentsch, J.; Hermle, M.; Roth-Foelsch, A.; Kaufmann, K.; Hagendorf, C. *Proceedings of the 4th International Conference on Crystalline Silicon Photovoltaics (Siliconpv 2014)* **2014**, *55*, 834-844.

47. Kato, Y.; Jung, M.; Lee, M.; Qi, Y. *Org. Electron.* **2014**, *15*, 721-728.

48. Schnabel, W. *Polymers and Light*; Wiley-VCH Verlag GmbH & Co. KGaA, 2007.

49. Rånby, B.; Rabek, J. *Photodegradation, Photo-Oxidation, and Photostabilization of Polymers: Principles and Applications*; John Wiley & Sons, 1975.

50. Walzak, M.; Flynn, S.; Foerch, R.; Hill, J.; Karbashewski, E.; Lin, A.; Strobel, M. *J Adhes Sci Technol* **1995**, *9*, 1229-1248.

51. Fuchs, B.; Süß, R.; Nimptsch, A.; Schiller, J. *Chroma* **2009**, *69*, 95-105.

52. Wilson, I. D. *Journal of Chromatography A* **1999**, *856*, 429-442.